Investigations into dianionic scorpionate ligands and their metal complexes

by

Elizabeth Nicole Cooper

B.S., Fort Hays State University, 2017

A THESIS

submitted in partial fulfillment of the requirements for the degree

MASTER OF SCIENCE

Department of Chemistry
College of Arts and Sciences

KANSAS STATE UNIVERSITY
Manhattan, Kansas

2021

Approved by:

Major Professor
Peter E. Sues

Copyright

Abstract

Ligand design helps to define reactivity in coordination complexes and organometallic chemistry. Ligand characteristics greatly influence the reactivity of transition metal complexes and simple changes in the steric or electronic properties of a ligand can drastically affect the activity and selectivity of a catalyst. Scorpionate ligands are an easily tunable and display flexible binding modes in that they can act as bidentate or tridentate donors. In literature scorpionate ligands with charged donors are underrepresented and this is an area with great potential to explore and discover new organometallic complexes with novel reactivity. Inspired by scorpionate ligands and phenolate ligands throughout the literature, a set of eight neutral ligands were synthesized and utilized in the generation of metal complexes. These novel ligands were diphenolate ligands with a nitrogen or oxygen containing tail. The steric hinderance of these structures was varied using the *ortho* substituents on the phenol groups. The various tails also allowed the binding strength of the ligands to be varied. Studies on the activity of the complexes bearing these scorpionate ligands were performed. The effect of the steric size of the ligands as well as binding strength of the tail were investigated.

Table of Contents

List of Figures vi
List of Tables viii
Acknowledgements ix
Chapter 1 - Introduction: Ligand Design in Inorganic Chemistry 1
1.1 Denticity 1
1.2 Ligand Charge 3
1.3 Donating Ability 3
1.4 Steric Hinderance and Tolman Cone Angles 4
1.5 Tridentate Ligand Design: Pincer Complexes 6
1.6 Tridentate Ligand Design: Scorpionate Ligands 8
1.7 References 13
Chapter 2 - Ring-Opening Polymerization of ε-Caprolactone Utilizing Aluminum Alkyl Complexes Bearing Dianionic Scorpionate Ligands 33
2.1 Introduction 33
2.2 Results and Discussion 35
Synthesis and characterization of scorpionate ligands 1-4. 35
Synthesis and characterization of aluminum complexes 5-8 40
ROP of ε-CL. 47
2.3 Conclusions 55
2.4 Experimental 56
2.4 Selected Crystal Data, Data Collection, and Refinement Parameters 70
2.5 Acknowledgements 73
2.6 References 74
Chapter 3 - Molybdenum and Tungsten Alkylidene Complexes 86
3.1 Olefin Metathesis 86
3.2 The Fischer-Tropsch Process and Alkane Metathesis 87
3.3 Current Olefin Metathesis Catalysts 89
3.4 Results and Discussion 91
3.5 Conclusions 103

3.6 Experimental 103
3.7 References 106
Chapter 4 - Conclusions and Future Work 109
4.1 Summary 109
4.2 Future Work 112
4.3 Experimental 115
4.4 References 117

List of Figures

Figure 1.1: Meridional versus facial binding of a tridentate ligand. 2
Figure 1.2: Binding modes from fully binding to fully dissociated. 2
Figure 1.3: Cone angle measurement. 4
Figure 1.4: Bite angle of a multidentate ligand. 5
Figure 1.5: β -diketiminate ligand. 5
Figure 1.6: Pincer ligand design. 6
Figure 1.7: Iridium pincer complexes for alkane hydrogenation and dehydrogenation. 7
Figure 1.8: General design of a scorpionate ligand. 8
Figure 1.9: Tris(methimazolyl)borate (Tm). 12
Figure 2.1: Examples of Aluminum ROP catalysts bearing bidentate (left), tridentate (middle), and tetratdenate (right) ligands. 34
Figure 2.2 General structures for tris(pyrazolyl)borate (left) and tris(pyrazolyl)methane (right) scorpionate ligands. 35
Figure 2.3: ORTEP3 representation (thermal ellipsoids at 50% probability) and atom numbering for: a) 2a, most of the hydrogens are omitted for clarity; and b) 4b, most of the hydrogens are omitted for clarity. 37
Figure 2.4: ORTEP3 representation (thermal ellipsoids at 50% probability) and atom numbering for: a) 5a; b) 6a; c) 6b; d) 7a; and e) 8a. 43
Figure 2.5: Proposed slow activation by aluminum-alkyl complexes followed by rapid ROP of ε-CL by alkoxide intermediates. 49
Figure 2.6: Proposed mechanism for the ROP of ε-CL using 5-8. 55
Figure 3.1: Olefin cross metathesis. 86
Figure 3.2: Mechanism of olefin metathesis. 87
Figure 3.3: Alkane distribution from Fischer-Tropsch process. 88
Figure 3.4: Alkane metathesis and potential side reactions. 88
Figure 3.5: Examples of Schrock-type (left) and Grubbs-type (right) olefin metathesis catalysts. 89
Figure 3.6: Molybdenum and tungsten based catalysts supported by a $[ONO]^{2-}$ ligand. 90

Figure 3.7: Molybdenum and tungsten based catalysts supported by $[MesON]^-$ and $[TripON]^-$ ligands. 91
Figure 3.8: The $Mo(NAr)(CHCMe_2Ph)(OTf)_2(DME)$ starting material. 91
Figure 3.9: Ligands 1-4. 92
Figure 3.10: Following the reaction between $Na_2$2a and $Mo(NAr)(CHCMe_2Ph)(OTf)_2(DME)$ by ^1H NMR spectroscopy in the alkylidene region. 93
Figure 3.11: ^1H NMR spectrum of alkylidene region of initial reaction between $Li_2$3b and $Mo(NAr)(CHCMe_2Ph)(OTf)_2(DME)$ in C_6D_6. 95
Figure 3.12: ^1H NMR spectrum of alkylidene region of initial reaction between $Li_2$2b and $Mo(NAr)(CHCMe_2Ph)(OTf)_2(DME)$ in C_6D_6. 95
Figure 3.13: ^1H NMR spectrum of alkylidene region of initial reaction between $Li_2$4b and $Mo(NAr)(CHCMe_2Ph)(OTf)_2(DME)$ in C_6D_6. 96
Figure 3.14: ORTEP3 representation (thermal ellipsoids at 50% probability) and atom numbering for $Mo(NAr)(CHCMe_2Ph)$(4b)(OTf) excluding most hydrogens for clarity. 97
Figure 3.15: ^1H NMR spectrum of the alkylidene region of $Mo(NAr)(CHCMe_2Ph)$(4b) taken in C_6D_6. 102
Figure 3.16: ^1H NMR spectrum of $Mo(NAr)(CHCMe_2Ph)$(4b) excluding the alkylidene region taken on 400 mHz in C_6D_6. 102
Figure 3.17: Unsymmetric binding of 4b to molybdenum. 103
Figure 4.1: ORTEP3 representation (thermal ellipsoids at 50% probability) and atom numbering for $Mo(NAr)(CHCMe_2Ph)$(4b)(OTf) excluding most hydrogens for clarity. 111
Figure 4.2: Cross metathesis with 1-hexene (top) and 1-octene (bottom). 113
Figure 4.3: Bicyclic monomers for polymerization. 114
Figure 4.4: a. Benzimidazole ligand (9) and b. the half-4b ligand. 114

List of Tables

Table 2.1: Selected bond lengths (Å) and angles (deg) for 2a and 4b. 38
Table 2.2: Selected bond lengths (Å) and angles (deg) for 5a.[a] 43
Table 2.3: Selected bond lengths (Å) and angles (deg) for 6a-b, 7a, and 8a. 46
Table 2.4: ROP of ε-caprolactone using 6a.[a] 47
Table 2.5: ROP of ε-caprolactone using 5-8.[a] 51
Table 2.6: Compounds 2a, 4b, 5a, and 6a. 70
Table 2.7: Compounds 6b, 7a, and 8a. 72
Table 3.1: Selected bond distances (Å) and angles (deg) for Mo(NAr)($CHCMe_2Ph$)(4b)(OTf). 98
Table 3.2: Selected crystal data, data collection, and refinement parameters. 98

Acknowledgements

I would like to thank many people, without whom this would not have been possible. First, I would like to thank Kansas State University for the funding and financial support as well as the opportunity to study and do research. Next, I would like to thank Dr. Peter E. Sues, who has mentored me throughout my research. I would also like to thank my former and current group members Casey Ackley, Logan Trowbridge, and Sachithra Somachandra and all previous members of the Sues group for their support and encouraging words. I would also like to thank my committee members Dr. Christer Aakeroy, Dr. Ryan Rafferty, and Dr. Urara Hasegawa. And last, but certainly not least, I would like to thank my family and friends for their support, especially my loving husband, parents, and siblings. Without the support of all these people, I would not have been able to accomplish what I have done to date. Thank you.

Chapter 1 - Introduction: Ligand Design in Inorganic Chemistry

In inorganic and organometallic chemistry, ligands have the power to dictate the reactivity of metal complexes. Although it is typically the metal that is the center of all activity for a coordination complex, the properties of the metal are often heavily influenced by the properties of the ligands that are bound.[1–5] The electronic and steric factors of the ligands are critically important and a simple change in one or both factors can drastically change the reactivity of the metal. Therefore, many varieties of ligands have been synthesized and utilized for various applications. These ligands can be classified according to their various properties including denticity, charge, donating ability, and steric bulk.

1.1 Denticity

Denticity is an important concept for ligands that helps to explain their binding modes. Denticity is commonly defined as the number of pairs of electrons that bind the ligand to a metal center, or how many bonds the ligand forms with a metal center. If a ligand binds through two donors, it is designated as bidentate and if the ligand binds through three donors, it is tridentate, etc. Higher denticity ligands have been developed, such as porphyrins,[25] but most ligands are monodentate, bidentate or tridentate.

The number of binding points, especially for tridentate and higher denticity ligands, can affect the overall geometry of a complex.[26] Ligands that have higher denticities are often not very flexible and must coordinate in specific orientations. For instance, a pincer ligand will bind to a metal in a *mer*- fashion, Figure 1.1.[27–36] The 2-2', 6'-2''-terpyridyl ligand also binds meridionally.[37] The other fashion in which a tridentate ligand can bind is *fac*-, which can be seen with scorpionate ligands,[38–41] 1,4,7-triazocyclononane (tacn),[42] and in bis-benzimidazole-ethanol ligands.[43] Meridional binding ligands add a robustness to the metal complex and allow for

Figure 1.1: Meridional versus facial binding of a tridentate ligand.

difficult bond breaking or forming reactions,[44–46] while facially binding ligands can give more reactive species.[41] Ligands in both binding classes can be varied and tuned through electronic and steric means which affects their binding strength as well as the overall metal complex. Electronic and steric factors and their effects will be discussed in later sections.

The total number of ligand binding points can affect the reactivity of a complex if a certain geometry is desired or if an open coordination site is needed. For a metal complex to react, an open site for an incoming molecule is needed for the metal complex to affect a chemical transformation. If a complex is already coordinatively saturated, ligand dissociation must occur first to allow an interaction to occur with another molecule.

Ligands can also be defined as hemi-labile, Figure 1.2. A hemi-labile ligand contains at least one atom that is strongly bound to the metal center, while one atom is weakly or reversibly bound to the metal. This can allow for metal complexes to be reactive and stabilized at the same time.[47] The weakly bound atom can dissociate to allow for an open coordination site, and then can bind once again to stabilize any reactive intermediates with vacant sites. Scorpionate ligands can fall into the category of being hemi-labile.[41]

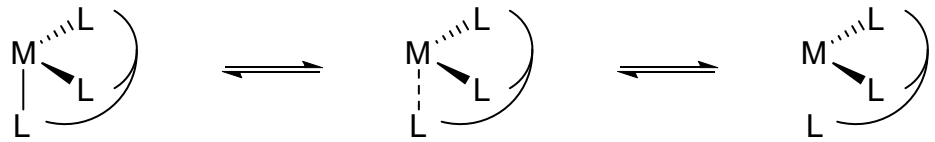

Figure 1.2: Binding modes from fully binding to fully dissociated.

1.2 Ligand Charge

Ligands can have a variety of charges, and although typically ligands are neutral or anionic, they can have multiple anionic charges as well. In other words, we can classify ligands based how many electrons they are donating to a metal center, as well as their overall charge. When talking about the charge of a ligand in general terms, X is used for an anionic ligand and L is used for a neutral ligand. For instance, a dianionic tridentate ligand would be LX_2. The charge of ligands is very important to consider and can be utilized to support metal centers with a wide range of oxidation states. Highly charged ligands are often found supporting complexes with metals in higher oxidation states, while neutral ligands are used more often in complexes with lower oxidation state metals.

1.3 Donating Ability

The electronic donating ability of ligands influences the amount of electron density at the metal center.[48] This effect was originally studied by looking at complexes containing carbonyl ligands. The C≡O stretching frequency is related to the electron density at the metal which influences the amount of back donation to the carbonyl. An example of this can be seen with $Ni(CO)_3L$ complexes where L was a trisubstituted phosphine ligand. These species have been studied to determine the electronic properties of phosphine ligands.[49] As the phosphine increases in electron donating ability the carbonyl stretching frequency decreases. This is due to an increase in electron density at the metal which leads to an increase in back donation to the carbonyl antibonding orbital. From most donating to most withdrawing, the phosphines contained alkyl substituents, followed by aromatic substituents, then oxygen containing substituents, and finally halide substituents. More electronegative substituents will provide greater electron-withdrawing effects making the metal less electron rich. This same effect can be

seen in all types of ligands and not just phosphines.[48,50–52] Electron density can also be seen in the shifts of NMR spectra. More electron density at the metal is consistent with shifts up-field in NMR spectra.[53]

The change in electron density at the metal center can affect its catalytic behavior. This change in behavior though can vary according to the catalytic mechanism.[54] An increase in electron density will facilitate oxidative addition, while decreasing electron density will facilitate faster β-hydride elimination as the electron count will increase by two at the metal center.[54]

1.4 Steric Hinderance and Tolman Cone Angles

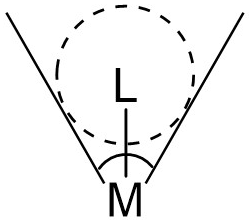

Figure 1.3: Cone angle measurement.

Along with electronic factors, steric hinderance greatly influences the behavior of ligands and organometallic complexes. The steric hinderance of a ligand can be described by its cone angle. This again was first discussed for phosphine ligands by Tolman.[49,55] Using space-filling models, increasing the steric size of the ligand increased the cone angle, Figure 1.3. The cone angle can help predict the number of ligands that will associate with a metal center. With large angles fewer ligands can bind.[56] Ligands with relatively small cone angles, PMe_3 PMe_2Ph and $PMePh_2$ with cone angles of 118°, 122°, and 136°, respectively, can fit up to four[57,58] or five[59] phosphine ligands around a molybdenum center. A more sterically hindered PPh_3 ligand has a cone angle of 145° and only two phosphine ligands bind to a molybdenum center.[60]

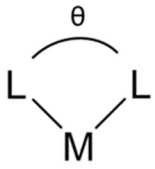

Figure 1.4: Bite angle of a multidentate ligand.

In the case of multidentate ligands, the bite angle can also be analyzed to determine the steric hinderance of the ligand, Figure 1.4. This angle also helps define the overall geometry of a metal complex. A larger bite angle results in more of the coordination sphere being occupied by the chelating ligand. This bite angle can be affected by increasing the steric bulk of substituents on the ligand. For β-diketiminate ligands, Figure 1.5, steric hinderance can be changed on the backbone or at the N-aryl substituents.[53] With smaller substituents, like H or Me, the bite angle is smaller, often causing metal complexes to form dimeric or polymeric complexes. Examples of this have been studied by looking at various analogues of the same β-diketiminate ligand with different substituents. For a $[LScCl_2]_n$ complex where L is a β-diketiminate ligand, when L contained a methyl substituent on the carbon bonded to the nitrogen (R^2 in Figure 1.5) n = 2, denoting the formation of a dimeric complex.[61] When this same complex L contained a *t*-butyl substituent in the same position, a monomeric complex formed and n = 1.[62] The same phenomenon was seen with $[LFeCl]_n$,[63–65] $[LFeF]_n$,[66] $[LCoCl]_n$,[67] $[LNiCl]_n$,[64,67,68] $[LNi(CO)]_n$,[69–71] $[LCuCl]_n$,[72–74] and $[LPd(\mu\text{-}OAc)]_n$[75,76] complexes. In addition to just forming dimeric or

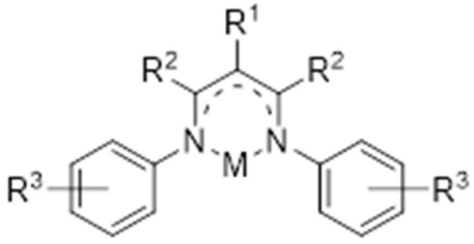

Figure 1.5: β -diketiminate ligand.

polymeric complexes, additional neutral ligands or solvents could be coordinated to complexes with smaller bite angles and less steric hinderance.[62,77–79]

Steric hinderance plays a vital role in the catalytic activity of a catalyst. Added steric hinderance can cause strain in intermediates which can raise activation energies and can slow down reactions.[53] Reduced catalytic activity due to steric hinderance can be seen with many types of ligands, including N,O-chelating ligands,[80] bis(N-heterocyclic carbene) ligands,[81] and phosphinamine ligands,[82] to name a few.

1.5 Tridentate Ligand Design: Pincer Complexes

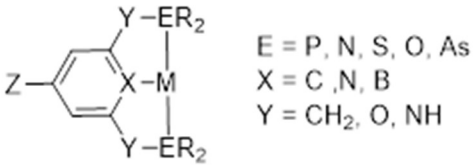

Figure 1.6: Pincer ligand design.

Taking the aforementioned factors into account, ligand design plays an integral part of inorganic and organometallic chemistry. Higher denticity ligands are of particular interest due to the stability they impart to complexes and the amount of control they provide with respect to the electronic and steric environment of the metal. One class of tridentate ligands is denoted as pincer ligands. An example of a complex bearing a pincer ligand is shown in Figure 1.6. This ligand structure was first reported in 1976 by Shaw and co-workers[83–85] as well as van Koten.[44] As first described, the term pincer was defined as $[2,6\text{-}(ECH_2)C_6H_3]^-$ where E was a neutral two-electron donor, typically either PR_2 or NR_2.[86,87] However, over the years, the definition of pincer ligands has expanded to include many more variations, Figure 1.6.[88] This modular structure allows both the electronic and steric factors within the ligand to be easily varied.[89] The E group is particularly modular and gives significant control over the resulting complex due to the close proximity to the metal center[90] Varying the R substituents on E allows for the steric demands of

the ligands to be tuned. The identity of the E group also allows for the electron donating ability of the pincer to be modified, and potentially provides a point to incorporate a labile donor.[86] The bridging Y group allows for tuning electronic effects as well.[91] The central X atom can also change the electronic density at the metal center.[92,93] Z allows for additional control over the electron density at the metal center without large effects on the steric hinderance of the ligand.[94]

As a generality most ligands that bind in a meridional fashion can be described as pincer ligands. As mentioned in earlier sections, these types of ligands tend to form more stable complexes with the ligand filling much of the coordination sphere around the metal center. This increased stability allows this ligand to be used in catalysts that require harsh and forcing reaction conditions.

A well-studied class of catalysts that uses pincer ligands are iridium pincer complexes which can be used for the dehydrogenation of alkenes. There are two main ligand structures used for the iridium pincer complexes, ($^{R}_{4}$PCP)IrH_2 and ($^{R}_{4}$POCOP)IrH_2, R=*i*-Pr, *t*-Bu, Figure 1.7.[27–32] There are other variants of these catalysts, but the two examples shown below are perhaps the most studied and most active alkane dehydrogenation catalysts available. Typically R=*i*-Pr is the more active variant between R=*i*-Pr and *t*-Bu due to the less sterically hindered metal center.[28,33] All of these iridium pincer catalysts require temperatures typically between 150°C and 250°C for

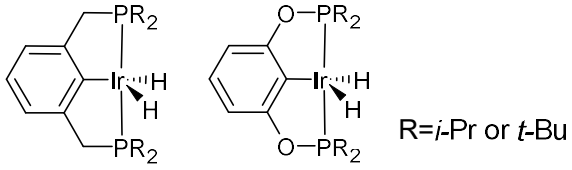

Figure 1.7: Iridium pincer complexes for alkane hydrogenation and dehydrogenation.

the dehydrogenation of alkanes.[33–35] The reason for this is that alkane carbon-hydrogen bonds are strong requiring approximately 28 or 30 kcal/mol to activate for *n*-alkanes at the internal position or terminal position, respectively.[95] At these elevated temperatures the pincer ligand is necessary

to stabilize the iridium complexes. Although iridium pincer complexes are the most prevalent examples of pincer complexes that can be found in literature, other compounds are known.[96–98]

1.6 Tridentate Ligand Design: Scorpionate Ligands

Another class of tridentate ligands are the scorpionate ligands. The first scorpionate ligands were developed by Trofimenko in the late 1960s.[38,99,100] The original general structure of the ligand class was [RR'B(pz)$_2$] where R and R' were pz, H, alkyl, aryl, F, OR, SR, or NR$_2$, and pz is a pyrazolyl group, Figure 1.8. Similar to pincer ligands, the definition of scorpionate ligands has expanded greatly since their initial discovery. The definition now includes tridentate ligands that bind facially. Often, scorpionate ligands are described as binding like a scorpion through its claws and stinging tail.[40] The term scorpionate can also refer to the tail of the ligand being labile.[41]

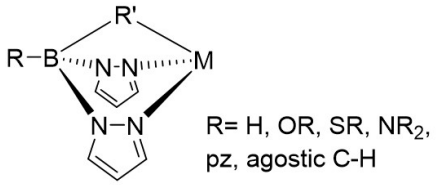

Figure 1.8: General design of a scorpionate ligand.

The binding of scorpionate ligands can be compared to a few other classes of ligands. When a scorpionate ligand is bidentate, an analog would be β-diketonates. When bound in a tridentate fashion, they are analogous in some ways to cyclopentadienyl or pentamethylcyclopentadienyl ligands.[101] While these analogies hold for the electronic behavior and number of electrons donated to the metal center, this analogy does not hold for the coordination geometry of the scorpionate ligand. As seen in Figure 1.8, the ligand is in a boat geometry when coordinated to the metal leaving the R' group in close proximity to the metal. This can lead to significant interaction between the R' group and the metal center. This is where the scorpion analogy can help visualize the binding. The two pz groups bind like two claws and

the R' group wraps around and 'stings' the metal center, like the tail of a scorpion. Further, there are subdivisions of scorpionate ligands, including homoscorpionate and heteroscorpionate species. In homoscorpionate ligands the tail is the same as the main chelating arms of the ligand. In heteroscorpionate ligands the tail has a different identity, leading to more opportunities to tune the ligand through electronic and steric means.[101]

The most studied of all scorpionate ligands are tris(pyrazolyl)borane (Tp) structures. These were the first scorpionates to be developed by Trofimenko and are the topic of many reviews.[41,101–116] The synthesis of these ligands has been well developed for many different substituted variants. Generally, the desired substituted pyrazole is heated with a borohydride anion, Scheme 1.1.[99,103] Through control of the reaction temperature, the degree of substitution can be controlled to form bis(pyrazolyl) versus tris(pyrazolyl) derivatives.[103] From here, when talking about tris(pyrazolyl)borane ligands, the following notation will be used Tp^x where x is the substituent in the 3-position of the pyrazolyl.

Scheme 1.1: Synthesis of bis(pyrazolyl)borate and tris(pyrazolyl)borate.

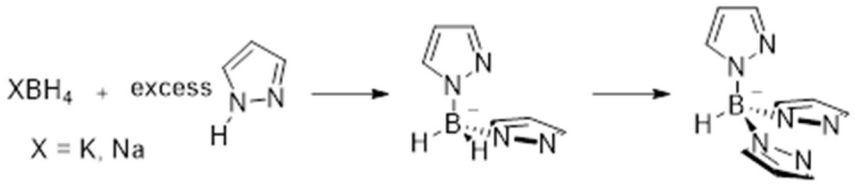

The substitution on the pyrazolyl moieties affects the coordination of the Tp^x ligand, both in terms of steric and electronic effects. With respect to steric effects, the substituents on the pyrazolyl groups can wrap around the metal center creating a more shielded species. In terms of cone angles, all Tp ligands have a cone angle greater than 180°, which can vary with the substituents utilized. The smallest cone angle is the unsubstituted Tp ligand at 184°, followed by Tp^{Me}, the 3,5-dimethylpryazolyl derivative, at 224°.[101] The cone angles for these derivatives as well as several other substituted Tp ligands have been determined by X-ray

crystallography.[101,117–119] The cone angle of a scorpionate ligand does limit the number of scorpionate ligands that can bind to a metal center. Looking at first row transition metals, Tp ligands with relatively small cone angles such as Tp, Tp^{Me}, Tp^{cpr}, Tp^{Tn}, where Me = methyl, cpr = cyclopentane, Tn = thiophene, are capable of forming $Tp^{x}{}_{2}M$ complexes, but do not form $Tp^{x}MX$ compounds, where X is an anionic ligand.[101,104,112–115] Ligands with intermediate cone angles, on the other hand, can form either $Tp^{x}{}_{2}M$ or $Tp^{x}MX$ species. Such ligands include $Tp^{i\text{-}Pr}$, $Tp^{i\text{-}Pr2}$, $Tp^{i\text{-}Pr,4\text{-}Br}$, $Tp^{i\text{-}Pr,Me}$, Tp^{Menth}, Tp^{Np}, Tp^{Ph}, and Tp^{Ar} where Menth = 7(R)-isopropyl-4(R)-methyl-4,5,6,7-tetrahydro, Np = neopentyl, and Ar is a number of substituted phenyl rings.[120–122] The most sterically hindered ligands, $Tp^{t\text{-}Bu}$, $Tp^{t\text{-}Bu,Me}$, $Tp^{t\text{-}Bu,\ Tn}$, $Tp^{t\text{-}Bu,\ i\text{-}Pr}$, Tp^{Ms}, Tp^{Ant}, Tp^{Trip}, where Ms = mesityl, Ant = anthracene, Trip = 9-triptycyl, only form $Tp^{x}MX$ species and do not form $Tp^{x}{}_{2}M$ complexes due to the large cone angle of the *fac* ligand.[122]

The electronic effects of substituents on Tp^{x} also influences metal complexes greatly. The substituent electronic effects were originally studied on Cr, Mo, and W complexes of the type $Tp^{x}M(CO)_{3}$.[123–126] The electronic effects were compared to those of $Cp^{x}M(CO)_{3}$ where Cp^{x} = substituted cyclopentadiene complexes containing the same metal since Tp^{x} and Cp^{x} are iso-electronic. From these studies, the Tp^{x} ligands followed a trend that was generally to be expected based on the electron donating or withdrawing capabilities of the individual substituents. For example, alkyl groups donated more electron density and phenyl groups as well as halogens were electron withdrawing in nature. The electron-donating ability of Tp^{x} could be ordered according to the series below:

Tp^{R2} (R=alkyl) > $Tp^{t\text{-}Bu}$ ≈ $Tp^{i\text{-}Pr}$ ≈ Tp^{Me} ≈ $Tp^{i\text{-}Pr}$ ≈ Tp^{Ms} > Tp > Tp^{Ph2} ≈ Tp^{Ph} > $Tp^{CF3,Tn}$ > $Tp^{i\text{-}Pr,4Br}$ > $Tp^{CF3,Me}$

In addition, Tp^x ligands have been used on almost all of the transition metals[101] as well as the p-block elements.[102]

Another well studied group of scorpionate ligands are the tris(pyrazolyl)methane ($HC(pz)_3$) family of compounds. Until the early 2000s, this was an understudied class of scorpionates, due to the low yielding synthesis of the ($HC(pz)_3$) ligands. The unsubstitued $HC(pz)_3$ ligand was developed in 1937 with the reaction of chloroform and the potassium salt of pyrazole, which had an isolated yield of 34%.[127] In 1984 an improved synthesis using pyrazole and chloroform using K_2CO_3 increased yields of $HC(3\text{-}Pz^{Me})_3$ to up to 60%, but the yield of $HC(pz)_3$ remained low at 24% yield.[128] Finally, in 2000 Reger and co-workers replaced K_2CO_3 in their synthesis with Na_2CO_3, and this gave higher percent yields for this ligand class.[129]

As with the Tp scorpionates, $HC(pz)_3$ ligands can be highly substituted. And as would be expected, the same trends in terms of steric hinderance and electronic effects can be seen for the carbon derivatives. Although the binding remains the same in many instances, there are some differences in metal complex reactivity between the boron and carbon analogues. One example of an extreme difference in reactivity was when $HC(pz)_3$ was reacted with $M(CO)_6$ (M=Group 6 metal), it formed an insoluble and involatile species. When Tp was reacted with the same group 6 metal carbonyls, it formed a very soluble substance that was sublimed with ease.[130] $HC(pz)_3$ ligands have also been covered in numerous reviews.[103,131]

In addition to borane and methane derivatives, there have been reports of silane derivatives of scorpionate ligands.[131–134] The carbon and boron derivatives have been investigated far more than the silane derivatives, though. Therefore, the silane derivatives remain an underdeveloped field.

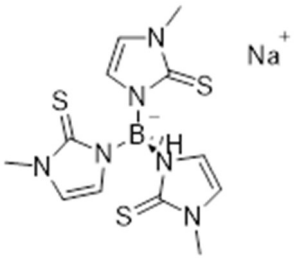

Figure 1.9: Tris(methimazolyl)borate (Tm).

Although the first scorpionate ligands were bound to metals through nitrogen atoms, sulfur derivatives have been reported in literature, Figure 1.9.[135,136] This allows for a large electronic and structural change. In general, these tris(methimazolyl)borate (Tm) derivatives and their metal complexes are more stable. This is especially the case with group 15 metals and even a group 16 metal, tellurium.[102,137] With Tp derivatives, metal complexes have been comprehensively studied for transition metals as well as group 13 and 14 metals, while group 15 Tp-metal complexes are rare. To study the difference between the soft Tm ligands and hard Tp ligands, Tm^{Me} was first added to $BiCl_3$ followed by addition of Tp to the reaction mixture. Instead of a mixed system of Tm^{Me} and Tp coordinated to the bismuth center, the formation of $[Bi(Tm^{Me})_2]^+[Na(Tp)_2]^-$ was observed.[138] This observation demonstrated the soft behavior Tm^{Me} versus the hard nature of Tp. Following hard-soft acid-base theory, the Tm^{Me} bound solely to the bismuth and Tp bound solely to sodium. Further, studies have shown that Tm^{Me} is a stronger electron donor than Tp and Cp. Comparing CO stretching frequencies for metal complexes utilizing Rh,[139,140] Mn,[141] Mo and W,[142,143] all species showed that the electron donating ability followed the trend: Tm^{Me} > Cp > Tp. This effect is to be expected as the sulfur donors in Tm^{Me} have lone pairs to donate to the metal center adding to the metal electron density. Another benefit of using sulfur donors on the scorpionate ligand is to better model metalloprotein active sites.[136]

While the scoprionate ligand class of molecules is widely studied and many variations of these ligands have been explored, there is still room for more exploration within this field. Scorpionate ligands with multiple anionic donors are, to the best of my knowledge, not widely reported in literature. Anionic oxygen donors would allow for an additional sub-class of current scorpionate ligands. Multiple anionic charges can support highly charged metal cations. Utilization of scorpionate ligands on highly charged metal centers without the use of additional anionic ligands could reveal new reactivity for those metal complexes.

This thesis will focus on the design and synthesis of a novel set of dianionic heteroscorpionate ligands and their coordination to metal complexes, including aluminum and molybdenum centers. This set of ligands will contain anionic oxygen donors as the pincers or 'claws' with nitrogen or oxygen containing tails. The steric hinderance on the 'claws' will also be varied. The influence of these ligands on complex reactivity will also be explored.

1.7 References

(1) Dzik, W. I.; van der Vlugt, J. I.; Reek, J. N. H.; de Bruin, B. Ligands That Store and Release Electrons during Catalysis. *Angewandte Chemie International Edition* **2011**, *50* (15), 3356–3358.

(2) Ikariya, T.; Murata, K.; Noyori, R. Bifunctional Transition Metal-Based Molecular Catalysts for Asymmetric Syntheses. *Org. Biomol. Chem.* **2006**, *4* (3), 393–406.

(3) Ikariya, T.; Blacker, A. J. Asymmetric Transfer Hydrogenation of Ketones with Bifunctional Transition Metal-Based Molecular Catalysts. *Acc. Chem. Res.* **2007**, *40* (12), 1300–1308.

(4) Gunanathan, C.; Milstein, D. Bond Activation and Catalysis by Ruthenium Pincer Complexes. *Chem. Rev.* **2014**, *114* (24), 12024–12087.

(5) Crabtree, R. H. Carbenes. Pincers, Chelates, and Abnormal Binding Modes. *Pure and Applied Chemistry* **2003**, *75* (4), 435–443.

(6) Pearson, R. G. Hard and Soft Acids and Bases. *J. Am. Chem. Soc.* **1963**, *85* (22), 3533–3539.

(7) Edwards, J. O.; Pearson, R. G. The Factors Determining Nucleophilic Reactivities. *J. Am. Chem. Soc.* **1962**, *84* (1), 16–24.

(8) Ahrland, S.; Chatt, J.; Davies, N. R. The Relative Affinities of Ligand Atoms for Acceptor Molecules and Ions. *Q. Rev. Chem. Soc.* **1958**, *12* (3), 265–276.

(9) Pearson, R. G.; Songstad, Jon. Application of the Principle of Hard and Soft Acids and Bases to Organic Chemistry. *J. Am. Chem. Soc.* **1967**, *89* (8), 1827–1836.

(10) Saville, B. The Concept of Hard and Soft Acids and Bases as Applied to Multi-Center Chemical Reactions. *Angewandte Chemie International Edition in English* **1967**, *6* (11), 928–939.

(11) Pearson, R. G. Acids and Bases. *Science* **1966**, *151* (3707), 172–177.

(12) Pearson, R. G. Hard and Soft Acids and Bases, HSAB, Part II: Underlying Theories. *J. Chem. Educ.* **1968**, *45* (10), 643.

(13) Ho, T.-L. Hard Soft Acids Bases (HSAB) Principle and Organic Chemistry. *Chem. Rev.* **1975**, *75* (1), 1–20.

(14) Huyskens, P.; Sobczyk, L.; Majerz, I. On a Hard/Soft Hydrogen Bond Interaction. *Journal of Molecular Structure* **2002**, *615* (1), 61–72.

(15) Vögtle, F.; Weber, E. Multidentate Acyclic Neutral Ligands and Their Complexation. *Angewandte Chemie International Edition in English* **1979**, *18* (10), 753–776.

(16) Komorowski, L. Electronegativity and Hardness in the Chemical Approximation. *Chemical Physics* **1987**, *114* (1), 55–71.

(17) Sankaralingam, M.; Lee, Y.-M.; Nam, W.; Fukuzumi, S. Amphoteric Reactivity of Metal–Oxygen Complexes in Oxidation Reactions. *Coordination Chemistry Reviews* **2018**, *365*, 41–59.

(18) Housecroft, C. E.; Sharpe, A. G. *Inorganic Chemistry*, Fourth Edition.; Pearson: New York, 2012.

(19) Miessler, G. M.; Fischer, P. J.; Tarr, D. A. *Inorganic Chemistry*, Fifth Edition.; Pearson: Boston, 2014.

(20) Elucidating the hard/soft acid/base principle: A perspective based on half-reactions: The Journal of Chemical Physics: Vol 124, No 19

(21) Hamisu, A. M.; Ariffin, A.; Wibowo, A. C. Cation Exchange in Metal-Organic Frameworks (MOFs): The Hard-Soft Acid-Base (HSAB) Principle Appraisal. *Inorganica Chimica Acta* **2020**, *511*, 119801.

(22) Yazaki, R.; Kumagai, N.; Shibasaki, M. Direct Catalytic Asymmetric Addition of Allyl Cyanide to Ketones via Soft Lewis Acid/Hard Brønsted Base/Hard Lewis Base Catalysis. *J. Am. Chem. Soc.* **2010**, *132* (15), 5522–5531.

(23) Nagaraj, P.; Ramesh, N. G. HSAB-Driven Regioselectivity Difference in the Lewis-Acid Catalyzed Reactions of 2-C-Substituted Glycals with Sulfur and Oxygen Nucleophiles: Direct versus Allylic Substitution. *Tetrahedron* **2011**, *67* (48), 9322–9328.

(24) Mayr, H.; Breugst, M.; Ofial, A. R. Farewell to the HSAB Treatment of Ambident Reactivity. *Angewandte Chemie International Edition* **2011**, *50* (29), 6470–6505.

(25) Bonnett, R. Photosensitizers of the Porphyrin and Phthalocyanine Series for Photodynamic Therapy. *Chem. Soc. Rev.* **1995**, *24* (1), 19–33.

(26) Smits, N. W. G.; van Dijk, B.; de Bruin, I.; Groeneveld, S. L. T.; Siegler, M. A.; Hetterscheid, D. G. H. Influence of Ligand Denticity and Flexibility on the Molecular Copper Mediated Oxygen Reduction Reaction. *Inorg. Chem.* **2020**, *59* (22), 16398–16409.

(27) Gupta, M.; Hagen, C.; Flesher, R. J.; Kaska, W. C.; Jensen, C. M. A Highly Active Alkane Dehydrogenation Catalyst: Stabilization of Dihydrido Rhodium and Iridium Complexes by a P–C–P Pincer Ligand. *Chem. Commun.* **1996**, No. 17, 2083–2084.

(28) Liu, F.; Goldman, A. S. Efficient Thermochemical Alkane Dehydrogenation and Isomerization Catalyzed by an Iridium Pincer Complex. *Chem. Commun.* **1999**, No. 7, 655–656.

(29) Göttker-Schnetmann, I.; Brookhart, M. Mechanistic Studies of the Transfer Dehydrogenation of Cyclooctane Catalyzed by Iridium Bis(Phosphinite) *p* -XPCP Pincer Complexes. *J. Am. Chem. Soc.* **2004**, *126* (30), 9330–9338.

(30) Göttker-Schnetmann, I.; White, P.; Brookhart, M. Iridium Bis(Phosphinite) p-XPCP Pincer Complexes: Highly Active Catalysts for the Transfer Dehydrogenation of Alkanes. *J. Am. Chem. Soc.* **2004**, *126* (6), 1804–1811.

(31) Göttker-Schnetmann, I.; White, P. S.; Brookhart, M. Synthesis and Properties of Iridium Bis(Phosphinite) Pincer Complexes (p-XPCP)IrH2, (p-XPCP)Ir(CO), (p-XPCP)Ir(H)(Aryl), and {(p-XPCP)Ir}2{μ-N2} and Their Relevance in Alkane Transfer Dehydrogenation. *Organometallics* **2004**, *23* (8), 1766–1776.

(32) Morales-Morales, D.; Redón, R.; Yung, C.; Jensen, C. M. Dehydrogenation of Alkanes Catalyzed by an Iridium Phosphinito PCP Pincer Complex. *Inorganica Chimica Acta* **2004**, *357* (10), 2953–2956.

(33) Xu, W.; Rosini, G. P.; Krogh-Jespersen, K.; Goldman, A. S.; Gupta, M.; Jensen, C. M.; Kaska, W. C. Thermochemical Alkane Dehydrogenation Catalyzed in Solution without the Use of a Hydrogen Acceptor. *Chem. Commun.* **1997**, No. 23, 2273–2274.

(34) Haenel, M. W.; Oevers, S.; Angermund, K.; Kaska, W. C.; Fan, H.-J.; Hall, M. B. Thermally Stable Homogeneous Catalysts for Alkane Dehydrogenation. *Angewandte Chemie International Edition* **2001**, *40* (19), 3596–3600.

(35) Punji, B.; Emge, T. J.; Goldman, A. S. A Highly Stable Adamantyl-Substituted Pincer-Ligated Iridium Catalyst for Alkane Dehydrogenation. *Organometallics* **2010**, *29* (12), 2702–2709.

(36) Renkema, K. B.; Kissin, Y. V.; Goldman, A. S. Mechanism of Alkane Transfer-Dehydrogenation Catalyzed by a Pincer-Ligated Iridium Complex. *J. Am. Chem. Soc.* **2003**, *125* (26), 7770–7771.

(37) McWhinnie, W. R.; Miller, J. D. The Chemistry of Complexes Containing 2,2′-Bipyridyl, 1, 10-Phenanthroline, or 2,2′,6′,2”-Terpyridyl as Ligands. In *Advances in Inorganic Chemistry and Radiochemistry*; Emeléus, H. J., Sharpe, A. G., Eds.; Academic Press, 1970; Vol. 12, pp 135–215.

(38) Trofimenko, S. Boron-Pyrazole Chemistry. *J. Am. Chem. Soc.* **1966**, *88* (8), 1842–1844.

(39) Trofimenko, Swiatoslaw. Coordination Chemistry of Pyrazole-Derived Ligands. *Chem. Rev.* **1972**, *72* (5), 497–509.

(40) Owen, G. R. Functional Group Migrations between Boron and Metal Centres within Transition Metal–Borane and –Boryl Complexes and Cleavage of H–H, E–H and E–E′ Bonds. *Chem. Commun.* **2016**, *52* (71), 10712–10726.

(41) Pettinari, C.; Pettinari, R.; Marchetti, F. Chapter Four - Golden Jubilee for Scorpionates: Recent Advances in Organometallic Chemistry and Their Role in Catalysis. In *Advances in Organometallic Chemistry*; Pérez, P. J., Ed.; Academic Press, 2016; Vol. 65, pp 175–260.

(42) Chaudhuri, P.; Wieghardt, K. The Chemistry of 1,4,7-Triazacyclononane and Related Tridentate Macrocyclic Compounds. In *Progress in Inorganic Chemistry*; John Wiley & Sons, Ltd, 1987; pp 329–436.

(43) Granelli, M.; Downward, A. M.; Deville, C.; Franco, A. R.; Guénée, L.; Besnard, C.; Williams, A. F. Coordination Chemistry of the Chiral, Facially Coordinating Tridentate Ligand 1,2-Bis(Benzimidazol-2-Yl)Ethanol with 3d Transition Metals. *European Journal of Inorganic Chemistry* **2018**, *2018* (37), 4181–4189.

(44) Koten, G. van; Timmer, K.; Noltes, J. G.; Spek, A. L. A Novel Type of Pt–C Interaction and a Model for the Final Stage in Reductive Elimination Processes Involving C–C Coupling at Pt; Synthesis and Molecular Geometry of [1,N,N′-η-2,6-Bis{(Dimethylamino)Methyl}-Toluene]Iodoplatinum(II) Tetrafluoroborate. *J. Chem. Soc., Chem. Commun.* **1978**, No. 6, 250–252.

(45) Taakili, R.; Canac, Y. NHC Core Pincer Ligands Exhibiting Two Anionic Coordinating Extremities. *Molecules* **2020**, *25* (9), 2231.

(46) Wang, Y.; Zhang, B.; Guo, S. Transition Metal Complexes Supported by N-Heterocyclic Carbene-Based Pincer Platforms: Synthesis, Reactivity and Applications. *European Journal of Inorganic Chemistry* **2021**, *2021* (3), 188–204.

(47) Grützmacher, H. Cooperating Ligands in Catalysis. *Angewandte Chemie International Edition* **2008**, *47* (10), 1814–1818.

(48) Flanagan, S. P.; Guiry, P. J. Substituent Electronic Effects in Chiral Ligands for Asymmetric Catalysis. *Journal of Organometallic Chemistry* **2006**, *691* (10), 2125–2154.

(49) Tolman, C. A. Steric Effects of Phosphorus Ligands in Organometallic Chemistry and Homogeneous Catalysis. *Chem. Rev.* **1977**, *77* (3), 313–348.

(50) Mealli, C.; Ienco, A.; Phillips, A. D.; Galindo, A. A Critical Review of Electronic Effects in Enediamido and α-Diimino Complexes of the Group 4 Metals. *European Journal of Inorganic Chemistry* **2007**, *2007* (18), 2556–2568.

(51) Jacobsen, E. N.; Zhang, W.; Guler, M. L. Electronic Tuning of Asymmetric Catalysts. *J. Am. Chem. Soc.* **1991**, *113* (17), 6703–6704.

(52) Nishiyama, H.; Yamaguchi, S.; Kondo, M.; Itoh, K. Electronic Substituent Effect of Nitrogen Ligands in Catalytic Asymmetric Hydrosilylation of Ketones: Chiral 4-Substituted Bis(Oxazolinyl)Pyridines. *J. Org. Chem.* **1992**, *57* (15), 4306–4309.

(53) Chen, C.; Bellows, S. M.; Holland, P. L. Tuning Steric and Electronic Effects in Transition-Metal β-Diketiminate Complexes. *Dalton Trans.* **2015**, *44* (38), 16654–16670.

(54) Liu, H.; Wang, W.-H.; Xiong, H.; Nijamudheen, A.; Ertem, M. Z.; Wang, M.; Duan, L. Efficient Iridium Catalysts for Formic Acid Dehydrogenation: Investigating the Electronic Effect on the Elementary β-Hydride Elimination and Hydrogen Formation Steps. *Inorg. Chem.* **2021**, *60* (5), 3410–3417.

(55) Tolman, C. A. Phosphorus Ligand Exchange Equilibriums on Zerovalent Nickel. Dominant Role for Steric Effects. *J. Am. Chem. Soc.* **1970**, *92* (10), 2956–2965.

(56) Anderson, S. N.; Hughes, D. L.; Richards, R. L. A Tris-Dinitrogne Complex. Preparation and Crystal Structure of Mer-[Mo(N2)3(PPrn2Ph)3]. *J. Chem. Soc., Chem. Commun.* **1984**, No. 15, 958–959.

(57) George, T. A.; Hayes, R. K.; Mohammed, M. Y.; Pickett, C. J. Reactions of Coordinated Dinitrogen. 23. Cis and Trans Isomers of Bis(Dinitrogen)Tetrakis(Dimethylphenylphosphine)Molybdenum. *Inorg. Chem.* **1989**, *28* (16), 3269–3270.

(58) Lazarowych, N. J.; Morris, R. H.; Ressner, J. M. Spectroscopic and Chemical Properties of Nitrogen-15-Enriched Molybdenum Dinitrogen Complexes Trans,Mer-Mo(N2)2(L)(PMePh2)3. *Inorg. Chem.* **1986**, *25* (22), 3926–3932.

(59) Carmona, E.; Marin, J. M.; Poveda, M. L.; Atwood, J. L.; Rogers, R. D. Preparation and Properties of Dinitrogen Trimethylphosphine Complexes of Molybdenum and Tungsten. 4. Synthesis, Chemical Properties, and x-Ray Structure of Cis-[Mo(N2)2(PMe3)4]. The Crystal and Molecular Structures of Trans-[Mo(C2H4)2(PMe3)4] and Trans,Mer-[Mo(C2H4)2(CO)(PMe3)3]. *J. Am. Chem. Soc.* **1983**, *105* (10), 3014–3022.

(60) Luck, R.; Morris, R. H.; Sawyer, J. F. Complexes [Mo(N2)(PPh3)2]2 and [Mo(CNR)(PPh3)2]2 (R = n-Butyl and Tert-Butyl) Containing Bridging .Eta.1,.Eta.6-Triphenylphosphine Ligands. The Molecular Structure of [Mo(.Mu.-.Eta.1,.Eta.6-PPh3)(PPh3)(CN(CH2)3Me)]2. *Organometallics* **1984**, *3* (7), 1009–1014.

(61) Hayes, P. G.; Piers, W. E.; Parvez, M. Cationic Organoscandium β-Diketiminato Chemistry: Arene Exchange Kinetics in Solvent Separated Ion Pairs. *J. Am. Chem. Soc.* **2003**, *125* (19), 5622–5623.

(62) Hayes, P. G.; Piers, W. E.; Lee, L. W. M.; Knight, L. K.; Parvez, M.; Elsegood, M. R. J.; Clegg, W. Dialkylscandium Complexes Supported by β-Diketiminato Ligands: Synthesis, Characterization, and Thermal Stability of a New Family of Organoscandium Complexes. *Organometallics* **2001**, *20* (12), 2533–2544.

(63) Smith, J. M.; Lachicotte, R. J.; Holland, P. L. Tuning Metal Coordination Number by Ancillary Ligandsteric Effects: Synthesis of a Three-Coordinate Iron(II)Complex. *Chem. Commun.* **2001**, No. 17, 1542–1543.

(64) Eckert, N. A.; Smith, J. M.; Lachicotte, R. J.; Holland, P. L. Low-Coordinate Iron(II) Amido Complexes of β-Diketiminates: Synthesis, Structure, and Reactivity. *Inorg. Chem.* **2004**, *43* (10), 3306–3321.

(65) Rodriguez, M. M.; Bill, E.; Brennessel, W. W.; Holland, P. L. N2 Reduction and Hydrogenation to Ammonia by a Molecular Iron-Potassium Complex. *Science* **2011**, *334* (6057), 780–783.

(66) Vela, J.; Smith, J. M.; Yu, Y.; Ketterer, N. A.; Flaschenriem, C. J.; Lachicotte, R. J.; Holland, P. L. Synthesis and Reactivity of Low-Coordinate Iron(II) Fluoride Complexes and Their Use in the Catalytic Hydrodefluorination of Fluorocarbons. *J. Am. Chem. Soc.* **2005**, *127* (21), 7857–7870.

(67) Holland, P. L.; Cundari, T. R.; Perez, L. L.; Eckert, N. A.; Lachicotte, R. J. Electronically Unsaturated Three-Coordinate Chloride and Methyl Complexes of Iron, Cobalt, and Nickel. *J. Am. Chem. Soc.* **2002**, *124* (48), 14416–14424.

(68) Wiencko, H. L.; Kogut, E.; Warren, T. H. Neutral β-Diketiminato Nickel(II) Monoalkyl Complexes. *Inorganica Chimica Acta* **2003**, *345*, 199–208.

(69) Horn, B.; Pfirrmann, S.; Limberg, C.; Herwig, C.; Braun, B.; Mebs, S.; Metzinger, R. N2 Activation in NiI–NN–NiI Units: The Influence of Alkali Metal Cations and CO Reactivity. *Zeitschrift für anorganische und allgemeine Chemie* **2011**, *637* (9), 1169–1174.

(70) Eckert, N. A.; Dinescu, A.; Cundari, T. R.; Holland, P. L. A T-Shaped Three-Coordinate Nickel(I) Carbonyl Complex and the Geometric Preferences of Three-Coordinate D9 Complexes. *Inorg. Chem.* **2005**, *44* (22), 7702–7704.

(71) Wiese, S.; Aguila, M. J. B.; Kogut, E.; Warren, T. H. β-Diketiminato Nickel Imides in Catalytic Nitrene Transfer to Isocyanides. *Organometallics* **2013**, *32* (8), 2300–2308.

(72) Jazdzewski, B. A.; Holland, P. L.; Pink, M.; Young, V. G.; Spencer, D. J. E.; Tolman, W. B. Three-Coordinate Copper(II)−Phenolate Complexes. *Inorg. Chem.* **2001**, *40* (24), 6097–6107.

(73) Spencer, D. J. E.; Reynolds, A. M.; Holland, P. L.; Jazdzewski, B. A.; Duboc-Toia, C.; Le Pape, L.; Yokota, S.; Tachi, Y.; Itoh, S.; Tolman, W. B. Copper Chemistry of β-Diketiminate Ligands: Monomer/Dimer Equilibria and a New Class of Bis(μ-Oxo)Dicopper Compounds. *Inorg. Chem.* **2002**, *41* (24), 6307–6321.

(74) Wiese, S.; Badiei, Y. M.; Gephart, R. T.; Mossin, S.; Varonka, M. S.; Melzer, M. M.; Meyer, K.; Cundari, T. R.; Warren, T. H. Catalytic C□H Amination with Unactivated Amines through Copper(II) Amides. *Angewandte Chemie International Edition* **2010**, *49* (47), 8850–8855.

(75) Hadzovic, A.; Song, D. Synthesis, Characterization, and Reactivity of a Versatile Dinuclear Palladium β-Diiminate Complex. *Organometallics* **2008**, *27* (6), 1290–1298.

(76) Hadzovic, A.; Song, D. Syntheses, Structures, and Reactivities of Novel Palladium β-Diiminato−Acetate Complexes. *Inorg. Chem.* **2008**, *47* (24), 12010–12017.

(77) Lee, L. W. M.; Piers, W. E.; Elsegood, M. R. J.; Clegg, W.; Parvez, M. Synthesis of Dialkylscandium Complexes Supported by β-Diketiminato Ligands and Activation with Tris(Pentafluorophenyl)Borane. *Organometallics* **1999**, *18* (16), 2947–2949.

(78) Basuli, F.; Bailey, B. C.; Tomaszewski, J.; Huffman, J. C.; Mindiola, D. J. A Terminal and Four-Coordinate Titanium Alkylidene Prepared by Oxidatively Induced α-Hydrogen Abstraction. *J. Am. Chem. Soc.* **2003**, *125* (20), 6052–6053.

(79) Basuli, F.; Bailey, B. C.; Watson, L. A.; Tomaszewski, J.; Huffman, J. C.; Mindiola, D. J. Four-Coordinate Titanium Alkylidene Complexes: Synthesis, Reactivity, and Kinetic Studies Involving the Terminal Neopentylidene Functionality. *Organometallics* **2005**, *24* (8), 1886–1906.

(80) Drover, M. W.; Love, J. A.; Schafer, L. L. 1,3-N,O-Complexes of Late Transition Metals. Ligands with Flexible Bonding Modes and Reaction Profiles. *Chem. Soc. Rev.* **2017**, *46* (10), 2913–2940.

(81) Gardiner, M. G.; Ho, C. C. Recent Advances in Bidentate Bis(N-Heterocyclic Carbene) Transition Metal Complexes and Their Applications in Metal-Mediated Reactions. *Coordination Chemistry Reviews* **2018**, *375*, 373–388.

(82) Guiry, P. J.; Saunders, C. P. The Development of Bidentate P,N Ligands for Asymmetric Catalysis. *Advanced Synthesis & Catalysis* **2004**, *346* (5), 497–537.

(83) Moulton, C. J.; Shaw, B. L. Transition Metal–Carbon Bonds. Part XLII. Complexes of Nickel, Palladium, Platinum, Rhodium and Iridium with the Tridentate Ligand 2,6-Bis[(Di-t-Butylphosphino)Methyl]Phenyl. *J. Chem. Soc., Dalton Trans.* **1976**, No. 11, 1020–1024.

(84) Crocker, C.; Errington, R. J.; Markham, R.; Moulton, C. J.; Shaw, B. L. Further Studies on the Interconversion of Large Ring and Cyclometallated Complexes of Rhodium, with the

Diphosphines But2P(CH2)5PBut2 and But2PCH2CHCHCH2PBut2. *J. Chem. Soc., Dalton Trans.* **1982**, No. 2, 387–395.

(85) Crocker, C.; Errington, R. J.; Markham, R.; Moulton, C. J.; Odell, K. J.; Shaw, B. L. Large-Ring and Cyclometalated Rhodium Complexes from Some Medium-Chain .Alpha.,.Omega.-Diphosphines. *J. Am. Chem. Soc.* **1980**, *102* (13), 4373–4379.

(86) Albrecht, M.; Koten, G. van. Platinum Group Organometallics Based on "Pincer" Complexes: Sensors, Switches, and Catalysts. *Angewandte Chemie International Edition* **2001**, *40* (20), 3750–3781.

(87) Morales-Morales, D. CHAPTER 9 - The Chemistry of PCP Pincer Phosphinite Transition Metal Complexes. In *The Chemistry of Pincer Compounds*; Morales-Morales, D., Jensen, C. M., Eds.; Elsevier Science B.V.: Amsterdam, 2007; pp 151–179.

(88) Choi, J.; MacArthur, A. H. R.; Brookhart, M.; Goldman, A. S. Dehydrogenation and Related Reactions Catalyzed by Iridium Pincer Complexes. *Chem. Rev.* **2011**, *111* (3), 1761–1779.

(89) Benito-Garagorri, D.; Kirchner, K. Modularly Designed Transition Metal PNP and PCP Pincer Complexes Based on Aminophosphines: Synthesis and Catalytic Applications. *Acc. Chem. Res.* **2008**, *41* (2), 201–213.

(90) van der Boom, M. E.; Milstein, D. Cyclometalated Phosphine-Based Pincer Complexes: Mechanistic Insight in Catalysis, Coordination, and Bond Activation. *Chem. Rev.* **2003**, *103* (5), 1759–1792.

(91) Polukeev, A. V.; Wendt, O. F. Iridium Complexes with Aliphatic, Non-Innocent Pincer Ligands. *Journal of Organometallic Chemistry* **2018**, *867*, 33–50.

(92) Leis, W.; Mayer, H. A.; Kaska, W. C. Cycloheptatrienyl, Alkyl and Aryl PCP-Pincer Complexes: Ligand Backbone Effects and Metal Reactivity. *Coordination Chemistry Reviews* **2008**, *252* (15), 1787–1797.

(93) Peris, E.; Crabtree, R. H. Recent Homogeneous Catalytic Applications of Chelate and Pincer N-Heterocyclic Carbenes. *Coordination Chemistry Reviews* **2004**, *248* (21), 2239–2246.

(94) Krogh-Jespersen, K.; Czerw, M.; Zhu, K.; Singh, B.; Kanzelberger, M.; Darji, N.; Achord, P. D.; Renkema, K. B.; Goldman, A. S. Combined Computational and Experimental Study of Substituent Effects on the Thermodynamics of H2, CO, Arene, and Alkane Addition to Iridium. *J. Am. Chem. Soc.* **2002**, *124* (36), 10797–10809.

(95) Kumar, A.; Bhatti, T. M.; Goldman, A. S. Dehydrogenation of Alkanes and Aliphatic Groups by Pincer-Ligated Metal Complexes. *Chemical Reviews* **2017**, *117* (19), 12357–12384.

(96) Wei, Z.; Jiao, H. Chapter Ten - Bifunctional Aliphatic PNP Pincer Catalysts for Hydrogenation: Mechanisms and Scope. In *Advances in Inorganic Chemistry*; van Eldik, R., Puchta, R., Eds.; Computational Chemistry; Academic Press, 2019; Vol. 73, pp 323–384.

(97) Zell, T.; Milstein, D. Hydrogenation and Dehydrogenation Iron Pincer Catalysts Capable of Metal–Ligand Cooperation by Aromatization/Dearomatization. *Acc. Chem. Res.* **2015**, *48* (7), 1979–1994.

(98) Gunanathan, C.; Milstein, D. Metal–Ligand Cooperation by Aromatization–Dearomatization: A New Paradigm in Bond Activation and “Green” Catalysis. *Acc. Chem. Res.* **2011**, *44* (8), 588–602.

(99) Trofimenko, Swiatoslaw. Transition Metal Poly(1-Pyrazolyl)Borates Containing Other Ligands. *J. Am. Chem. Soc.* **1967**, *89* (15), 3904–3905.

(100) Trofimenko, Swiatoslaw. Boron-Pyrazole Chemistry. IV. Carbon- and Boron-Substituted Poly[(1-Pyrazolyl) Borates]. *J. Am. Chem. Soc.* **1967**, *89* (24), 6288–6294.

(101) Trofimenko, S. Recent Advances in Poly(Pyrazolyl)Borate (Scorpionate) Chemistry. *Chem. Rev.* **1993**, *93* (3), 943–980.

(102) Reglinski, J.; Spicer, M. D. Chemistry of the P-Block Elements with Anionic Scorpionate Ligands. *Coordination Chemistry Reviews* **2015**, *297–298*, 181–207.

(103) Pettinari, C.; Santini, C. 1.10 - Polypyrazolylborate and Scorpionate Ligands. In *Comprehensive Coordination Chemistry II*; McCleverty, J. A., Meyer, T. J., Eds.; Pergamon: Oxford, 2003; pp 159–210.

(104) Parkin, G. Alkyl, Hydride, and Hydroxide Derivatives of the s- and p-Block Elements Supported by Poly(Pyrazolyl)Borato Ligation: Models for Carbonic Anhydrase, Receptors for Anions, and the Study of Controlled Crystallographic Disorder. In *Advances in Inorganic Chemistry*; Sykes, A. G., Ed.; Academic Press, 1995; Vol. 42, pp 291–393.

(105) Trofimenko, S. Scorpionates: Genesis, Milestones, Prognosis. *Polyhedron* **2004**, *23* (2), 197–203.

(106) Trofimenko, S. *Scorpionates: The Coordination Chemistry of Poly(Pyrazolyl)Borate Ligands*; Imperial College Press: London, 1999.

(107) Trofimenko, S. The Coordination Chemistry of Pyrazole-Derived Ligands. In *Progress in Inorganic Chemistry*; John Wiley & Sons, Ltd, 1986; pp 115–210.

(108) Trofimenko, S. Polypyrazolylborates, a New Class of Ligands. *Acc. Chem. Res.* **1971**, *4* (1), 17–22.

(109) McCleverty, J. A. Tilden Lecture. Alkoxy, Amido, Hydrazido, and Related Compounds of Molybdenum and Tungsten. *Chem. Soc. Rev.* **1983**, *12* (3), 331–360.

(110) Byers, P. K.; Canty, A. J.; Honeyman, R. T. Organometallic Chemistry of Palladium and Platinum with Poly(Pyrazol-1-Yl)Alkanes and Poly(Pyrazol-1-Yl)Borates. In *Advances in Organometallic Chemistry*; Stone, F. G. A., West, R., Eds.; Academic Press, 1992; Vol. 34, pp 1–65.

(111) Kitajima, N.; Tolman, W. B. Coordination Chemistry with Sterically Hindered Hydrotris(Pyrazolyl)Borate Ligands: Organometallic and Bioinorganic Perspectives. In *Progress in Inorganic Chemistry*; John Wiley & Sons, Ltd, 1995; pp 419–531.

(112) Reger, D. L. Poly (Pyrazolyl)Borate Complexes of Gallium and Indium. *Coordination Chemistry Reviews* **1996**, *147*, 571–595.

(113) Janiak, C. (Organo)Thallium (I) and (II) Chemistry: Syntheses, Structures, Properties and Applications of Subvalent Thallium Complexes with Alkyl, Cyclopentadienyl, Arene or Hydrotris(Pyrazolyl)Borate Ligands. *Coordination Chemistry Reviews* **1997**, *163*, 107–216.

(114) Christoph Janiak. HYDROTRIS(PYRAZOLYL)BORATE THALLIUM(I) [TpTI(I)] CHEMISTRY SYNTHESES AND APPLICATIONS. *Main Group Metal Chemistry* **1998**, *21* (1), 33–50.

(115) McCleverty, J. A.; Ward, M. D. The Role of Bridging Ligands in Controlling Electronic and Magnetic Properties in Polynuclear Complexes. *Acc. Chem. Res.* **1998**, *31* (12), 842–851.

(116) Ward, M. D.; McCleverty, J. A.; Jeffery, J. C. Coordination and Supramolecular Chemistry of Multinucleating Ligands Containing Two or More Pyrazolyl-Pyridine 'Arms.' *Coordination Chemistry Reviews* **2001**, *222* (1), 251–272.

(117) Calabrese, J. C.; Domaille, P. J.; Trofimenko, S.; Long, G. J. Hydrotris[3,(2'-Thienyl)Pyrazol-1-Yl]Borate: A Ligand of Remarkably Low Steric Requirements. *Inorg. Chem.* **1991**, *30* (13), 2795–2801.

(118) Rheingold, A. L.; Ostrander, R. L.; Haggerty, B. S.; Trofimenko, S. Homoscorpionate (Tris(Pyrazolyl)Borate) Ligands Containing Tethered 3-Phenyl Groups. *Inorg. Chem.* **1994**, *33* (17), 3666–3676.

(119) Rheingold, A. L.; Haggerty, B. S.; Trofimenko, S. A Novel Homoscorpionate Ligand and Its Unusual Bonding in a Molybdenum Complex. *J. Chem. Soc., Chem. Commun.* **1994**, No. 17, 1973–1974.

(120) Kitajima, N.; Fujisawa, K.; Morooka, Y. Tetrahedral Copper(II) Complexes Supported by a Hindered Pyrazolylborate. Formation of the Thiolato Complex, Which Closely Mimics the Spectroscopic Characteristics of Blue Copper Proteins. *J. Am. Chem. Soc.* **1990**, *112* (8), 3210–3212.

(121) Kitajima, N.; Fujisawa, K.; Hikichi, S.; Morooka, Y. Formation of (.Mu.-Hydroxo)(.Mu.-Azido) Dinuclear Copper Complex from .Mu.-.Eta.2:.Eta.2-Peroxo Complex. *J. Am. Chem. Soc.* **1993**, *115* (17), 7874–7875.

(122) Trofimenko, S.; Calabrese, J. C.; Kochi, J. K.; Wolowiec, S.; Hulsbergen, F. B.; Reedijk, J. Spectroscopic Analysis, Coordination Geometry, and x-Ray Structures of Nickel(II) Compounds with Sterically Demanding Tris(Pyrazolyl)Borate Ligands and Azide or (Thio)Cyanate Anions. Crystal and Molecular Structures of Bis[(.Mu.-Thiocyanato-N,S)(Hydrotris(3-Isopropyl-4-Bromopyrazol-1-Yl)Borato)Nickel(II)]-3-Heptane and (Thiocyanato-N)(Hydrotris(3-Tert-Butyl-5-Methylpyrazol-1-Yl)Borato)Nickel(II). *Inorg. Chem.* **1992**, *31* (19), 3943–3950.

(123) Skagestad, V.; Tilset, M. Thermodynamics of Heterolytic and Homolytic Metal-Hydrogen Bond Cleavage Reactions of 18-Electron and 17-Electron Group 6 Hydridotris(Pyrazolyl)Borate Metal Hydrides. *J. Am. Chem. Soc.* **1993**, *115* (12), 5077–5083.

(124) MacNeil, J. H.; Watkins, W. C.; Baird, M. C.; Preston, K. F. Synthesis and Characterization of New Chromium-Centered Radicals of the Type {.Eta.3-Tris(Pyrazolyl)Borato}Cr(CO)2L (L = CO, PMe3): EPR Spectra of Organochromium and -Molybdenum Compounds Undergoing Subtle Jahn-Teller Distortions. *Organometallics* **1992**, *11* (8), 2761–2762.

(125) Curtis, M. David.; Shiu, K. Bei.; Butler, W. M.; Huffman, J. C. Metal-Metal Multiple Bonds. Part 17. Syntheses, Structures, and Molecular Orbital Analysis of Hydridotris(Pyrazolyl)Borate (Tp) Molybdenum Carbonyls: Paramagnetic TpMo(CO)3 and Triply Bonded Tp2Mo2(CO)4 (Mo.Tplbond.Mo). *J. Am. Chem. Soc.* **1986**, *108* (12), 3335–3343.

(126) Shiu, K.-B.; Lee, L.-Y. Organotransition-Metal Complexes of Multidentate Ligands: IV. Facile Formation of a Heat- and Air-Stable, 17-Electron Radical, Tp′ Mo(CO)3, and a Sulfur-Bridged Dimer, [Tp′ Mo(CO)2]2S (Tp′ = Hydridotris(3,5-Dimethylpyrazol-1-Yl)Borate). *Journal of Organometallic Chemistry* **1988**, *348* (3), 357–360.

(127) HücKel, W.; Chneider, H. B. N-Tripyrazolyl-methan. *Berichte der deutschen chemischen Gesellschaft (A and B Series)* **1937**, *70* (9), 2024–2026.

(128) Juliá, S.; Mazo, J. M. del; Avila, L.; Elguero, J. Improved Synthesis of Polyazolylmethanes Under Solid-Liquid Phase-Transfer Catalysis. *Organic Preparations and Procedures International* **1984**, *16* (5), 299–307.

(129) Reger, D. L.; Grattan, T. C.; Brown, K. J.; Little, C. A.; Lamba, J. J. S.; Rheingold, A. L.; Sommer, R. D. Syntheses of Tris(Pyrazolyl)Methane Ligands and {[Tris(Pyrazolyl)Methane]Mn(CO)3}SO3CF3 Complexes: Comparison of Ligand Donor Properties. *Journal of Organometallic Chemistry* **2000**, *607* (1), 120–128.

(130) Trofimenko, S. Geminal Poly(1-Pyrazolyl)Alkanes and Their Coordination Chemistry. *J. Am. Chem. Soc.* **1970**, *92* (17), 5118–5126.

(131) Bigmore, H. R.; Lawrence, S. C.; Mountford, P.; Tredget, C. S. Coordination, Organometallic and Related Chemistry of Tris(Pyrazolyl)Methane Ligands. *Dalton Trans.* **2005**, No. 4, 635–651.

(132) Pullen, E. E.; Rabinovich, D.; Incarvito, C. D.; Concolino, T. E.; Rheingold, A. L. Syntheses and Structures of Methyltris(Pyrazolyl)Silane Complexes of the Group 6 Metals. *Inorg. Chem.* **2000**, *39* (7), 1561–1567.

(133) Vepachedu, S.; Stibrany, R. T.; Knapp, S.; Potenza, J. A.; Schugar, H. J. Tris(3,5-Dimethylpyrazol-1-Yl)Methylsilane. *Acta Cryst C* **1995**, *51* (3), 423–426.

(134) Pullen, E. E.; Rheingold, A. L.; Rabinovich, D. Methyltris(Pyrazolyl)Silanes: New Tripodal Nitrogen-Donor Ligands. *Inorganic Chemistry Communications* **1999**, *2* (5), 194–196.

(135) Parkin, G. Applications of Tripodal [S3] and [Se3] L2X Donor Ligands to Zinc, Cadmium and Mercury Chemistry: Organometallic and Bioinorganic Perspectives. *New J. Chem.* **2007**, *31* (12), 1996–2014.

(136) Spicer, M. D.; Reglinski, J. Soft Scorpionate Ligands Based on Imidazole-2-Thione Donors. *European Journal of Inorganic Chemistry* **2009**, *2009* (12), 1553–1574.

(137) Dodds, C. A.; Kennedy, A. R.; Reglinski, J.; Spicer, M. D. Pushing the Frontiers of Hard and Soft Scorpionate Chemistry. *Inorg. Chem.* **2004**, *43* (2), 394–395.

(138) Reglinski, J.; Spicer, M. D.; Garner, M.; Kennedy, A. R. Structural Consequences of the Use of Hard and Soft Tripodal Ligands during Metathesis Reactions: Synthesis of the [Bis(Hydrotris(Methimazolyl)Borato]Bismuth(III) [Bis(Hydrotris(Pyrazolyl)Borato]Sodiate. *J. Am. Chem. Soc.* **1999**, *121* (10), 2317–2318.

(139) Garcia, R.; Paulo, A.; Domingos, Â.; Santos, I. Rhenium(I) Organometallic Complexes with Novel Bis(Mercaptoimidazolyl)Borates and with Hydrotris(Mercaptoimidazolyl)Borate: Chemical and Structural Studies. *Journal of Organometallic Chemistry* **2001**, *632* (1), 41–48.

(140) Garcia, R.; Domingos, Â.; Paulo, A.; Santos, I.; Alberto, R. Reactivity of [Re{κ3-H(μ-H)B(TimMe)2}(CO)3] (TimMe = 2-Mercapto-1-Methylimidazolyl) toward Neutral Substrates. *Inorg. Chem.* **2002**, *41* (9), 2422–2428.

(141) Graham, L. A.; Fout, A. R.; Kuehne, K. R.; White, J. L.; Mookherji, B.; Marks, F. M.; Yap, G. P. A.; Zakharov, L. N.; Rheingold, A. L.; Rabinovich, D. Manganese(I) Poly(Mercaptoimidazolyl)Borate Complexes: Spectroscopic and Structural Characterization of Mn···H–B Interactions in Solution and in the Solid State. *Dalton Trans.* **2005**, No. 1, 171–180.

(142) Garner, M.; Lehmann, M.-A.; Reglinski, J.; Spicer, M. D. Soft (S3-Donor) Scorpionate Complexes of Molybdenum and Tungsten Carbonyls. *Organometallics* **2001**, *20* (24), 5233–5236.

(143) Foreman, M. R. St.-J.; Hill, A. F.; White, A. J. P.; Williams, D. J. Hydrotris(Methimazolyl)Borato Alkylidyne Complexes of Tungsten1. *Organometallics* **2003**, *22* (19), 3831–3840.

Chapter 2 - Ring-Opening Polymerization of ε-Caprolactone Utilizing Aluminum Alkyl Complexes Bearing Dianionic Scorpionate Ligands

2.1 Introduction

Petroleum-based polymers such as polyethylene and polypropylene have found widespread commercial use due to their chemical stability and physical durability. As such, they are produced on million tonne (Mt) scales globally every year, with over 359 Mt produced in 2018.[1,2] The desirable properties of petroleum-based plastics, however, causes problems when it comes to their disposal. Polyethylene and polypropylene polymers are not biodegradable and persist in natural environments. The most dramatic example of this is the Great Pacific Garbage Patch, which is estimated to have a surface area of 1.6 million square kilometers, or roughly twice the size of Texas.[3–6] In addition, petroleum feedstocks are rapidly depleting, making the use of petroleum-based plastics unsustainable in the long term.[7–9] The development of biodegradable polymers, therefore, is highly desirable and has received increasing attention in recent years.[10–12] Polyesters such as polylactide and polycaprolactone (PCL), which are generated through the ring-opening polymerization (ROP) of lactide and ε-caprolactone (ε-CL), respectively, are particularly promising because of their favorable degradation properties, and renewable feedstocks.[12,13]

Metal-mediated processes have been a specific area of interest for the ROP of cyclic esters as well-defined biodegradable polymers with controlled chain lengths are produced.[14,15] Aluminum-based systems are especially attractive due to the large abundance of the metal, its low cost, and its high Lewis acidity.[14,16–18] When developing catalytic systems, though, the

ancillary ligands surrounding the aluminum center play a key role in determining the reactivity and selectivity of the catalyst. Over the past several decades, aluminum complexes bearing bidentate,[19–31] tridentate,[32–37] and tetradentate[35,38,39] ligands have been explored in the literature, a selection of which are shown in Figure 2.1.[15,40–45] Notably, aluminum alkyl complexes supported by salen[46–51] or salan[52–54] ligands have seen particular success in this field. These species form five-coordinate pre-catalysts that can polymerize cyclic esters with narrow PDIs after being activated with benzyl alcohol.

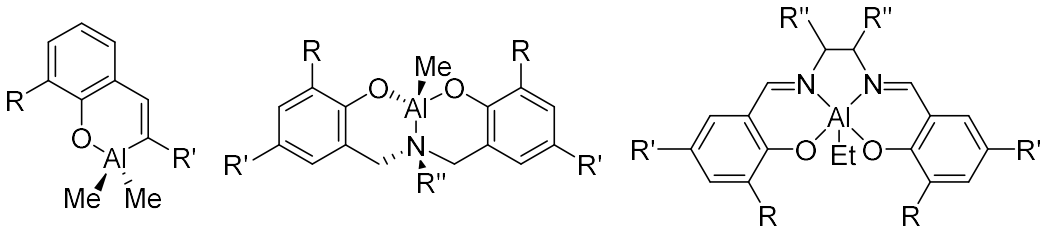

Figure 2.1: Examples of Aluminum ROP catalysts bearing bidentate (left), tridentate (middle), and tetratdenate (right) ligands.

Scorpionate ligands, on the other hand, were first developed in the late 1960s by Trofimenko, and include species like tris(pyrazolyl)borate[5,56] and tris(pyrazolyl)methane (Figure 2.2[57] The defining features of these ligands are a *fac* coordination geometry and the ability to interchange between tridentate and bidentate binding modes.[58,59] This hemilability can lead to higher reactivity levels over other tridentate ligands, such as pincer ligands, which tend to form very stable complexes.[60,61] Moreover, scorpionate ligands are extremely versatile in that their bonding strengths, electronic parameters, and steric encumbrance can be readily tuned. Since their development, complexes incorporating these types of ligands have been widely studied for medical purposes,[62] catalysis,[63] as well as other applications.[62,64,65] Surprisingly, despite their versatility, to the best of our knowledge, only a handful of scorpionate ligands have been explored on aluminum centers.[66–68] Martínez *et. al.* investigated a family of aluminum scorpionate complexes for the catalytic synthesis of cyclic carbonates from epoxides and carbon

dioxide.[66,69–71] Additionally, aluminum scorpionate complexes have been utilized by the Otero group, and others, to affect the ROP of lactide and ε-CL.[67,71–75] By increasing the steric bulk of the tridentate ligands, more control over polymerization was seen and products with narrower PDIs were generated.[74] It would therefore be of great interest to further explore this underutilized ligand class in the context of aluminum catalyzed ROP of cyclic esters .

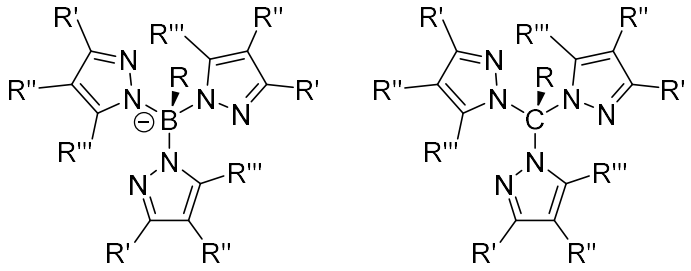

Figure 2.2 General structures for tris(pyrazolyl)borate (left) and tris(pyrazolyl)methane (right) scorpionate ligands.

Herein, the facile synthesis of dianionic scorpionate ligands with two phenolate donors and a third hemilabile "tail" is reported, as is their characterization. In addition, the first metal complexes bearing these tridentate ligands, tetrahedral aluminum alkyl compounds, are discussed and the coordination geometry of the ligands is investigated. Lastly, the catalytic activity of the aluminum species for the ROP of ε-CL is explored with respect the steric demands of the ligands, and the nature of the hemilabile "tail". With respect to nomenclature, throughout this chapter the scorpionate ligands will be named according to their neutral donor functionality (**1** for methoxy; **2** for dimethylamino; **3** for imidazolyl; **4** for N-methylimidazolyl) and the substituents *ortho* to the phenol groups (**a** for methyl; **b** for *tert*-butyl), while the aluminum complexes will be named according to the bound scorpionate ligand (**5a-b** for **1a-b**; **6a-b** for **2a-b**; **7a-b** for **3a-b**; **8a-b** for **4a-b**).

2.2 Results and Discussion

Synthesis and characterization of scorpionate ligands 1-4.

Compounds **1-4** were synthesized using a Friedel-Crafts alkylation reaction under acidic conditions.[76,77] Two equivalents of phenol (2,4-dimethylphenol for **a**, or 2-*tert*-butyl-4-methylphenol for **b**), as well as one equivalent of protected aldehyde (methoxyacetaldehyde dietheylacetal for **1**, or dimethylaminoacetaldehyde diethylacetal for **2**) or aldehyde (2-imidazolecarboxaldehyde for **3**, or 1-methyl-2-imidazolecarboxaldehyde for **4**) were combined in an acetic acid/sulfuric acid mixture to yield **1-4** as white solids in poor to moderate yields (24-50%, Scheme 2.1. For ease of isolation, the dimethylamino variants were first isolated as hydrochloride salts, **2a·HCl** and **2b·HCl**, and then neutralized with base to give the desired neutral scorpionate ligands, **2a** and **2b**.

Scheme 2.1: General synthetic procedure for scorpionate ligands 1-4.

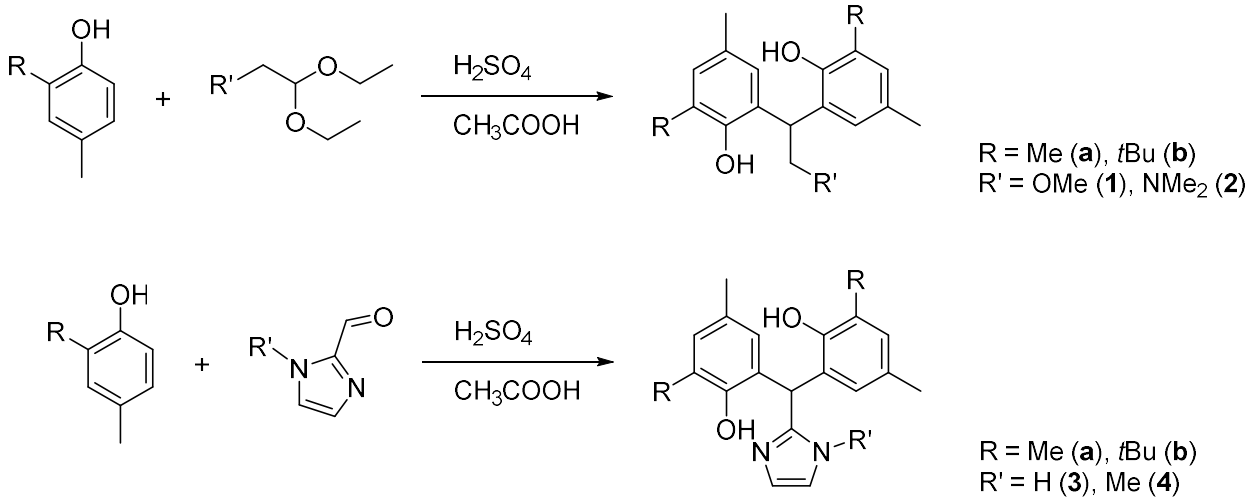

The ^{1}H NMR spectra of compounds **1-4** exhibited several diagnostic peaks that confirmed the presence of the proposed structures. All eight scorpionate ligands showed the disappearance of the hydrogen *ortho* to the phenol moiety, as well as the loss of its coupling to the adjacent *meta*-hydrogen. Moreover, the appearance of a triplet between 4.5 and 5.1 ppm (C*H*-CH$_2$) in **1a-b** and **2a-b**, as well as a doublet between 3.0 and 3.8 ppm (CH-C*H*$_2$) indicated that the methoxy and dimethylamino "tails" had been incorporated. For **3a-b** and **4a-b**, on the

other hand, the appearance of a singlet between 5.7 and 6.0 ppm (tertiary carbon) revealed that the imidazolyl and N-methylimidazolyl functionalities had been installed.

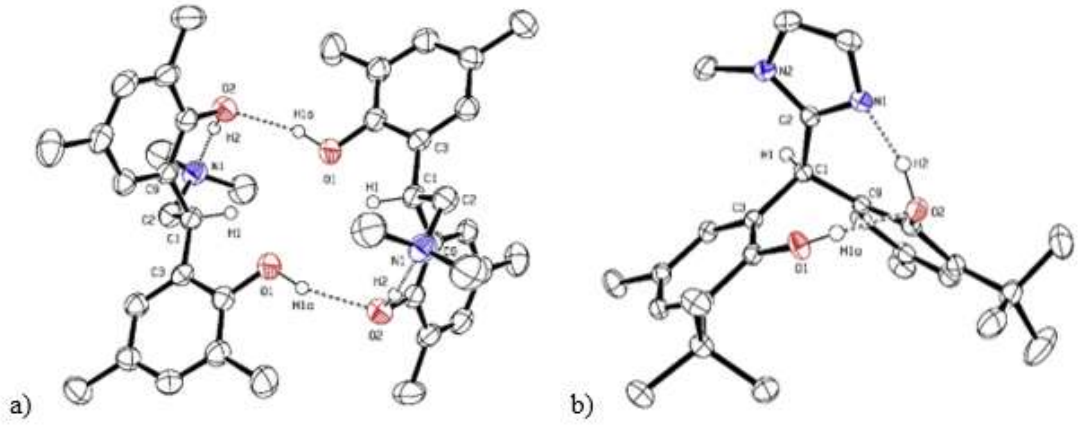

Figure 2.3: ORTEP3 representation (thermal ellipsoids at 50% probability) and atom numbering for: a) 2a, most of the hydrogens are omitted for clarity; and b) 4b, most of the hydrogens are omitted for clarity.

In addition to NMR experiments, compounds **2a** and **4b** were characterized in the solid state utilizing single crystal X-ray diffraction (Figure 2.3**Error! Reference source not found.**). In both tridentate ligands, the central tertiary carbon linking the two phenol moieties and the "tail" functionality (dimethylamino in **2a**; N-methylimidazolyl in **4b**) adopts a distorted tetrahedral geometry (for notable bond lengths and angles see Table 2.1). The C-C-C bond angles are all larger than the optimal 109.5° angle for a perfect tetrahedron, with values of 112.9(6)°, 111.0(6)°, and 111.8(6)° in **2a**, as well as 110.8(2)°, 117.8(4)°, and 114.3(4)° in **4b**, for C(3)-C(1)-C(9), C(2)-C(1)-C(9), and C(2)-C(1)-C(3), respectively. This is likely due to steric strain between the three large substituents. In order to compensate for these larger bond angles, the C-C-H bond angles are all compressed below 109.5°. Interestingly, while the largest C-C-C bond angle for the tertiary carbon in **2a**, 112.9(6)°, is between the two largest substituents (the phenol groups), in **4b** this is actually the smallest C-C-C bond angle for the tertiary carbon, 110.8(2)°. This disparity can be attributed to the difference in hydrogen bonding exhibited by the

two scorpionate species (Figure 2.3). In **2a**, both inter- and intramolecular hydrogen bonding occurs: one hydroxyl group is hydrogen bonded to the dimethylamino moiety (H(2)···N(1), 1.67 Å, intramolecular), whereas the other hydroxyl group is hydrogen bonded to the oxygen of an adjacent molecule (H(1a)···O(2), 1.94 Å, intermolecular). As such, in the solid state **2a** forms hydrogen bonded dimers where the ligand donors (O(1), O(2), and N(1)) are oriented in roughly the same direction as the tertiary carbon's C(1)-H(1) bond. For **4b**, in contrast, only intramolecular hydrogen bonding can be seen: one hydroxyl functionality is hydrogen bonded to the imdazole nitrogen (H(2)···N(1), 1.56 Å), while the other hydroxyl is hydrogen bonded to the oxygen atom of the adjacent phenol (H(1a) ···O(2), 1.82 Å). It is believed that the interaction between the two hydroxyl groups in **4b** compresses the C(3)-C(1)-C(9) bond angle, which is why it is smaller than the other C-C-C bond angles discussed above. Additionally, it is hypothesized that the *tert*-butyl groups in **4b** prevent hydrogen bonded dimers from forming. For **2a**, the methyl groups *ortho* to the phenol groups point towards each other in adjacent molecules and increased steric bulk in these positions could disrupt intermolecular hydrogen bonding.

Table 2.1: Selected bond lengths (Å) and angles (deg) for 2a and 4b.

	2a	**4b**
	Bond Lengths (Å)	
C(1)-C(2)	1.542(9)	1.513(4)
C(1)-C(3)	1.515(9)	1.542(4)
C(1)-C(9)	1.537(6)	1.541(4)
C(1)-H(1)	0.99(6)	0.99
H(1a)···O(2)	1.94	1.82
H(2)···N(1)	1.67	1.56

	Bond Angles (deg)	
C(2)-C(1)-C(3)	111.8(6)	114.3(4)
C(2)-C(1)-C(9)	111.0(6)	117.8
C(3)-C(1)-C(9)	112.9(6)	110.8
C(2)-C(1)-H(1)	108.0(4)	104.3
C(3)-C(1)-H(1)	105.8(4)	104.1
C(9)-C(1)-H(1)	106.8(3)	103.8
O(1)-(H1a)-O(2)	162.3	175.0
O(2)-H(2)-N(1)	163.4	162.8

The modular nature of the synthetic procedure outlined above (Scheme 2.1) is particularly exciting as it represents a general route for accessing a wide variety of scorpionate ligands using commercially available reagents where the steric and electronic properties of the targeted species can be readily varied. A wide range of "tail" groups were tolerated, including imidazolyl, amino, and ethereal functionalities, and it is hypothesized many other groups will be tolerated as well. As such, the donating ability of the hemi-labile donor can be easily tuned to increase or decrease binding strength. Moreover, the scope of this reaction was not limited to free aldehydes as protected aldehydes could also be utilized. A limitation of this procedure, however, is that a strong acid is needed to facilitate the Friedel-Crafts alkylation, which precludes the used of acid-sensitive functionalities.

With respect to the phenol starting materials, reagents with methyl and *tert*-butyl substituents *ortho* to the hydroxyl groups were successfully utilized. This suggested that the formation of the tridentate compounds was relatively insensitive to steric encumbrance in those positions, and that a wide variety of alkyl substituents would be tolerated. This provides a

convenient avenue for varying the bulkiness of the targeted scorpionate compounds by simply changing the nature of the phenol starting materials. It should be noted, though, that initial attempts to utilize phenols with electron rich aryl groups *ortho* to the hydroxyl moieties were unsuccessful. It is likely that the increased conjugation decreased the nucleophilicity of phenol ring, which prevented the reaction from proceeding.

Scheme 2.2: General synthetic procedure for scorpionate complexes 5-8.

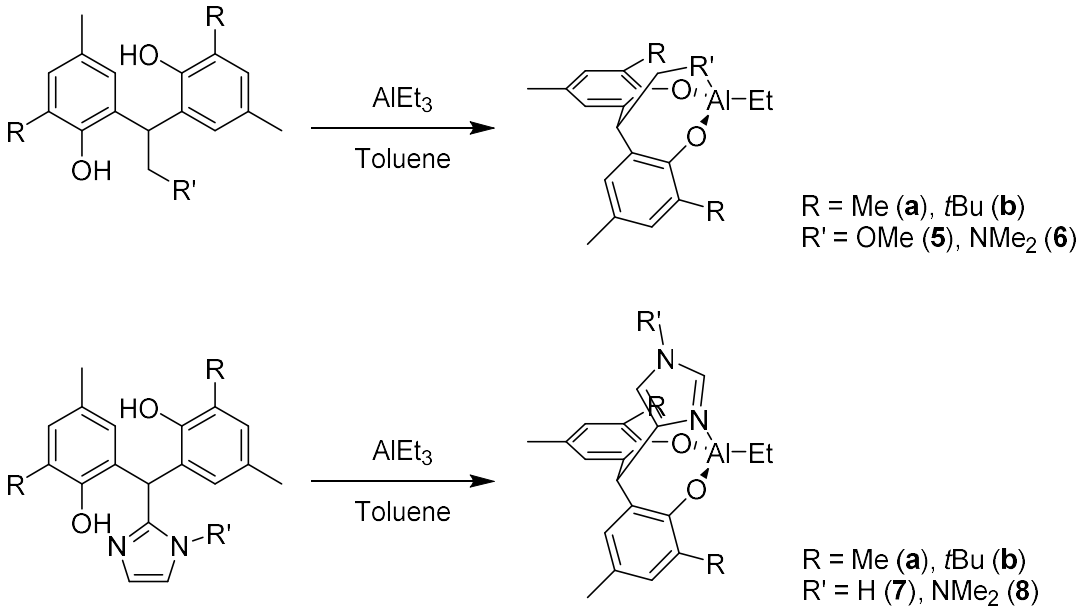

Synthesis and characterization of aluminum complexes 5-8

In order to probe the binding mode of compounds **1-4**, the scorpionate ligands were combined with triethylaluminum and the resulting complexes were characterized. The bisphenol species were cleanly deprotonated at room temperature in benzene leading to the evolution of ethane gas and the formation of four-coordinate aluminum complexes, **5-8**, which could be isolated as white solids in poor to good yields (27-83%, Scheme 2.2). The only exception was **4b**, which initially formed an asymmetric, mono-deprotonated aluminum intermediate with two ethyl groups and only one phenolate donor bound to the metal center, as determined by ^{1}H NMR spectroscopy. Heating this species at 70°C, however, yielded the desired product, **8b**.

The ^{1}H NMR spectra of compounds **5-8** (except **5a** which will be addressed separately below) all showed characteristic peaks that were shifted from the free ligand forms. Additionally, the absence of the hydroxyl signals between 10 and 11 ppm was notable, as was the presence of ethyl peaks: a triplet between 1.4 and 1.7 ppm (Al-CH_2CH_3), as well as a quartet between 0.3 and 0.8 ppm (Al-CH_2CH_3).

In addition to NMR spectroscopy, complexes **5a**, **6a-b**, **7a-b**, and **8a** were characterized in the solid state utilizing single crystal X-ray diffraction (Figure 2.4). The solvent and most to all of the hydrogens are omitted for clarity in Figure 2.4. In all six structures, the aluminum centers adopted distorted tetrahedral coordination geometries. Unlike the other five compounds, however, **5a** formed dimeric species where the ethereal "tail" of the scorpionate ligand was not bound to aluminum. Instead, a phenoxide donor bridged between two metal centers generating a diamond shaped core with bond angles of 99.78(9)° and 80.22(9)° for Al(1)-O(1)-Al(1)* and O(1)-Al(1)-O(1)*, respectively, as well as an Al(1)-Al(1)* distance of 2.819(2) Å. Additionally, the O(1)-Al(1)-O(2) angle was slightly compressed, 109.0(1)°, likely because of the bidentate binding mode of **1a**. All of the O-Al-C bond angles, in contrast, were significantly larger than the optimal 109.5° angle for a perfect tetrahedron: 112.2(2)°, 118.9(2)°, and 121.2(2)° for O(1)-Al(1)-C(1E), C(1E)-Al(1)-O(1)*, and O(2)-Al(1)-C(1E), respectively. It is hypothesized that the weaker binding ability of the methoxy group, as well as the sterically unencumbered methyl substituents *ortho* to the oxygen donors allowed this structure to form. Interestingly, the asymmetric binding mode of the bisphenolate ligand in **5a** is similar to the protonated ligand **2a** in the solid state, in that the oxygen donors, O(1), O(2), and O(3), are all oriented in roughly the same direction as the tertiary carbon's C-H bond, C(1)-H(1). As such, the C-C-H and C-C-C

bond angles for the tertiary carbon in **5a** are similar to those seen in **2a** (for notable bond lengths and angles see Table 2.2).

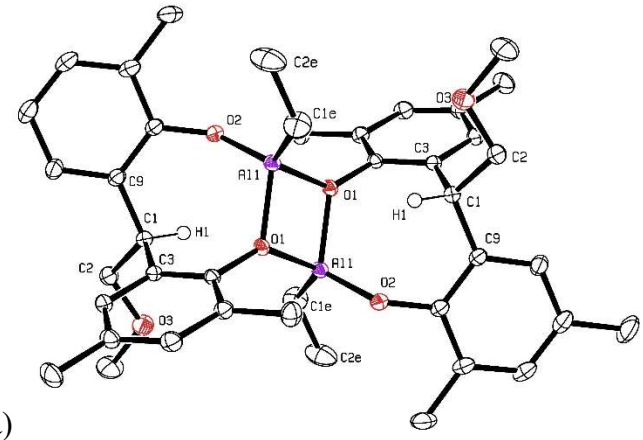

a)

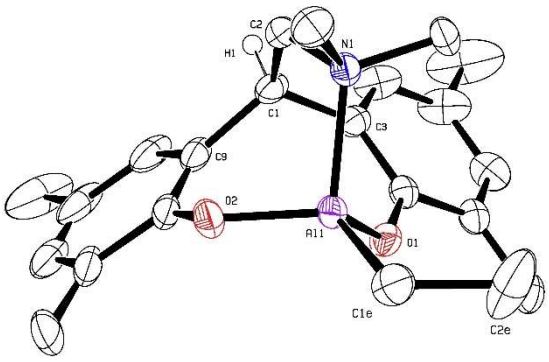

b)

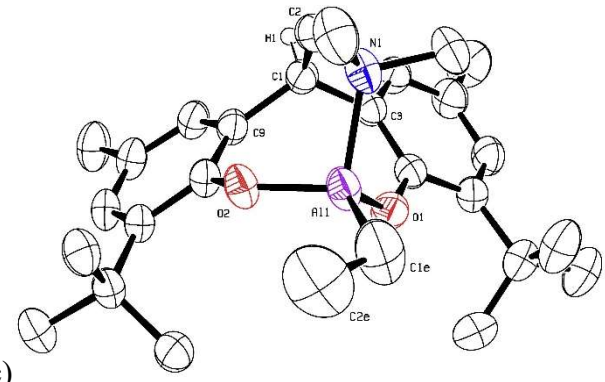

c)

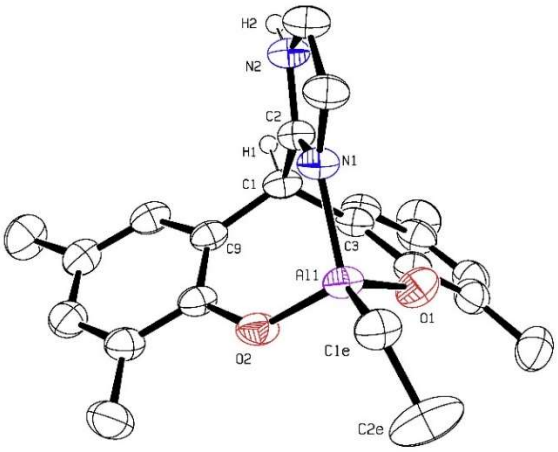

d)

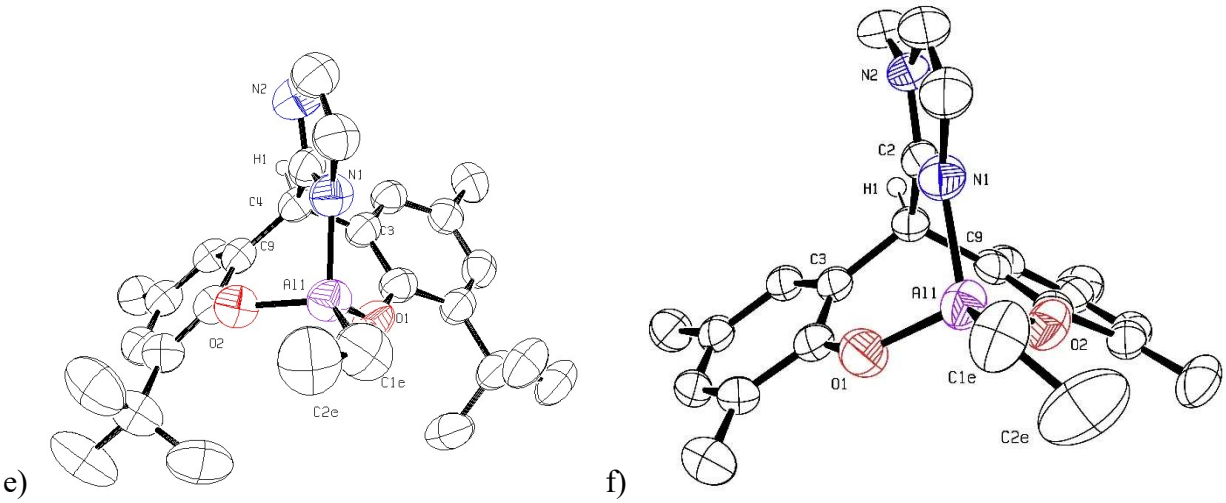

e) f)

Figure 2.4: ORTEP3 representation (thermal ellipsoids at 50% probability) and atom numbering for: a) 5a; b) 6a; c) 6b; d) 7a; and e) 7b; f) 8a.

Table 2.2: Selected bond lengths (Å) and angles (deg) for 5a.[a]

	5a
	Bond Lengths (Å)
Al(1)-Al(1)	2.819(2)
Al(1)-O(1)	1.854(2)
Al(1)-O(1)[b]	1.832(2)
Al(1)-O(2)	1.713(2)
Al(1)-C(1E)	1.941(4)
	Bond Angles (deg)
Al(1)-O(1)-Al(1)	99.78(9)°
O(1)-Al(1)-O(1)	80.22(9)°
O(1)-Al(1)-O(2)	109.0(1)°
O(1)-Al(1)-O(2)[c]	108.0(1)°
O(1)-Al(1)-C(1E)	112.2(2)°

O(1)-Al(1)-C(1E)[d]	118.9(2)°
O(2)-Al(1)-C(1E)	121.2(2)°
C(2)-C(1)-C(3)	111.0(2)
C(2)-C(1)-C(9)	112.2(2)
C(3)-C(1)-C(9)	111.7(2)
C(2)-C(1)-H(1)	107.2
C(3)-C(1)-H(1)	107.2
C(9)-C(1)-H(1)	107.2

[a] The asymmetric unit of **5a** only includes half of the dimeric species, and as such the labels for both halves of the dimer are identical.

[b] This bond length describes the Al-O bond distance to the oxygen donor from the half of the dimer not displayed in the asymmetric unit.

[c] This bond angle describes the O-Al-C bond angle with the oxygen donor from the half of the dimer not displayed in the asymmetric unit.

[d] This bond angle describes the O-Al-C bond angle with the oxygen donor from the half of the dimer not displayed in the asymmetric unit.

While **5a** is dimeric in the solid state, in solution the structure appears to be somewhat dynamic. The ^{1}H NMR spectrum showed multiple compounds in solution, with the monomeric complex as the major species. It is believed that the hemilabile "tail" is bound to the metal in this monomeric structure due to the symmetric environment of the scorpionate ligand, in contrast to the asymmetric binding mode seen in the crystal structure. Additionally, similar chemical shifts were seen for this major species and **5b**; both complexes displayed characteristic peaks that were shifted from the free ligand forms including an overlapping doublet and triplet between 3.67 and

3.72 ppm (for CH-C*H*$_2$ and C*H*-CH$_2$ in the tail functionality). The other unidentified compounds in solution are hypothesized to be dimers, trimers, and other clusters, but due to their relatively low concentrations, full characterization was not possible. It should also be noted that identical ^{1}H NMR spectra were obtained using single crystals suitable for X-ray diffraction and amorphous powders obtained through precipitation. This suggests that the various compounds in solution are in equilibrium with each other and can interconvert at room temperature. This is likely due the lability of the methoxy group, as well as the sterically unencumbered methyl substituents *ortho* to the phenolate donors. Analogous behavior was not seen for **5b**, which we attribute to the bulkiness of the *tert*-butyl groups preventing bridging of the phenolate donors.

In contrast to **5a**, the crystal structures of complexes **6a**, **6b**, **7a**, **7b**, and **8a** were all monomeric in nature, with the scorpionate ligand adopting a tridentate binding mode (Figure 2.4). The Al(1)-N(1) bond distances were 1.981(6), 1.967(4), 1.909(3), 1.92(4) and 1.909(9) Å for **6a**, **6b**, **7a, 7b** and **8a**, respectively, which followed expected trends. The stronger imidazole donors formed shorter bonds with the metal in comparison to the weaker dimethylamino donors. Within the imidazole donors, the bulkier **7b** had a longer bond due to the larger steric hinderance. When considering the coordination geometry about the aluminum center, the O(1)-Al(1)-N(1) and O(2)-Al(1)-N(1) bond angles were both significantly compressed (likely due to the tridentate binding mode of the scorpionate ligands), whereas the O(1)-Al(1)-O(2) bond angle was much more open (see Table 2.3). The only exception was **7a-b**, which had a significantly smaller O(1)-Al(1)-O(2) bond angle of 102.7(2)° and 106.3(8)° respectively. It is unclear why **7a-b** was such an outlier, but this could be due to crystal packing effects. In order to compensate for these smaller bond angles, the N(1)-Al(1)-C(1E), O(1)-Al(1)-C(1E), and O(2)-Al(1)-C(1E) bond angles were all larger than 109.5°. Notably, the coordination mode of the bisphenolate

ligands in **6a**, **6b**, **7a**, **7b**, and **8a** is somewhat similar to the protonated ligand **4b** in the solid state, in that the oxygen and nitrogen donors, O(1), O(2), and N(1), are all oriented in the opposite direction of the tertiary carbon's C-H bond, C(1)-H(1). As such, the C-C-H and C-C-C bond angles for the tertiary carbon in **6a**, **6b**, **7a**, **7b**, and **8a** are fairly similar to those seen in **4b** (for notable bond lengths and angles see Table 2.3).

Table 2.3: Selected bond lengths (Å) and angles (deg) for 6a-b, 7a-b, and 8a.

	6a	**6b**	**7a**	**7b**	**8a**
			Bond Lengths (Å)		
Al(1)-N(1)	1.981(6)	1.967(4)	1.909(3)	1.92(4)	1.909(9)
Al(1)-O(1)	1.738(6)	1.726(4)	1.734(3)	1.72(6)	1.730(6)
Al(1)-O(2)	1.735(6)	1.725(3)	1.750(3)	1.76(6)	1.732(6)
Al(1)-C(1E)	1.996(9)	1.947(4)	1.942(4)	1.92(4)	1.95(1)
			Bond Angles (deg)		
O(1)-Al(1)-N(1)	103.7(3)	102.2(2)	100.3(2)	103.1(8)	101.5(4)
O(2)-Al(1)-N(1)	98.6(3)	98.6(2)	104.5(2)	95.2(6)	99.8(6)
O(1)-Al(1)-O(2)	111.7(3)	110.4(2)	102.7(2)	106.3(8)	109.5(4)
N(1)-Al(1)-C(1E)	113.5(3)	112.8(3)	114.6(2)	116.2(8)	115.0(5)
O(1)-Al(1)-C(1E)	112.0(3)	116.7(3)	116.3(2)	116.3(3)	115.1(5)
O(2)-Al(1)-C(1E)	115.9(3)	114.1(3)	116.3(2)	116.6(4)	114.1(4)
C(2)-C(1)-C(3)	116.9(6)	116.6(4)	115.3(3)	110.1(5)	115.4(6)
C(2)-C(1)-C(9)	114.6(6)	115.5(3)	111.9(3)	119.3(1)	115.1(6)
C(3)-C(1)-C(9)	114.4(6)	114.8(3)	116.5(3)	113.4(4)	113.8(6)
C(2)-C(1)-H(1)	102.7	102.2	103.7	104.0(0)	103.4

C(3)-C(1)-H(1)	102.7	102.2	103.7	103.9(6)	103.4
C(9)-C(1)-H(1)	102.7	102.2	103.7	104.1(0)	103.5

ROP of ε-CL.

Previously, four- and five-coordinate aluminum alkyl complexes have been used to affect the polymerization of cyclic esters in the presence of a co-catalyst, usually benzyl alcohol or *iso*-propanol (BnOH or *i*PrOH). To the best of our knowledge, though, very few aluminum alkyl species are catalytically active for these types of transformations without the use of an alcohol activator.[47,78,79] With complexes **5-8** in hand, their activity for the ROP ε-CL was explored under various conditions (Scheme 2.3). According to the standards for ε-CL ROP established by Redshaw *et al.* these scorpionate complexes displayed moderate to good catalytic efficiencies.[80]

Scheme 2.3: ROP of ε-caprolactone utilizing aluminum alkyl complexes.

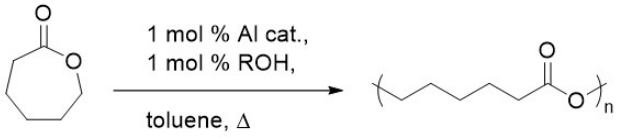

Table 2.4: ROP of ε-caprolactone using 6a.[a]

Catalyst	[Al]:[ROH]: [ε-CL]	ROH	Temp. (°C)	Conv. (%)[b]	M_n (g/mol)[c]	M_n (g/mol)[d]	M_w/M_n
6a	1:0:100	N/A	rt	1	N/A	N/A	N/A
6a	1:0:100	N/A	50	7	N/A	N/A	N/A
6a	1:0:100	N/A	110	99	N/A	109455	1.98
6a	1:1:100	EtOH	rt	35	5220	5547	1.18
6a	1:1:100	EtOH	50	97	14199	16931	1.28
6a[e]	1:1:100	EtOH	50	89	14542	16550	1.36

6a	1:1:100	*i*PrOH	rt	46	6262	7860	1.35
6a	1:1:100	*i*PrOH	50	98	11817	16038	1.35
6a[e]	1:1:100	*i*PrOH	50	99	12330	18063	1.41
6a[e]	1:10:100	*i*PrOH	50	83	1658	1863	1.51

[a] Conditions: Toluene, 1 M ε-CL, 1 hr. All entries are the average of multiple runs with a standard deviation ≤2.5%.

[b] Conversions determined by ^{1}H NMR spectroscopy following established procedures.[81,82]

[c] Molecular weights determined by ^{1}H NMR spectroscopy following established procedures.[81,82]

[d] Molecular weights determined by GPC/SEC.

[e] The alcohol was added to the aluminum species and stirred for 5 min. prior to addition of ε-CL in order to pre-activate the catalyst.

Initial catalytic studies were performed using **6a**, as the dimethylamino complex was anticipated to display intermediate activity between **5**, with weakly bound ethereal groups, and **7-8**, with strongly bound imidazole functionalities. A catalyst to substrate ratio, [Al]:[ε-CL], of 1:100 was used, and reactions were allowed to proceed for one hour. In particular, the effects of temperature and the type of alcohol activator utilized were investigated (Table 2.4). In the absence of a co-catalyst, little to no polymerization was observed at room temperature and at 50°C, as expected. However, if the temperature was increased to 110°C in toluene, near complete polymerization was observed after one hour and high molecular weight species were generated (discussed further below). It is hypothesized that the high temperatures were needed to overcome the large kinetic barrier associated with a 1,2-migratory insertion of an alkyl group

into an ester carbonyl functionality. Once this step was completed, however, a significantly more active aluminum-alkoxide intermediate was formed, which rapidly performed ROP (Figure 2.5).

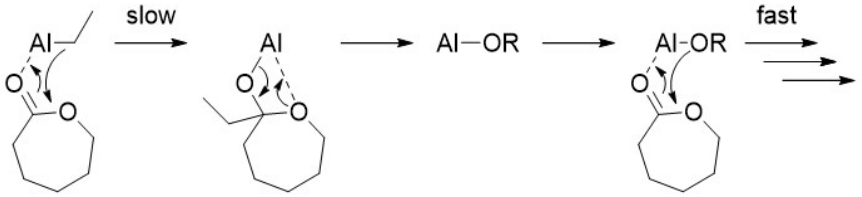

Figure 2.5: Proposed slow activation by aluminum-alkyl complexes followed by rapid ROP of ε-CL by alkoxide intermediates.

When an alcohol co-catalyst was utilized, the catalytic activity of **6a** increased greatly. This was evident from the 35 and 46 % conversions observed at room temperature when activating the alkyl species with one equivalent of EtOH or *i*PrOH, respectively. At higher temperatures of 50°C, on the other hand, the ROP reactions proceeded to completion, with 97 and 98% conversions for EtOH and *i*PrOH, respectively. Interestingly, the less sterically hindered and more acidic EtOH co-catalyst gave products with higher molecular weights than predicted for a polymer with 100 monomer subunits in comparison to *i*PrOH (theoretical M_n = 11414 g/mol). This suggested that EtOH may have caused partial decomposition of the aluminum alkyl pre-catalyst. This hypothesis was further supported when **6a** was pre-activated with alcohol prior to ε-CL addition. The lower polydispersity, though, suggests that EtOH more uniformly activated **6a** compared to *i*PrOH, likely due to the increased steric hinderance of *i*PrOH. For *i*PrOH very similar results were seen with and without pre-activation, but for EtOH, pre-activation gave increased polymer molecular weights, higher polydispersity, and lower catalytic conversions (likely due to increased amounts of pre-catalyst decomposition before substrate addition). It was also found that if more than one equivalent of *i*PrOH was utilized as a co-catalyst, the excess alcohol acted as a chain transfer agent and very short oligomers were formed with a higher polydispersity.

Once ROP conditions were optimized with **6a**, the catalytic activities of all the aluminum scorpionate complexes **5-8** were explored (Table 2.5). When no co-catalyst was used, the results seen for **5-8** were similar to those obtained with **6a**, as discussed above. In general, no polymerization was observed at room temperature or at 50°C, but once temperatures reached 110°C, nearly full conversion was achieved over a one-hour period. Moreover, all the products generated under these conditions had high molecular weights and polydispersity index between 1.63 and 2.35. There were two notable outliers to this trend, however: **5b**, which was unusually active, and **6b**, which was unusually inactive. For **5b**, 62% conversion was observed at 50°C, whereas for **6b** only 49% conversion was seen at 110°C. The reasons for these discrepancies are currently unclear, but the weak donating ability of the hemilabile "tail" in **5b** could lead to increased catalytic activity for this species. It might be expected that **5a** should also exhibit increased catalytic activity, but due to its dynamic structure in solution (forming dimers, trimers, and other clusters) it is possible that these species are inactive and slow down catalysis. In fact, even with the addition of *i*PrOH, **5a** showed lower activity than initially anticipated based on the binding strength of the ethereal "tail" (see below). **6b**, on the other hand, is the most sterically hindered complex of the scorpionate series, which could explain its poor catalytic activity under these conditions. For **5a**, **5b**, and **6b** the molecular weight was between 109,455 and 137,815 indicate only a small fraction of the catalyst was active. Interestingly, **5a** had the lowest polydispersity, suggesting that the small percentage of activated species were more uniformly activated compared to **5b** which is more sterically hindered. The steric and donating effects in catalysts **7-8** had minimal effect, although the slightly reduced molecular weights in **7a** and **8a** indicate that more of the species were active compared to their more sterically hindered

analogues of **7b** and **8b**. There was minimal change in the polydispersity in **7-8** when no co-catalyst was used.

Table 2.5: ROP of ε-caprolactone using 5-8.[a]

Catalyst	ROH	Temp. (°C)	Conv. (%)[b]	M_n (g/mol)[c]	M_n (g/mol)[d]	M_w/M_n
5a	N/A	rt	2	N/A	N/A	N/A
5a	N/A	50	2	N/A	N/A	N/A
5a	N/A	110	98	N/A	137815	1.63
5a	*i*PrOH	rt	4	N/A	N/A	N/A
5a	*i*PrOH	50	18	N/A	N/A	N/A
5a	*i*PrOH	110	99	10618	21091	1.31
5b	N/A	rt	7	N/A	N/A	N/A
5b	N/A	50	62	N/A	52048	1.40
5b	N/A	110	>99	N/A	109643	2.35
5b	*i*PrOH	rt	16	N/A	N/A	N/A
5b	*i*PrOH	50	96	9305	17733	1.11
5b	*i*PrOH	110	98	8621	14618	1.75
6a	N/A	rt	1	N/A	N/A	N/A
6a	N/A	50	7	N/A	N/A	N/A
6a	N/A	110	99	N/A	109455	1.98
6a	*i*PrOH	rt	46	6262	7860	1.35
6a	*i*PrOH	50	98	11817	16038	1.35
6a	*i*PrOH	110	94	11132	15613	1.72

6b	N/A	rt	0	N/A	N/A	N/A
6b	N/A	50	0	N/A	N/A	N/A
6b	N/A	110	49	N/A	27038	1.72
6b	*i*PrOH	rt	0	N/A	N/A	N/A
6b	*i*PrOH	50	0	N/A	N/A	N/A
6b	*i*PrOH	110	98	9115	14520	1.84
7a	N/A	rt	0	N/A	N/A	N/A
7a	N/A	50	14	N/A	N/A	N/A
7a	N/A	110	99	N/A	34386	1.86
7a	*i*PrOH	rt	0	N/A	N/A	N/A
7a	*i*PrOH	50	48	4854	6009	1.21
7a	*i*PrOH	110	96	11931	13462	1.77
7b	N/A	rt	0	N/A	N/A	N/A
7b	N/A	50	2	N/A	N/A	N/A
7b	N/A	110	98	N/A	39336	1.78
7b	*i*PrOH	rt	1	N/A	N/A	N/A
7b	*i*PrOH	50	32	3998	4522	1.30
7b	*i*PrOH	110	99	10732	15453	1.72
8a	N/A	rt	0	N/A	N/A	N/A
8a	N/A	50	2	N/A	N/A	N/A
8a	N/A	110	99	N/A	37965	1.82
8a	*i*PrOH	rt	2	N/A	N/A	N/A
8a	*i*PrOH	50	69	7669	11138	1.14

8a	*i*PrOH	110	95	10390	11891	1.73
8b	N/A	rt	0	N/A	N/A	N/A
8b	N/A	50	0	N/A	N/A	N/A
8b	N/A	110	95	N/A	43485	1.77
8b	*i*PrOH	rt	0	N/A	N/A	N/A
8b	*i*PrOH	50	1	N/A	N/A	N/A
8b	*i*PrOH	110	98	13814	15307	1.80

[a] Conditions: Toluene, [Al]:[*i*PrOH]:[ε-CL] = 1:1:100 or 1:0:100, 1 M ε-CL, 1 hr. All entries are the average of multiple runs with a standard deviation ≤2.5%

[b] Conversions determined by ^{1}H NMR spectroscopy following established procedures.[81,82]

[c] Molecular weights determined by ^{1}H NMR spectroscopy following established procedures.[81,82]

[d] Molecular weights determined by GPC/SEC.

Once again, very similar to the results obtained with **6a**, the use of *i*PrOH as a co-catalyst greatly increased the catalytic efficiency of **5-8**. Moreover, when considering the molecular weights of the products, the addition of alcohol led to clean activation of the aluminum alkyl species, and generation of polymer chains approximately 100 monomer subunits long. When considering the general trends seen for **5-8**, the less sterically hindered complexes with methyl substituents *ortho* to the phenolate donors were more active at lower temperatures when compared to the species with *tert*-butyl groups in these positions. This could be attributed to more facile binding of ε-CL by the less bulky catalysts, but more studies are needed. In addition, the aluminum complexes with more labile "tail" functionalities generally showed higher

activities at lower temperatures. This suggests that de-coordination of one of the scorpionate ligand arms is necessary to allow catalysis to proceed. A major outlier, however, was **5a**, which displayed lower catalytic conversions than expected at 50°C, given the binding strength of the ethereal "tail" and the steric bulk about the metal center. As discussed above, it is hypothesized that the multi-metallic bridging species formed in solution are responsible for these observations, but at higher temperatures the monomeric form is favored due to entropy. Furthermore, **5b** showed slightly lower polymer chain lengths than expected, which became even shorter as the temperature was increased to 110°C. This could be due to partial decomposition of pre-catalyst due to the more labile tail, which would lead to a slight excess of alcohol in solution. The excess alcohol could then act as a chain transfer agent to generate shorter polymer chains (as seen previously with **6a** when 10 equivalents of *i*PrOH was used). The increase to 110°C also caused an increase in the polydispersity for **5-8**, likely due to a slower reaction with *i*PrOH versus insertion of caprolactone into the aluminum-alkoxide bond at 110°C. The increase in polydispersity correlated to the thermal changes but does not correlate strongly to steric hinderance or donating ability of the tail. The one outlier was **5a** with a polydispersity index of 1.31 versus 1.72-1.84 for **5b** and **6-8**. It is proposed that the clusters of **5a** cleanly and more uniformly activate at 110°C than the activation of **5b** and **6-8** at 110°C.

Based on the ROP results that were obtained, we propose a catalytic mechanism involving initial formation of an aluminum-alkoxide complex, and de-coordination of the scorpionate "tail" prior to ε-CL coordination. As such, the aluminum center would alternate between 3- and 4-coordinate intermediates, as shown in Figure 2.6**Error! Reference source not found.**. It should be noted, however, that an alternative five-coordinate pathway cannot be ruled

out at this time, and further mechanistic studies are needed to differentiate between possible mechanisms.

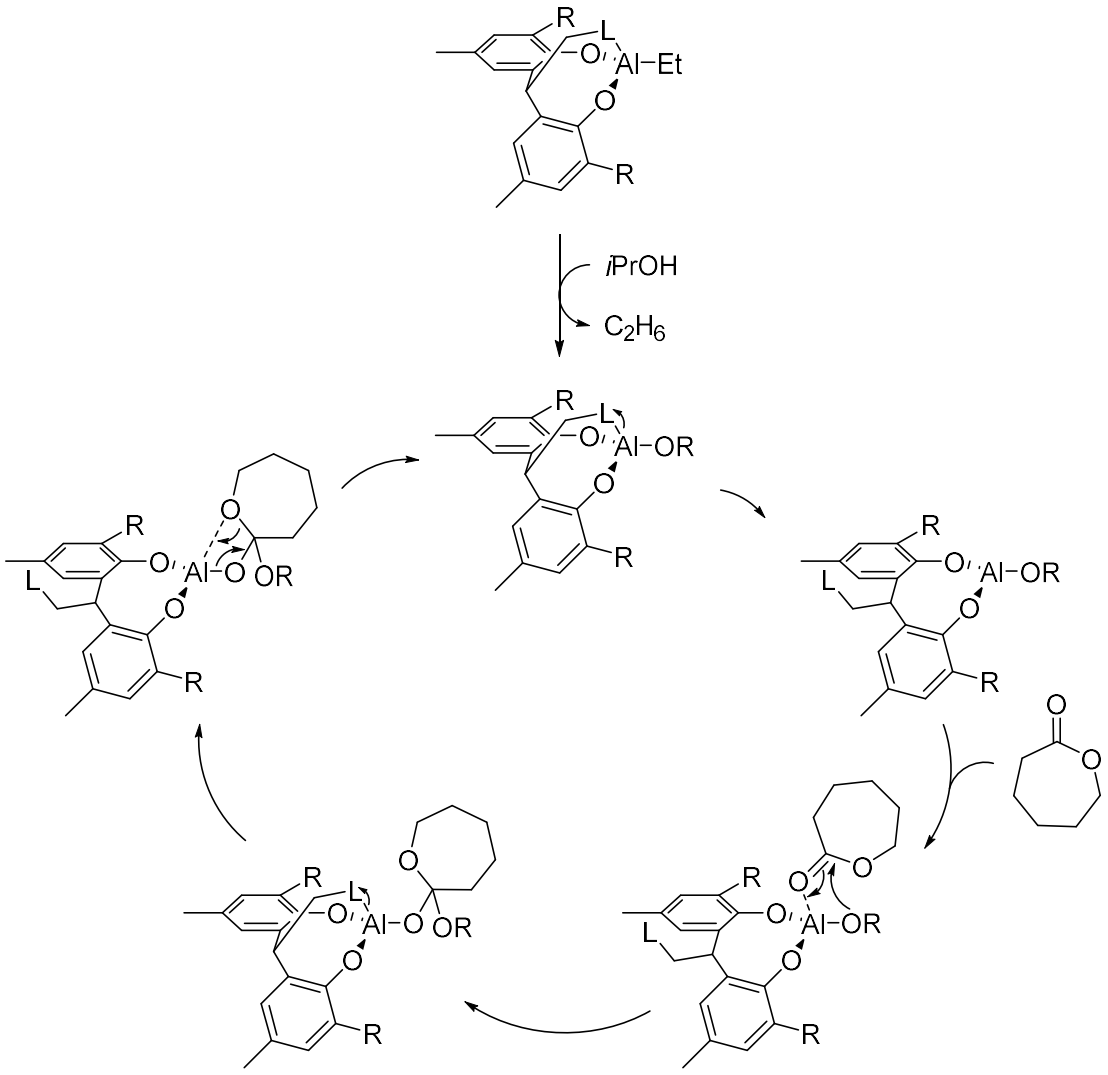

Figure 2.6: Proposed mechanism for the ROP of ε-CL using 5-8.

2.3 Conclusions

In summary, a family of scorpionate ligands **1-4** were synthesized using a modular Friedel-Crafts alkylation reaction starting with commercially available reagents. The steric and electronic properties of the targeted compounds could be readily varied, and a wide range of "tail" groups could be incorporated, including imidazolyl, amino, and ethereal functionalities.

This allowed the binding strength of the hemi-labile neutral donor to be easily tuned. In order to investigate the binding modes of these ligands, they were combined with triethylaluminum to generate tetrahedral complexes **5-8**. The variable binding strength of the scorpionate "tail" followed expected trends, with **5a** forming bridging dimers in the solid state due to the weak donating ability of the ethereal moiety, and the decreased steric bulk *ortho* to the phenolate donors. Interestingly, the tridentate ligands displayed fairly flexible binding modes, with bond angles between 98 and 112°, indicating that they should be compatible with octahedral or trigonal bipyramidal coordination geometries. In addition, the aluminum alkyl complexes were found to be active catalysts for the ROP of ε-CL, both with and without the use of an alcohol co-catalyst. Higher activities and cleaner activations were seen, however, when one equivalent of *i*PrOH was employed. Unsurprisingly, the steric size of the scorptionate ligand as well as the donating ability of the "tail" influenced the polymerization of ε-CL. Less sterically hindered complexes were able to polymerize ε-CL with more ease, as were species with more weakly bound neutral donors. It is believed that de-coordination of the scorpionate "tail" is required for polymerization, and that the aluminum center alternates between 3- and 4-coordinate intermediates during the catalytic cycle, but more studies are needed to elucidate the mechanism of ROP with these systems.

2.4 Experimental

General Considerations. All procedures and manipulations were performed under an argon or nitrogen atmosphere using standard Schlenk-line and glove box techniques unless stated otherwise. Solvents were dried and deoxygenated under argon using a LC Technology Solutions Inc. SP-1 stand-alone solvent purification system. All alcohols were dried and distilled over activated magnesium (magnesium turnings and a crystal of iodine) under a nitrogen atmosphere.

Deuterated solvents were purchased from Cambridge Isotope Laboratories, Sigma Aldrich, Acros Organics, or Alfa Aesar degassed, and dried over activated molecular sieves prior to use. All other reagents were purchased from commercial sources and utilized without further purification unless stated otherwise. NMR spectra were recorded at ambient temperature and pressure using a Bruker 400 MHz spectrometer (400 MHz for ^{1}H, and 100 MHz for ^{13}C). The ^{1}H and ^{13}C NMR spectra were measured relative to partially deuterated solvent peaks but are reported relative to tetramethylsilane (TMS). The elemental analyses were performed at the University of Rochester, Department of Chemistry, on a PerkinElmer 2400 Series II Analyzer. Single crystal X-ray data for compounds **2a** and **7b** were collected using a Bruker Proteum diffractometer equipped with dual CCD detectors (Apex II and Platinum 135) and a shared Bruker MicroStar microfocus rotating anode generator running at 45 mA and 60 kV (Cu Kα λ = 1.54178 Å for **2a** and **7b**). The data collection strategy was calculated using the Bruker APEX2 software package to ensure desired data redundancy and percent completeness. Unit cell determination, initial indexing, data collection, frame integration, Lorentz-polarization corrections and final cell parameter calculations were carried out using the Bruker APEX2 software package. An absorption correction was performed using the SADABS. Single crystal X-ray data for compounds **5a**, **6a-b**, **7a**, and **8a** were collected using a Rigaku XtaLAB Synergy-S diffractometer equipped with a HyPix-6000HE Hybrid Photon Counting (HPC) detector and dual Mo and Cu microfocus sealed X-ray source (Mo Kα λ = 0.71073 Å for **5a**; Cu Kα λ = 1.54184 Å for **6a-b**, **7a**, and **8a**). The data collection strategy was calculated using CrysAlisPro to ensure desired data redundancy and percent completeness. Unit cell determination, initial indexing, data collection, frame integration, Lorentz-polarization corrections and final cell parameter calculations were carried out using CrysAlisPro. An absorption correction was

performed using the SCALE3 ABSPACK scaling algorithm embedded within CrysAlisPro. The structures (**2a**, **5a**, **6a-b**, **7a-b**, and **8a**) were solved using ShelXT structure solution program using Intrinsic Phasing and refined by Least Squares using ShelXL program. All non-hydrogen atoms were refined anisotropically. Hydrogen atom positions were calculated geometrically and refined using the riding model. Olex2 was used for the preparation of the publication materials. The polymers were characterized by size exclusion chromatography (SEC) using anEcoSEC GPC system with an RI detector from TOSOH. The column set installed in this instrument consists of the following three columns: 2 Tosoh TSKgel SuperMultiporeHZ-M; 4.6×150 mm; 4 μm; and a TSKgel SuperMultiporeHZ-M guard. The calibration range is ≈600 to 1,000,000daltons using either PS standards. The operating flow rates are 0.35 ml/min for both the reference cell and the sample cell. Column temperature and detector temperature are set at 40 °C. Sample injection volume is 10 uL. Polymer solutions were prepared in THF to make a final concentration of about 1-1.5 mg/mL. The samples were allowed to dissolve for 1-2 hours and filtered through a 0.2 μm pore size PTFE filters into autosampler vials. Some samples were sonicated for 30sto facilitate dissolution prior to filtration. The spectra were analyzed using the EcoSEC Analysis software

Synthesis of 1a. A mixture of 0.537 g (1 equiv., 3.62 mmol) methoxyacetaldehyde diethylacetal and 0.885 g (2 equiv., 7.24 mmol) 2,4-dimethylphenol in 10 mL acetic acid was stirred for 15 minutes. The solution was then cooled to 0°C and 6.6 mL of 1:3 sulfuric acid:acetic acid was added. The reaction was allowed to stir for two days at room temperature. The reaction was then cooled to 0°C and diluted with 20 mL H_2O. The reaction was neutralized with 30 mL of 10 M NaOH, allowed to warm to room temperature, and then extracted three times using 50 mL ethyl acetate. The organic layers were combined, then washed twice with 50 mL water, dried

with Na_2SO_4, filtered, and concentrated in vacuo. The product was stirred in 30 mL hexanes, isolated by filtration, and washed with an additional 20 mL hexanes to give a white solid. Yield: 0.569 g (52.4%). **^{1}H NMR** (400 MHz, C_6D_6) δ: 6.87 (s, 2H, Aromatic-C*H*), 6.73 (s, 2H, Aromatic-C*H*), 6.14 (s, 2H, -O*H*), 4.78 (t, 1H, C*H*CH_2, J = 6.2 Hz), 3.80 (d, 2H, CHC*H*$_2$, J = 6.2 Hz), 2.85 (s, 3H, O-C*H*$_3$), 2.12 (s, 6H, Aromatic-C*H*$_3$), and 2.08 (s, 6H, Aromatic-C*H*$_3$) ppm. **^{13}C NMR** (100 MHz, C_6D_6) δ: 151.02 (Aromatic-*C*), 130.70 (Aromatic-*C*H), 129.49 (Aromatic-*C*), 126.70 (Aromatic-*C*H), 125.60 (Aromatic-*C*), 77.54 (CH*C*H_2), 58.67 (O-*C*H_3), 40.34 (*C*HCH$_2$), 20.82 (Aromatic-*C*H_3), and 16.36 (Aromatic-*C*H_3) ppm. Anal. Calcd for $C_{19}H_{24}O_3$: C, 75.97; H, 8.05; N, 0.00. Found: C, 75.56; H, 8.20; N, 0.01.

Synthesis of 1b. A mixture of 0.541 g (1 equiv., 3.65 mmol) methoxyacetaldehyde diethylacetal and 1.202 g (2 equiv., 7.32 mmol) 2-*tert*-butyl-4-methylphenol in 10 mL acetic acid was stirred for 15 minutes. The solution was then cooled to 0°C and 6.6 mL of 1:3 sulfuric acid:acetic acid was added. The reaction was allowed to stir for two days at room temperature. The reaction was then cooled to 0°C and diluted with 20 mL H_2O. The reaction was neutralized with 30 mL of 10 M NaOH, allowed to warm to room temperature, and then extracted three times using 50 mL ethyl acetate. The organic layers were combined, then washed twice with 50 mL water, dried with Na_2SO_4, filtered, and concentrated in vacuo. The residue was recrystallized from cold hexanes to give a white solid. Yield: 0.355 g (25.2%). **^{1}H NMR** (400 MHz, C_6D_6) δ: 7.12 (s, 2H, Aromatic-C*H*), 6.76 (s, 2H, Aromatic-C*H*), 6.30 (s, 2H, -O*H*), 4.55 (t, 1H, C*H*CH_2, J = 6.5 Hz), 3.65 (d, 2H, CHC*H*$_2$, J = 6.5 Hz), 2.75 (s, 3H, O-C*H*$_3$), 2.13 (s, 6H, Aromatic-C*H*$_3$), and 1.51 (s, 18H, C-(C*H*$_3$)$_3$) ppm. **^{13}C NMR** (100 MHz, C_6D_6) δ: 151.63 (Aromatic-*C*), 138.03 (Aromatic-*C*), 129.15 (Aromatic-*C*), 128.39 (Aromatic-*C*), 126.99 (Aromatic-*C*H), 125.77 (Aromatic-*C*H), 78.27 (CH*C*H_2), 58.40 (O-*C*H_3), 39.61 (*C*HCH$_2$), 34.70 (*C*-(CH$_3$)$_3$), 29.72 (C-

(CH$_3$)$_3$), and 20.82 (Aromatic-CH$_3$) ppm. Anal. Calcd for $C_{25}H_{36}O_3$: C, 78.08; H, 9.44; N, 0.00. Found: C, 78.30; H, 9.61; N, 0.02.

Synthesis 2a·HCl. A mixture of 0.594 g (1 equiv., 3.68 mmol) dimethylaminoacetaldehyde diethylacetal and 0.884 g (2 equiv., 7.24 mmol) 2,4-dimethylphenol in 10 ml acetic acid was stirred for 15 minutes. The reaction was then cooled to 0°C and 6.6 mL of 1:3 sulfuric acid:acetic acid was added. The reaction was allowed to stir for two days at room temperature. The reaction was then cooled to 0°C and was diluted with 20 mL H_2O. The reaction was neutralized with 30 mL of 10 M NaOH, allowed to warm to room temperature, and then extracted three times using 50 mL ethyl acetate. The organic layers were combined, then washed twice with 50 mL water, dried with Na_2SO_4, filtered, and concentrated in vacuo. The residue was then dissolved in 50 mL methanol and 0.5 mL 12 M HCl was added. After stirring for 15 minutes the solvent was removed in vacuo. The residue was then stirred in 75 mL ether for several hours, isolated by filtration, and washed with 20 mL ether to give a white powder. Yield: 0.582 g (45.9%). **^{1}H NMR** (400 MHz, DMSO-d$_6$) δ: 9.30 (s, 1H, -NH), 8.48 (s, 2H, -OH), 6.88 (s, 2H, Aromatic-CH), 6.81 (s, 2H, Aromatic-CH), 5.18 (t, 1H, CHCH$_2$, J = 7.4 Hz), 3.70 (d, 2H, CHCH_2, J = 7.4 Hz), 2.75 (s, 6H, N-(CH_3)$_2$), 2.16 (s, 6H, Aromatic-CH_3), and 2.15 (s, 6H, Aromatic-CH_3) ppm. **^{13}C NMR** (100 MHz, DMSO-d$_6$) δ: 150.50 (Aromatic-C), 130.41 (Aromatic-CH), 128.61 (Aromatic-C), 127.96 (Aromatic-C), 126.80 (Aromatic-CH), 125.66 (Aromatic-C), 59.79 (CHCH$_2$), 43.48 (N-(CH$_3$)$_2$), 34.03 (CHCH$_2$), 20.94 (Aromatic-CH$_3$), and 17.32 (Aromatic-CH$_3$) ppm. Anal. Calcd for [$C_{20}H_{28}ClNO_2$]0.25[H_2O]: C, 67.78; H, 8.11; N, 3.95. Found: C, 67.45; H, 8.21; N, 3.96.

Synthesis of 2b·HCl. A mixture of 0.584 g (1 equiv., 3.62 mmol) dimethylaminoacetaldehyde diethylacetal and 1.178 g (2 equiv., 7.17 mmol) 2-*tert*-butyl-4-

methylphenol in 10 mL acetic acid was stirred for 15 minutes. The solution was then cooled to 0°C and 6.6 mL of 1:3 sulfuric acid:acetic acid was added. The reaction was allowed to stir for two days at room temperature. The reaction was then cooled to 0°C and diluted with 20 mL H_2O. The reaction was neutralized with 30 mL of 10 M NaOH, allowed to warm to room temperature, and then extracted three times using 50 mL ethyl acetate. The organic layers were combined, then washed twice with 50 mL water, dried with Na_2SO_4, filtered, and concentrated in vacuo. The residue was then dissolved in 50 mL methanol and 0.5 mL 12 M HCl was added. After stirring for 15 minutes, the solvent was removed in vacuo. The residue was then dissolved using 75 mL ether and stirred for several hours causing the formation of a precipitate. The solid was isolated by filtration and washed with 20 mL ether to give a white powder. Yield: 0.622 g (39.5%). **^{1}H NMR** (400 MHz, DMSO-d_6) δ: 9.16 (s, 1H, -N*H*), 8.79 (s, 2H, -O*H*), 6.92 (s, 4H, Aromatic-C*H*), 5.40 (t, 1H, C*H*CH_2, J = 7.5 Hz), 3.80 (app. t, 2H, CHC*H*$_2$), 2.80 (d, 6H, N-(C*H*$_3$)$_2$, J = 4.8 Hz), 2.21 (s, 6H, Aromatic-C*H*$_3$), and 1.34 (s, 18H, C-(C*H*$_3$)$_3$) ppm. **^{13}C NMR** (100 MHz, DMSO-d_6) δ: 150.42 (Aromatic-*C*), 139.39 (Aromatic-*C*), 129.63 (Aromatic-*C*), 126.52 (Aromatic-*C*), 125.71 (Aromatic-*C*H), 59.58 (*C*HCH$_2$), 44.16 (N-(*C*H$_3$)$_2$), 35.00 (*C*-(CH$_3$)$_3$), 33.56 (*C*HCH$_2$), 30.28 (C-(*C*H$_3$)$_3$), and 21.42 (Aromatic-*C*H$_3$) ppm. Anal. Calcd for $C_{26}H_{40}ClNO_2$: C, 71.94; H, 9.29; N, 3.23. Found: C, 71.52; H, 9.43; N, 3.21.

Synthesis of 2a. A suspension of 0.0355 g LiOH (1 equiv., 1.48 mmol) in 5 mL DCM was added to 0.513 g MAEMP·HCl (1 equiv., 1.47 mmol) in 5 mL DCM. The solution was stirred for 2 hours then filtered through celite. The filtrate was dried using Na_2SO_4, filtered, and the solvent was removed in vacuo. The product was isolated as a white solid. Yield: 0.295 g (64.1%). Crystals suitable for X-ray diffraction studies were grown from the slow diffusion of pentane into a toluene solution of **2a** at -30°C. **^{1}H NMR** (400 MHz, D_2O) δ: 6.88 (s, 2H,

Aromatic-C*H*), 6.85 (s, 2H, Aromatic-C*H*), 5.09 (t, 1H, C*H*CH_2, *J* = 8.0 Hz), 3.69 (d, 2H, CHC*H*$_2$, *J* = 8.0 Hz), 2.82 (s, 6H, N-(C*H*$_3$)$_2$), 2.10 (s, 6H, Aromatic-C*H*$_3$), 2.09 (s, 6H, Aromatic-C*H*$_3$) ppm. **^{13}C NMR** (100 MHz, D_2O) δ: 148.77 (Aromatic-*C*), 131.28 (Aromatic-*C*), 130.68 (Aromatic-*C*H), 126.87 (Aromatic-*C*), 126.60 (Aromatic-*C*), 125.86 (Aromatic-*C*H), 60.44 (CH*C*H$_2$), 43.31 (N-(*C*H$_3$)$_2$), 33.41 (*C*HCH$_2$), 19.51 (Aromatic-*C*H$_3$), 15.63 (Aromatic-*C*H$_3$) ppm. Anal. Calcd for $C_{20}H_{27}NO_2$: C, 76.64; H, 8.68; N, 4.47. Found: C, 76.70; H, 8.95; N, 4.42.

Synthesis of 2b. A suspension of 0.0316 g LiOH (1 equiv., 1.32 mmol) in 5 mL DCM was added to 0.567 g MAETBMP·HCl (1 equiv., 1.31 mmol) in 5 mL DCM. The solution was stirred for 2 hours then filtered through celite. The filtrate was dried using Na_2SO_4, filtered, and the solvent removed in vacuo. The product was isolated as a white solid. Yield: 0.375 g (72.1%). **^{1}H NMR** (400 MHz, D_2O) δ: 9.20 (s, 2H, -O*H*), 6.84 (br s, 2H, Aromatic-C*H*), 6.46 (s, 2H, Aromatic-C*H*), 4.76 (t, 1H, C*H*CH_2, *J* = 5.7 Hz), 2.96 (d, 2H, CHC*H*$_2$, *J* = 5.6 Hz), 2.33 (s, 6H, N-(C*H*$_3$)$_2$), 2.10 (s, 6H, Aromatic-C*H*$_3$), and 1.36 (s, 18H, C-(C*H*$_3$)$_3$) ppm. **^{13}C NMR** (100 MHz, D_2O) δ: 152.47 (Aromatic-*C*), 137.94 (Aromatic-*C*), 132.34 (Aromatic-*C*), 127.31 (Aromatic-*C*H), 127.01 (Aromatic-*C*), 125.55 (Aromatic-*C*H), 67.03 (CH*C*H$_2$), 45.32 (N-(*C*H$_3$)$_2$), 38.46 (*C*HCH$_2$), 34.96 (*C*-(CH$_3$)$_3$), 30.29 (C-(*C*H$_3$)$_3$), and 21.39 (Aromatic-*C*H$_3$) ppm. Anal. Calcd for $C_{26}H_{39}NO_2$: C, 78.34; H, 10.12; N, 3.51. Found: C, 78.19; H, 10.05; N, 3.57.

Synthesis of 3a. A mixture of 0.325 g (1 equiv., 3.39 mmol) 2-imidazolecarboxaldehyde and 0.877 g (2 equiv., 7.18 mmol) 2,4-dimethylphenol in 10 mL acetic acid was stirred for 15 minutes. The solution was then cooled to 0°C and 6.6 mL of 1:3 sulfuric acid:acetic acid was added. The reaction was allowed to stir for two days at room temperature. The reaction was then cooled to 0°C and diluted with 20 mL H_2O. The reaction was neutralized with 30 mL of 10 M NaOH, allowed to warm to room temperature, and then extracted three times using 50 mL ethyl

acetate. The organic layers were combined, then washed twice with 50 mL water, dried with Na_2SO_4, filtered, and concentrated in vacuo. The resulting residue was washed through a silica gel plug using 5% ethyl acetate in hexanes. The silica gel plug was then washed with ethyl acetate to elute the product. The resulting filtrate was concentrated in vacuo to give a white solid. Yield: 0.519 g (47.5%). **^{1}H NMR** (400 MHz, DMSO-d_6) δ: 11.0 (br s, 3H, -O*H*, -N*H*), 7.00 (s, 2H, Imidazole-C*H*), 6.88 (s, 2H, Aromatic-C*H*), 6.75 (s, 2H, Aromatic-C*H*), 5.75 (s, 1H, C*H*), and 2.11 (s, 12H, Aromatic-CH_3) ppm. **^{13}C NMR** (100 MHz, DMSO-d_6) δ: 150.72 (Aromatic-*C*), 149.64 (Aromatic-*C*), 129.74 (Aromatic-*C*H), 128.24 (Aromatic-*C*H), 127.52 (Aromatic-*C*), 126.81 (Aromatic-*C*), 125.16 (Aromatic-*C*), 120.87 (Imidazole-*C*H), 42.34 (*C*H), 21.13 (Aromatic-*C*H_3), and 16.77 (Aromatic-*C*H_3) ppm. Anal. Calcd for $[C_{20}H_{22}N_2O_2]0.25[H_2O]$: C, 73.48; H, 6.94; N, 8.57. Found: C, 73.31; H, 7.01; N, 8.71.

Synthesis of 3b. A mixture of 0.329 g (1 equiv., 3.42 mmol) 2-imidazolecarboxaldehyde and 1.104 g (2 equiv., 6.72 mmol) 2-*tert*-butyl-4-methylphenol in 10 mL acetic acid was stirred for 15 minutes. The solution was then cooled to 0°C and 6.6 mL of 1:3 sulfuric acid:acetic acid was added. The reaction was allowed to stir for two days at room temperature. The reaction was then cooled to 0°C and diluted with 20 mL H_2O. The reaction was neutralized with 30 mL of 10 M NaOH, allowed to warm to room temperature, and then extracted three times using 50 mL ethyl acetate. The organic layers were combined, then washed twice with 50 mL water, dried with Na_2SO_4, filtered, and concentrated in vacuo. The resulting residue was washed through a silica gel plug using 5% ethyl acetate in hexanes. The silica gel plug was then washed with ethyl acetate to elute the product. The resulting filtrate was concentrated in vacuo to give a residue, which was dissolved in pentane, filtered, and then dried under reduced pressure to give a white solid. Yield: 0.337 g (24%). **^{1}H NMR** (400 MHz, DMSO-d_6) δ: 10.75 (s, 2H, -O*H*), 7.01 (s, 4H,

Aromatic-C*H*), 6.88 (s, 2H, Imidazole-C*H*), 5.79 (s, 1H, C*H*), 2.12 (s, 6H, Aromatic-C*H*$_3$), and 1.35 (s, 18H, C-(C*H*$_3$)$_3$) ppm. **^{13}C NMR** (100 MHz, DMSO-d$_6$) δ: 151.59 (Aromatic-*C*), 149.88 (Aromatic-*C*), 138.81 (Aromatic-*C*), 129.83(Aromatic-*C*), 129.03 (Aromatic-*C*H), 127.90 (Aromatic-*C*), 126.42 (Imidazole-*C*H), 121.34 (Aromatic-*C*H), 43.47 (*C*H), 35.02 (*C*-(CH$_3$)$_3$), 30.34 (C-(*C*H$_3$)$_3$), and 21.22 (Aromatic-*C*H$_3$) ppm. Anal. Calcd for $C_{26}H_{34}N_2O_2$: C, 76.81; H, 8.43; N, 6.89. Found: C, 76.59; H, 8.63; N, 6.76.

Synthesis of 4a. A mixture of 0.385 g (1 equiv., 3.50 mmol) 1-methyl-2-imidazolecarboxaldehyde and 0.851 g (2 equiv., 6.96 mmol) 2,4-dimethylphenol in 10 mL acetic acid was stirred for 15 minutes. The solution was then cooled to 0°C and 6.6 mL of 1:3 sulfuric acid:acetic acid was added. The reaction was allowed to stir for two days at room temperature. The reaction was then cooled to 0°C and diluted with 20 mL H_2O. The reaction was neutralized with 30 mL of 10 M NaOH, allowed to warm to room temperature, and then extracted three times using 50 mL ethyl acetate. The organic layers were combined, then washed twice with 50 mL water, dried with Na_2SO_4, filtered, and concentrated in vacuo. The resulting oil was dissolved in 20 mL 5% ethyl acetate in hexanes and stirred causing the formation of a precipitate. The resulting suspension was filtered and washed with minimal hexanes to yield the product as a white solid. Yield: 0.438 g (37.4%). **^{1}H NMR** (400 MHz, DMSO-d$_6$) δ: 10.00 (s, 2H, -O*H*), 7.11 (s, 1H, Imidazole-C*H*), 6.87 (s, 1H, Imidazole-C*H*), 6.84 (s, 2H, Aromatic-C*H*), 6.76 (s, 2H, Aromatic-C*H*), 5.79 (s, 1H, C*H*), 3.63 (s, 3H, N-C*H*$_3$), 2.11 (s, 6H, Aromatic-C*H*$_3$), and 2.10 (s, 6H, Aromatic-C*H*$_3$) ppm. **^{13}C NMR** (100 MHz, DMSO-d$_6$) δ: 151.18 (Aromatic-C), 150.09 (Aromatic-C), 130.34 (Aromatic-*C*H), 128.71 (Aromatic-*C*H), 127.47 (Aromatic-*C*), 125.67 (Aromatic-*C*), 125.00 (Imidazole-*C*H), 121.70 (Imidazole-*C*H), 33.01 (N-*C*H$_3$), 20.82

(Aromatic-*C*CH_3), and 17.21 (Aromatic-*C*CH_3) ppm. Anal. Calcd for [$C_{21}H_{24}N_2O_2$]0.25[H_2O]: C, 73.98; H, 7.24; N, 8.22. Found: C, 74.23; H, 7.19; N, 8.19.

Synthesis of 4b. A mixture of 0.395 g (1 equiv., 3.6 mmol) 1-methyl-2-imidazolecarboxaldehyde and 1.193 g (2 equiv., 7.3 mmol) 2-*tert*-butyl-4-methylphenol in 10 mL acetic acid was stirred for 15 minutes. The solution was then cooled to 0°C and 6.6 mL of 1:3 sulfuric acid:acetic acid was added. The reaction was allowed to stir for two days at room temperature. The reaction was then cooled to 0°C and diluted with 20 mL H_2O. The reaction was neutralized with 30 mL of 10 M NaOH, allowed to warm to room temperature, and then extracted three times using 50 mL ethyl acetate. The organic layers were combined, then washed twice with 50 mL water, dried with Na_2SO_4, filtered, and concentrated in vacuo. The resulting oil was dissolved in 20 mL 5% ethyl acetate in hexanes and stirred. The resulting solution was filtered to yield the solid product as a white powder. Yield: 0.627 g (49%). Crystals suitable for X-ray diffraction studies were grown from a toluene solution of **4b** cooled to -30°C. **^{1}H NMR** (400 MHz, C_6D_6) δ: 10.07 (s, 2H, -O*H*), 7.10 (s, 2H, Aromatic-C*H*), 6.91 (s, 2H, Aromatic-C*H*), 6.72 (s, 1H, Imidazole-C*H*), 5.94 (s, 1H, Imidazole-C*H*), 5.11 (s, 1H, C*H*), 2.54 (s, 3H, N-CH_3), 2.15 (s, 6H, Aromatic-CH_3), and 1.50 (s, 18 H, C-(CH_3)$_3$) ppm. **^{13}C NMR** (100 MHz, C_6D_6) δ: 152.32 (Aromatic-C), 149.00 (Aromatic-C), 139.84 (Aromatic-C), 128.74 (Aromatic-*C*H), 128.64 (Aromatic-*C*H), 124.92(Imidazole-*C*H), 120.59 (Imidazole-*C*H), 47.32 (*C*H), 34.86 (*C*-(CH$_3$)$_3$), 31.84 (N-*C*H_3), 29.80 (C-(*C*H_3)$_3$), and 20.72 (Aromatic-*C*H_3) ppm. Anal. Calcd for $C_{27}H_{36}N_2O_2$: C, 77.10; H, 8.62; N, 6.66. Found: C, 76.78; H, 8.74; N, 6.65.

Synthesis of 5a. To a solution of 90.3 mg **1a** (1 equiv., 0.300 mmol) in 6 mL benzene, 0.30 mL 1.0 M Al(Et)$_3$ in hexanes (1 equiv., 0.30 mmol) was added and stirred 10 minutes. The solvent was then removed in vacuo and the resulting residue was stirred in 5 mL pentane for an

hour. The product was then isolated as a white solid by filtration and washed with minimal pentane to give a white powder. Yield: 55.2 mg, (52.0%). Crystals suitable for X-ray diffraction studies were grown from the slow evaporation of a benzene solution of **5a** at room temperature. **^{1}H NMR** (400 MHz, C_6D_6) δ: 6.87 (s, 2H, Aromatic-C*H*), 6.77 (s, 2H, Aromatic-C*H*), 3.71-3.67 (m, 3H, C*H*CH_2, CHC*H*$_2$), 2.46 (s, 3H, O-C*H*$_3$), 2.38 (s, 6H, Aromatic-C*H*$_3$), 2.18 (s, 6H, Aromatic-C*H*$_3$), 1.43 (t, 3H, Al-CH_2C*H*$_3$, *J* = 8.2 Hz), and 0.30 (q, 2H, Al-C*H*$_2$$CH_3$, *J* = 8.2 Hz) ppm. **^{13}C NMR** (100 MHz, C_6D_6) δ: 154.67 (Aromatic-*C*), 131.26 (Aromatic-*C*H), 129.67 (Aromatic-*C*H), 129.05 (Aromatic-*C*), 128.59 (Aromatic-*C*), 126.98 (Aromatic-*C*), 83.61 (CH*C*H_2), 60.80 (O-*C*H_3), 51.71 (*C*HCH_2), 20.64 (Aromatic-*C*H_3), 17.38 (Aromatic-*C*H_3), 8.81 (Al-CH_2*C*H_3), and -4.96 (Al-*C*H_2CH_3) ppm. Anal. Calcd for $AlC_{21}H_{27}O_3$: C, 71.17; H, 7.68; N, 0.00. Found: C, 70.81; H, 7.94; N, -0.19.

Synthesis of 5b. To a solution of 113.2 mg **1b** (1 equiv., 0.30 mmol) in 6 mL benzene, 0.30 mL 1.0 M $Al(Et)_3$ in hexanes (1 equiv., 0.30 mmol) was added and stirred overnight. The solvent was then removed in vacuo and the resulting residue was stirred in 5 mL pentane for an hour. The product was then isolated as a white solid by filtration and washed with minimal pentane. Yield: 107 mg, (82.3%). **^{1}H NMR** (400 MHz, C_6D_6) δ: 7.13 (s, 2H, Aromatic-C*H*), 6.78 (s, 2H, Aromatic-C*H*), 3.72-3.69 (m, 3H, C*H*CH_2, CHC*H*$_2$), 2.51 (s, 3H, O-C*H*$_3$), 2.19 (s, 6H, Aromatic-C*H*$_3$), 1.60 (s, 18H, C-(C*H*$_3$)$_3$), 1.51 (t, 3H, Al-CH_2C*H*$_3$, *J* = 8.2 Hz), and 0.35 (q, 2H, Al-C*H*$_2$$CH_3$, *J* = 8.2 Hz) ppm. **^{13}C NMR** (100 MHz, C_6D_6) δ: 155.23 (Aromatic-*C*), 139.65 (Aromatic-*C*), 130.18 (Aromatic-*C*), 130.01 (Aromatic-*C*H), 127.45 (Aromatic-*C*), 126.79 (Aromatic-*C*H), 83.41 (CH*C*H_2), 60.77 (O-*C*H_3), 52.27 (*C*HCH_2), 35.33 (*C*-(CH_3)$_3$), 30.15 (C-(*C*H_3)$_3$), 20.99 (Aromatic-*C*H_3), 8.73 (Al-CH_2*C*H_3), and -4.69 (Al-*C*H_2CH_3) ppm. Anal. Calcd for $AlC_{27}H_{39}O_3$: C, 73.94; H, 8.96; N, 0.00. Found: C, 73.70; H, 9.12; N, -0.17.

Synthesis of 6a. To a solution of 95.0 mg **2a** (1 equiv., 0.30 mmol) in 6 mL benzene, 0.30 mL 1.0 M $Al(Et)_3$ in hexanes (1 equiv., 0.30 mmol) was added and stirred overnight. The solvent was then removed in vacuo and the resulting residue was stirred in 5 mL pentane for an hour. The product was then isolated as a white solid by filtration and washed with minimal pentane. Yield: 92.9 mg, (83.3%). Crystals suitable for X-ray diffraction studies were grown from a toluene solution of **6a** cooled to -30°C. **^{1}H NMR** (400 MHz, C_6D_6) δ: 6.84 (s, 2H, Aromatic-C*H*), 6.78 (s, 2H, Aromatic-C*H*), 3.71 (t, 1H, C*H*CH_2, J = 3.9 Hz), 2.66 (d, 2H, CHC*H*$_2$, J = 3.9 Hz), 2.37 (s, 6H, Aromatic-C*H*$_3$) 2.17 (s, 6H, Aromatic-C*H*$_3$), 1.68 (s, 6H, N-(C*H*$_3$)$_2$), 1.49 (t, 3H, Al-CH_2C*H*$_3$, J = 8.2 Hz), and 0.28 (q, 2H, Al-C*H*$_2$$CH_3$, J = 8.2 Hz) ppm. **^{13}C NMR** (100 MHz, C_6D_6) δ: 154.80 (Aromatic-*C*), 130.98 (Aromatic-*C*H), 129.62 (Aromatic-*C*) 129.52 (Aromatic-*C*H), 128.78 (Aromatic-*C*), 126.90 (Aromatic-*C*), 66.40 (CH*C*H_2), 50.55 (*C*HCH_2), 46.35 (N-(*C*H$_3$)$_2$), 20.68 (Aromatic-*C*H_3), 17.32 (Aromatic-*C*H_3), 9.44 (Al-CH_2*C*H_3), and -4.63 (Al-*C*H_2CH_3) ppm.

Synthesis of 6b. To a solution of 236 mg **2b** (1 equiv., 0.595 mmol) in 12 mL benzene, 0.60 mL 1.0 M $Al(Et)_3$ in hexanes (1 equiv., 0.60 mmol) was added and stirred overnight. The solvent was then removed in vacuo and the product was dissolved in 1 mL pentane. Upon cooling to -30°C a precipitate formed, which was isolated by filtration and washed with 1 mL cold pentane to give a white powder. Yield: 72.5 mg, (27.1%). Crystals suitable for X-ray diffraction studies were grown from a pentane solution of **6b** cooled to -30°C. **^{1}H NMR** (400 MHz, C_6D_6) δ: 7.11 (s, 2H, Aromatic-C*H*), 6.80 (s, 2H, Aromatic-C*H*), 3.72 (t, 1H, C*H*CH_2, J = 3.9 Hz), 2.60 (d, 2H, CHC*H*$_2$, J = 3.9 Hz), 2.19 (s, 6H, Aromatic-C*H*$_3$), 1.68 (s, 6H, N-(C*H*$_3$)$_2$), 1.59 (s, 18H, C(C*H*$_3$)$_3$) 1.54 (t, 3H, Al-CH_2C*H*$_3$, J = 8.2 Hz), and 0.29 (q, 2H, Al-C*H*$_2$$CH_3$, J = 8.2 Hz) ppm. **^{13}C NMR** (100 MHz, C_6D_6) δ: 155.33 (Aromatic-*C*), 139.32 (Aromatic-*C*), 131.19

(Aromatic-*C*), 130.11 (Aromatic-*C*H), 127.13 (Aromatic-*C*), 126.67 (Aromatic-*C*H), 66.20 (*C*HCH$_2$), 51.16 (CH*C*H$_2$), 46.20 (N-(*C*H$_3$)$_2$), 35.30 (*C*-(CH$_3$)$_3$), 30.03 (C-(*C*H$_3$)$_3$), 21.02 (Aromatic-*C*H$_3$), 9.27 (Al-CH$_2$*C*H$_3$), and -4.52 (Al-*C*H$_2$CH$_3$) ppm.

Synthesis of 7a. To a solution of 96.8 mg **3a** (1 equiv., 0.30 mmol) in 6 mL benzene, 0.30 mL 1.0 M Al(Et)$_3$ in hexanes (1 equiv., 0.30 mmol) was added and stirred overnight. The solvent was then removed in vacuo and the resulting residue was stirred in 5 mL pentane for an hour. The product was then isolated as a white solid by filtration and washed with minimal pentane. Yield: 59.3 mg, (52.5%). Crystals suitable for X-ray diffraction studies were grown from a toluene solution of **7a** cooled to -30°C. **^{1}H NMR** (400 MHz, C$_6$D$_6$) δ: 7.99 (s, 1H, -N*H*), 6.83 (s, 2H, Aromatic-C*H*), 6.81 (s, 2H, Aromatic-C*H*), 6.20 (s, 1H, Imidazole-C*H*), 5.65 (s, 1H, Imidazole-C*H*), 4.45 (s, 1H, C*H*), 2.32 (s, 6H, Aromatic-C*H$_3$*), 2.21 (s, 6H, Aromatic-C*H$_3$*), 1.64 (t, 3H, Al-CH$_2$C*H$_3$*, *J* = 8.2 Hz), and 0.77 (q, 2H, Al-C*H$_2$*CH$_3$, *J* = 8.2 Hz) ppm. **^{13}C NMR** (100 MHz, C$_6$D$_6$) δ: 154.69 (Aromatic-*C*), 149.17 (Aromatic-*C*), 131.48 (Aromatic-*C*H), 130.22 (Aromatic-*C*), 129.22 (Aromatic-*C*H), 126.14 (Aromatic-*C*), 125.64 (Aromatic-*C*), 122.86 (Imidazole-*C*H), 115.39 (Imidazole-*C*H), 51.77 (*C*H), 20.24 (Aromatic-*C*H$_3$), 17.15 (Aromatic-*C*H$_3$), 8.98 (Al-CH$_2$*C*H$_3$), and -4.65 (Al-*C*H$_2$CH$_3$) ppm.

Synthesis of 7b. To a solution of 119 mg **3b** (1 equiv., 0.29 mmol) in 6 mL benzene, 0.30 mL 1.0 M Al(Et)$_3$ in hexanes (1 equiv., 0.30 mmol) was added and stirred overnight. The solvent was then removed in vacuo and the resulting residue was stirred in 5 mL pentane for an hour. The product was then isolated as a white solid by filtration and washed with minimal pentane. Yield: 80.2 mg, (59.2%). Crystals suitable for X-ray diffraction studies were grown from the slow diffusion of pentane into a toluene solution of **7b** at -30°C. **^{1}H NMR** (400 MHz, C$_6$D$_6$) δ: 7.81 (s, 1H, -N*H*), 7.15 (s, 2H, Aromatic-C*H*), 6.89 (s, 2H, Aromatic-C*H*), 6.21 (s, 1H,

Imidazole-C*H*), 5.67 (s, 1H, Imidazole-C*H*), 4.56 (s, 1H, C*H*), 2.25 (s, 6H, Aromatic-CH_3) 1.71 (t, 3H, Al-CH_2CH_3, J = 8.2 Hz), 1.57 (s, 18H, C-$(CH_3)_3$), and 0.72 (q, 2H, Al-CH_2CH_3, J = 8.2 Hz) ppm. **^{13}C NMR** (100 MHz, C_6D_6) δ: 155.81 (Aromatic-*C*), 149.65 (Aromatic-*C*), 141.13 (Aromatic-*C*), 130.11 (Aromatic-*C*H), 128.59 (Aromatic-*C*), 127.63 (Aromatic-*C*H), 126.45 (Aromatic-*C*), 123.17 (Imidazole-*C*H), 115.78 (Imidazole-*C*H), 52.56 (*C*H), 35.53 (*C*-$(CH_3)_3$), 30.06 (C-(*C*$H_3)_3$), 20.96 (Aromatic-*C*H_3), 9.40 (Al-CH_2*C*H_3), and -4.22 (Al-*C*H_2CH_3) ppm. Anal. Calcd for $[AlC_{28}H_{37}N_2O_2]0.2[C_5H_{12}]$ C, 73.33; H, 8.36; N, 5.90. Found: C, 72.92; H, 8.32; N, 5.57.

Synthesis of 8a. To a solution of 102 mg **4a** (1 equiv., 0.30 mmol) in 6 mL benzene, 0.30 mL 1.0 M $Al(Et)_3$ in hexanes (1 equiv., 0.30 mmol) was added and stirred overnight. The solvent was then removed in vacuo and the resulting residue was stirred in 5 mL pentane for an hour. The product was then isolated as a white solid by filtration and washed with minimal pentane. Yield: 76.2 mg, (65%). Crystals suitable for X-ray diffraction studies were grown from the slow diffusion of pentane into a toluene solution of **8a** at -30°C. **^{1}H NMR** (400 MHz, C_6D_6) δ: 6.88 (s, 2H, Aromatic-C*H*), 6.85 (s, 2H, Aromatic-C*H*), 6.33 (s, 1H, Imidazole-C*H*), 5.38 (s, 1H, Imidazole-C*H*), 4.79 (s, 1H, C*H*), 2.39 (s, 6H, Aromatic-C*H*$_3$), 2.24 (s, 3H, N-C*H*$_3$), 2.21 (s, 6H, Aromatic-C*H*$_3$), 1.71 (t, 3H, Al-CH_2C*H*$_3$, J = 8.2 Hz), and 0.75 (q, 2H, Al-C*H*$_2$$CH_3$, J = 8.2 Hz) ppm. **^{13}C NMR** (100 MHz, C_6D_6) δ: 155.67 (Aromatic-*C*), 149.40 (Aromatic-*C*), 131.93 (Aromatic-*C*), 130.74 (Aromatic-*C*H), 129.72 (Aromatic-*C*H), 126.10 (Aromatic-*C*), 125.29 (Aromatic-*C*), 121.58 (Imidazole-*C*H), 120.96 (Imidazole-*C*H), 49.95 (*C*H), 32.38 (N-*C*H_3), 20.64 (Aromatic-*C*H_3), 17.96 (Aromatic-*C*H_3), 9.50 (Al-CH_2*C*H_3), and -4.28 (Al-*C*H_2CH_3) ppm.

Synthesis of 8b. To a solution of 128 mg **4b** (1 equiv., 0.30 mmol) in 6 mL benzene, 0.30 mL 1.0 M $Al(Et)_3$ in hexanes (1 equiv., 0.30 mmol) was added and stirred overnight at 70°C.

The solvent was then removed in vacuo and the resulting residue was stirred in 5 mL pentane for an hour. The product was then isolated as a white solid by filtration and washed with minimal pentane. Yield: 84.1 mg, (59%). **^{1}H NMR** (400 MHz, C_6D_6) δ: 6.89 (s, 2H, Aromatic-C*H*), 6.33 (s, 2H, Imidazole-C*H*), 5.31 (s, 1H, Imidazole-C*H*), 4.82 (s, 1H, C*H*), 2.25 (s, 6H, Aromatic-C*H*$_3$), 2.18 (s, 3H, N-C*H*$_3$), 1.79 (t, 3H, Al-CH$_2$C*H*$_3$, J = 8.2 Hz), 1.64 (s, 18H, C(C*H*$_3$)$_3$), and 0.80 (q, 2H, Al-C*H*$_2$CH$_3$, J = 8.2 Hz) ppm. **^{13}C NMR** (100 MHz, C_6D_6) δ: 156.44 (Aromatic-*C*), 149.36 (Aromatic-*C*), 141.06 (Aromatic-*C*), 130.21 (Aromatic-*C*H), 128.59 (Aromatic-*C*), 127.08 (Aromatic-*C*), 125.89 (Aromatic-*C*), 121.22 (Imidazole-*C*H), 121.09 (Imidazole-*C*H), 50.31 (*C*H), 35.58 (*C*-(CH$_3$)$_3$)), 32.34 (N-*C*H$_3$), 30.05 (C-(*C*H$_3$)$_3$), 21.00 (Aromatic-*C*H$_3$), 9.53 (Al-CH$_2$*C*H$_3$), and -4.36 (Al-*C*H$_2$CH$_3$) ppm.

General procedure for ROP of ε-CL. Stock solutions of aluminum catalyst (0.0133 M), *i*PrOH (0.08 M), and ε-CL (8 M) in toluene were prepared. 0.75 mL of the aluminum stock solution was added to a Schlenk flask and cycled onto a Schlenk-line. The solution was heated for 5 minutes at the desired temperature. 0.125 mL of the *i*PrOH stock solution and 0.125 mL of the ε-CL stock solution were then added. The reaction was allowed to stir at the desired temperature for 1 hour, and then quenched with 0.35 mL of a 3% acetic acid in ether solution. The solvent was removed in vacuo and the solid was analyzed using ^{1}H NMR spectroscopy. The solid was then washed with hexanes and dried for GPC-SEC analysis. The final concentrations in the catalytic mixture were 0.01 M catalyst, 0.01 M *i*PrOH, and 1 M ε-CL.

2.4 Selected Crystal Data, Data Collection, and Refinement Parameters

Table 2.6: Compounds 2a, 4b, 5a, and 6a.

	2a	**4b**	**5a·(C_6H_6)**	**6a·0.5(C_7H_8)**
empirical formula	$C_{20}H_{27}NO_2$	$C_{27}H_{36}N_2O_2$	$C_{27}H_{33}AlO_3$	$C_{22.5}H_{34}AlNO_2$

FW	313.42	420.58	432.51	413.51
lattice type	triclinic	triclinic	triclinic	orthorhombic
space group	P-1	P-1	P-1	$P2_12_12_1$
T, K	200	150(1)	100(1)	100(1)
a, Å	8.856(1)	8.5063(4)	9.3659(6)	14.1132(6)
b, Å	10.263(2)	9.4462(4)	11.3066(6)	17.5444(6)
c, Å	11.695(2)	15.3065(9)	12.7160(9)	18.9129(6)
α, deg	106.43(1)	90.368(4)	114.544(6)	90
β, deg	106.39(1)	105.880(4)	94.983(6)	90
γ, deg	106.89(1)	92.076(4)	94.895(6)	90
V, $Å^3$	895.4(2)	1182.02(9)	1209.3(2)	4683.0(3)
Z	2	2	2	8
ρ_{calc}/Mg m^{-3}	1.162	1.182	1.188	1.173
μ(Cu/Mo, Kα) mm^{-1}	0.580 (Cu)	0.576 (Cu)	0.109 (Mo)	0.908(Cu)
F(000)	340	456	464	1784
cryst size, mm^3	0.07 x 0.03 x 0.01	0.24 x 0.15 x 0.08	0.40 x 0.13 x 0.06	0.41 x 0.11 x 0.01
range θ collected, deg	4.294 to 70.082	3.002 to 77.216	1.998 to 33.481	3.436 to 77.364
reflns collected/unique	11116/2225	18435/4648	23722/6980	35927/9333
abs cor	Semi-empirical from equivalents			

Max and min transmn coeff.	0.7533 and 0.6544	1.0000 and 0.7636	1.000 and 0.702	1.0000 and 0.5883
goodness of fit	1.044	1.030	1.055	1.057
$R_1(I>2\sigma(I))^a$	0.0460	0.0387	0.0441	0.0412
wR_2 (all data)^a	0.1264	0.1027	0.1314	0.1102
peak and hole, e Å^{-3}	0.187 and -0.173	0.271 and -0.250	0.635 and -0.376	0.456 and -0.395

^{a} Definition of R indices: $R_1 = \Sigma(F_O - F_C)/\Sigma(F_O)$; $wR_2 = [\Sigma[w(F_O^2 - F_C^2)^2]/[\Sigma[w(F_O^2)^2]]^{1/2}$

Table 2.7: Compounds 6b, 7a, and 8a.

	6b	**7a·(C_7H_8)**	**7b·0.5(C_7H_8)**	**8a·0.5(C_7H_8)**
empirical formula	$C_{28}H_{42}AlNO_2$	$C_{29}H_{33}AlN_2O_2$	$C_{31.5}H_{41}AlN_2O_2$	$C_{26.5}H_{31}AlN_2O_2$
FW	451.60	468.55	506.64	436.51
lattice type	monoclinic	monoclinic	monoclinic	monoclinic
space group	$P12_1/n1$	$P12_1/c1$	C12/c1	$P12_1/n1$
T, K	200(1)	200(1)	199(9)	200(2)
a, Å	9.1905(3)	10.6313(3)	26.6686(15)	8.824(2)
b, Å	14.1181(3)	19.0072(6)	26.9237(14)	13.722(2)
c, Å	20.6824(3)	13.1128(3)	17.9976(10)	20.238(4)
α, deg	90	90	90	90
β, deg	91.110(3)	103.709(3)	108.690(4)	90.33(2)
γ, deg	90	90	90	90
V, Å^3	2683.1(1)	2574.2(1)	12241.1(12)	2450.3(9)

Z	4	4	16	4
ρ_{calc}/Mg m^{-3}	1.118	1.209	1.100	1.183
μ(Cu/Mo, Kα) mm^{-1}	0.827 (Cu)	0.902 (Cu)	0.789 (Cu)	0.910(Cu)
F(000)	984	1000	4368	932
cryst size, mm^3	0.37 x 0.25 x 0.14	0.33 x 0.04 x 0.03	0.083 x 0.077 x 0.02	0.20 x 0.04 x 0.02
range θ collected, deg	3.791 to 77.339	4.178 to 77.240	2.398 to 70.289	2.183 to 70.249
reflns collected/unique	24920/5258	33309/4859	39225/6921	19390/3459
abs cor				
Max and min transmn coeff.	1.000 and 0.325	1.000 and 0.501	0.7534 and 0.5876	0.7533 and 0.5607
goodness of fit	1.074	1.101	1.021	1.042
R_1(I>2σ(I))[a]	0.0464	0.0424	0.0697	0.0608
wR_2 (all data)[a]	0.1319	0.1197	0.2302	0.1776
peak and hole, e Å^{-3}	0.452 and -0.477	0.292 and -0.296	0.305 and -0.449	0.400 and -0.243

[a] Definition of R indices: $R_1 = \Sigma(F_O - F_C)/\Sigma(F_O)$; $wR_2 = [\Sigma[w(F_O^2 - F_C^2)^2]/[\Sigma[w(F_O^2)^2]]^{1/2}$

2.5 Acknowledgements

We acknowledge the NSF-MRI grants CHE-0923449 and CHE-2018414, which were used to purchase the single-crystal X-ray diffractometers and associated software employed in

this study, as well as the NSF-MRI grant CHE-1826982, which was used to purchase the Bruker 400 MHz spectrometer.

2.6 References

(1) Xu, W.; Chen, W.-Q.; Jiang, D.; Zhang, C.; Ma, Z.; Ren, Y.; Shi, L. Evolution of the Global Polyethylene Waste Trade System. *Ecosyst. Health Sustain.* **2020**, *6* (1), 1-16.

(2) Jubinville, D.; Esmizadeh, E.; Saikrishnan, S.; Tzoganakis, C.; Mekonnen, T. A Comprehensive Review of Global Production and Recycling Methods of Polyolefin (PO) Based Products and Their Post-Recycling Applications. *Sustain. Mater. Techno.* **2020**, *25*, e00188.

(3) Lebreton, L.; Slat, B.; Ferrari, F.; Sainte-Rose, B.; Aitken, J.; Marthouse, R.; Hajbane, S.; Cunsolo, S.; Schwarz, A.; Levivier, A.; Noble, K.; Debeljak, P.; Maral, H.; Schoeneich-Argent, R.; Brambini, R.; Reisser, J. Evidence That the Great Pacific Garbage Patch Is Rapidly Accumulating Plastic. *Sci. Rep.* **2018**, *8* (1), 4666.

(4) Law, K. L.; Morét-Ferguson, S. E.; Goodwin, D. S.; Zettler, E. R.; DeForce, E.; Kukulka, T.; Proskurowski, G. Distribution of Surface Plastic Debris in the Eastern Pacific Ocean from an 11-Year Data Set. *Environ. Sci. Technol.* **2014**, *48* (9), 4732–4738.

(5) Jambeck, J. R.; Geyer, R.; Wilcox, C.; Siegler, T. R.; Perryman, M.; Andrady, A.; Narayan, R.; Law, K. L. Plastic Waste Inputs from Land into the Ocean. *Science* **2015**, *347* (6223), 768-771.

(6) Eriksen, M.; Lebreton, L. C. M.; Carson, H. S.; Thiel, M.; Moore, C. J.; Borerro, J. C.; Galgani, F.; Ryan, P. G.; Reisser, J. Plastic Pollution in the World's Oceans: More than 5 Trillion Plastic Pieces Weighing over 250,000 Tons Afloat at Sea. *PLoS ONE* **2014**, *9* (12), e111913.

(7) Zhang, X.; Fevre, M.; Jones, G. O.; Waymouth, R. M. Catalysis as an Enabling Science for Sustainable Polymers. *Chem. Rev.* **2018**, *118* (2), 839–885.

(8) Vroman, I.; Tighzert, L. Biodegradable Polymers. *Materials* **2009**, *2* (2), 307-344.

(9) Nayak, P. L. Biodegradable Polymers: Opportunities and Challenges. *J. Macromol. Sci. Polymer Rev.* **1999**, *39* (3), 481–505.

(10) Galbis, J. A.; García-Martín, M. de G.; de Paz, M. V.; Galbis, E. Synthetic Polymers from Sugar-Based Monomers. *Chem. Rev.* **2016**, *116* (3), 1600–1636.

(11) Guillaume, S. M.; Kirillov, E.; Sarazin, Y.; Carpentier, J.-F. Beyond Stereoselectivity, Switchable Catalysis: Some of the Last Frontier Challenges in Ring-Opening Polymerization of Cyclic Esters. *Chem. Eur. J.* **2015**, *21* (22), 7988–8003.

(12) Panchal, S. S.; Vasava, D. V. Biodegradable Polymeric Materials: Synthetic Approach. *ACS Omega* **2020**, *5* (9), 4370–4379.

(13) Ashter, S. A. 1 - Introduction. In *Introduction to Bioplastics Engineering*; Ashter, S. A., Ed.; Plastics Design Library; William Andrew Publishing: Oxford, 2016; pp 1–17.

(14) Wei, Y.; Wang, S.; Zhou, S. Aluminum Alkyl Complexes: Synthesis, Structure, and Application in ROP of Cyclic Esters. *Dalton Trans.* **2016**, *45* (11), 4471–4485.

(15) Dechy-Cabaret, O.; Martin-Vaca, B.; Bourissou, D. Controlled Ring-Opening Polymerization of Lactide and Glycolide. *Chem. Rev.* **2004**, *104* (12), 6147–6176.

(16) Wu, J.; Yu, T.-L.; Chen, C.-T.; Lin, C.-C. Recent Developments in Main Group Metal Complexes Catalyzed/Initiated Polymerization of Lactides and Related Cyclic Esters. *Coord. Chem. Rev.* **2006**, *250* (5), 602–626.

(17) Jianming, R.; Anguo, X.; Hongwei, W.; Hailin, Y. Review – Recent Development of Ring-Opening Polymerization of Cyclic Esters Using Aluminum Complexes. *Des. Monomers Polym.* **2014**, *17* (4), 345–355.

(18) Gao, J.; Zhu, D.; Zhang, W.; Solan, G. A.; Ma, Y.; Sun, W.-H. Recent Progress in the Application of Group 1, 2 & 13 Metal Complexes as Catalysts for the Ring Opening Polymerization of Cyclic Esters. *Inorg. Chem. Front.* **2019**, *6* (10), 2619–2652.

(19) Wang, Y.; Ma, H. Exploitation of Dinuclear Salan Aluminum Complexes for Versatile Copolymerization of ε-Caprolactone and L-Lactide. *Chem. Commun.* **2012**, *48* (53), 6729–6731.

(20) Wang, Y.; Ma, H. Aluminum Complexes of Bidentate Phenoxy-Amine Ligands: Synthesis, Characterization and Catalysis in Ring-Opening Polymerization of Cyclic Esters. *J. Organomet. Chem.* **2013**, *731*, 23–28.

(21) Chen, L.; Li, W.; Yuan, D.; Zhang, Y.; Shen, Q.; Yao, Y. Syntheses of Mononuclear and Dinuclear Aluminum Complexes Stabilized by Phenolato Ligands and Their Applications in the Polymerization of ε-Caprolactone: A Comparative Study. *Inorg. Chem.* **2015**, *54* (10), 4699–4708.

(22) Li, W.; Wu, W.; Wang, Y.; Yao, Y.; Zhang, Y.; Shen, Q. Bimetallic Aluminum Alkyl Complexes as Highly Active Initiators for the Polymerization of ε-Caprolactone. *Dalton Trans.* **2011**, *40* (43), 11378–11381.

(23) Kaler, S.; McKeown, P.; Ward, B. D.; Jones, M. D. Aluminium(Iii) and Zinc(Ii) Complexes of Azobenzene-Containing Ligands for Ring-Opening Polymerisation of ε-Caprolactone and Rac-Lactide. *Inorg. Chem. Front.* **2021**, *8* (3), 711–719.

(24) Yu, X.; Zhang, C.; Wang, Z. Controlled Polymerization of ϵ-Caprolactone Using Aluminum and Zinc Complexes with Iminophosphorane Ligands. *ChemistrySelect* **2020**, *5* (1), 426–429.

(25) Diteepeng, N.; Wilson, I. A. P.; Buffet, J.-C.; Turner, Z. R.; O'Hare, D. L- and Rac-Lactide Polymerisation Using Scandium and Aluminium Permethylindenyl Complexes. *Polym. Chem.* **2020**, *11* (39), 6308–6318.

(26) Campirán-Martínez, A.; Jancik, V.; Martínez-Otero, D.; Hernández-Balderas, U.; Zavala-Segovia, N.; Moya-Cabrera, M. Linkage Isomerism in Dinuclear Al and Ga Organometallic Complexes: Structural and Reactivity Consequences. *Organometallics* **2020**, *39* (10), 1799–1813.

(27) Bouyahyi, M.; Roisnel, T.; Carpentier, J.-F. Aluminum Complexes of Bidentate Fluorinated Alkoxy-Imino Ligands: Syntheses, Structures, and Use in Ring-Opening Polymerization of Cyclic Esters. *Organometallics* **2012**, *31* (4), 1458–1466.

(28) Wang, P.; Hao, X.; Cheng, J.; Chao, J.; Chen, X. Aluminum Chelates Supported by β-Quinolyl Enolate Ligands: Synthesis and ROP of ε-CL. *Dalton Trans.* **2016**, *45* (22), 9088–9096.

(29) Zhang, Q.; Zhang, W.; Rajendran, N. M.; Liang, T.; Sun, W.-H. Thermo-Enhanced Ring-Opening Polymerization of ε-Caprolactone: The Synthesis, Characterization, and Catalytic Behavior of Aluminum Hydroquinolin-8-Olates. *Dalton Trans.* **2017**, *46* (24), 7833–7843.

(30) Nakonkhet, C.; Nanok, T.; Wattanathana, W.; Chuawong, P.; Hormnirun, P. Aluminium Complexes Containing Salicylbenzothiazole Ligands and Their Application in the Ring-Opening Polymerisation of Rac-Lactide and ε-Caprolactone. *Dalton Trans.* **2017**, *46* (33), 11013–11030.

(31) Sumrit, P.; Chuawong, P.; Nanok, T.; Duangthongyou, T.; Hormnirun, P. Aluminum Complexes Containing Salicylbenzoxazole Ligands and Their Application in the Ring-Opening Polymerization of Rac-Lactide and ε-Caprolactone. *Dalton Trans.* **2016**, *45* (22), 9250–9266.

(32) Ma, W.-A.; Wang, Z.-X. Synthesis and Characterisation of Aluminium(Iii) and Tin(Ii) Complexes Bearing Quinoline-Based N,N,O-Tridentate Ligands and Their Catalysis in the Ring-Opening Polymerisation of ε-Caprolactone. *Dalton Trans.* **2011**, *40* (8), 1778–1786.

(33) Chuang, H.-J.; Su, Y.-C.; Ko, B.-T.; Lin, C.-C. Synthesis and Structural Characterization of Aluminum Complexes Supported by NNO-Tridentate Ketiminate Ligands: Efficient Catalysts for Ring-Opening Polymerization of l-Lactide. *Inorg. Chem. Commun.* **2012**, *18*, 38–42.

(34) Sun, W.-H.; Shen, M.; Zhang, W.; Huang, W.; Liu, S.; Redshaw, C. Methylaluminium 8-Quinolinolates: Synthesis, Characterization and Use in Ring-Opening Polymerization (ROP) of ε-Caprolactone. *Dalton Trans.* **2011**, *40* (11), 2645–2653.

(35) Chen, C.-T.; Huang, C.-A.; Huang, B.-H. Aluminium Metal Complexes Supported by Amine Bis-Phenolate Ligands as Catalysts for Ring-Opening Polymerization of ε-Caprolactone. *Dalton Trans.* **2003**, *19*, 3799–3803.

(36) Hild, F.; Neehaul, N.; Bier, F.; Wirsum, M.; Gourlaouen, C.; Dagorne, S. Synthesis and Structural Characterization of Various N,O,N-Chelated Aluminum and Gallium Complexes for the Efficient ROP of Cyclic Esters and Carbonates: How Do Aluminum and Gallium Derivatives Compare ? *Organometallics* **2013**, *32* (2), 587–598.

(37) Gao, B.; Li, X.; Duan, R.; Duan, Q.; Li, Y.; Pang, X.; Zhuang, H.; Chen, X. Hemi-Salen Aluminum Catalysts Bearing N, N, O-Tridentate Type Binaphthyl-Schiff-Base Ligands for the Living Ring-Opening Polymerisation of Lactide. *RSC Adv.* **2015**, *5* (37), 29412–29419.

(38) Meduri, A.; Cozzolino, M.; Milione, S.; Press, K.; Sergeeva, E.; Tedesco, C.; Mazzeo, M.; Lamberti, M. Yttrium and Aluminium Complexes Bearing Dithiodiolate Ligands: Synthesis and Application in Cyclic Ester Polymerization. *Dalton Trans.* **2015**, *44* (41), 17990–18000.

(39) Rajendran, N. M.; Xi, Y.; Zhang, W.; Braunstein, P.; Liang, T.; Sun, W.-H. Magnesium and Aluminum Complexes Bearing Bis(5,6,7-Trihydro Quinolyl)-Fused Benzodiazepines for ε-Caprolactone Polymerization. *Inorg. Chem. Front.* **2016**, *3* (10), 1317–1325.

(40) Huang, W.-Y.; Chuang, S.-J.; Chunag, N.-T.; Hsiao, C.-S.; Datta, A.; Chen, S.-J.; Hu, C.-H.; Huang, J.-H.; Lee, T.-Y.; Lin, C.-H. Aluminium Complexes Containing Bidentate and Symmetrical Tridentate Pincer Type Pyrrolyl Ligands: Synthesis, Reactions and Ring Opening Polymerization. *Dalton Trans.* **2011**, *40* (28), 7423–7433.

(41) Dagorne, S.; Le Bideau, F.; Welter, R.; Bellemin-Laponnaz, S.; Maisse-François, A. Well-Defined Cationic Alkyl– and Alkoxide–Aluminum Complexes and Their Reactivity with ε-Caprolactone and Lactides. *Chem. Eur. J.* **2007**, *13* (11), 3202–3217.

(42) Fneich, B. N.; Das, A.; Kirschbaum, K.; Mason, M. R. Bidentate and Tridentate Coordination Modes of Bis(3-Methylindolyl)-2-Pyridylmethane in Complexes of Aluminum and Gallium: Structural Characterization of Bridging N-Indolide in a Dialuminum Complex. *J. Organomet. Chem.* **2018**, *872*, 12–23.

(43) Hair, G. S.; Battle, S. L.; Decken, A.; Cowley, A. H.; Jones, R. A. Synthesis and Characterization of 8-(Dimethylamino)-1-Naphthyl Derivatives of Aluminum, Gallium, and Indium. *Inorg. Chem.* **2000**, *39* (1), 27–31.

(44) Zheng, W.; Roesky, H. W. Alkynyl Aluminium Compounds: Bonding Modes and Structures. *J. Chem. Soc., Dalton Trans.* **2002**, *14*, 2787–2796.

(45) Huang, Y.-T.; Wang, W.-C.; Hsu, C.-P.; Lu, W.-Y.; Chuang, W.-J.; Chiang, M. Y.; Lai, Y.-C.; Chen, H.-Y. The Ring-Opening Polymerization of ε-Caprolactone and l-Lactide Using Aluminum Complexes Bearing Benzothiazole Ligands as Catalysts. *Polym. Chem.* **2016**, *7* (26), 4367–4377.

(46) Nomura, N; Ishii, R.; Akakura, M.; Aoi, K. Stereoselective Ring-Opening Polymerization of Racemic Lactide Using Aluminum-Achiral Ligand Complexes: Exploration of a Chain-End Control Mechanism. *J. Am. Chem. Soc.* **2002**, *124*, 5938-5939.

(47) Du, H.; Pang, X.; Yu, H.; Zhuang, X.; Chen, X.; Cui, D.; Wang, X.; Jing, X. Polymerization of Rac-Lactide Using Schiff Base Aluminum Catalysts: Structure, Activity, and Stereoselectivity. *Macromolecules* **2007**, *40* (6), 1904–1913.

(48) Tang, Z.; Chen, X.; Pang, X.; Yang, Y.; Zhang, X.; Jing, X. Stereoselective Polymerization of Rac-Lactide Using a Monoethylaluminum Schiff Base Complex. *Biomacromolecules* **2004**, *5* (3), 965–970.

(49) Tang, Z.; Yang, Y.; Pang, X.; Hu, J.; Chen, X.; Hu, N.; Jing, X. Controlled and Stereospecific Polymerization of Rac-Lactide with a Single-Site Ethyl Aluminum and Alcohol Initiating System. *J. Appl. Polym. Sci.* **2005**, *98* (1), 102–108.

(50) Nomura, N.; Ishii, R.; Yamamoto, Y.; Kondo, T. Stereoselective Ring-Opening Polymerization of a Racemic Lactide by Using Achiral Salen– and Homosalen–Aluminum Complexes. *Chem. Eur. J.* **2007**, *13* (16), 4433–4451.

(51) Bolley, A.; Mameri, S.; Dagorne, S. Controlled and Highly Effective Ring-Opening Polymerization of α-Chloro-ε-Caprolactone Using Zn- and Al-Based Catalysts. *J. Polym. Sci.* **2020**, *58* (9), 1197–1206.

(52) Hormnirun, P.; Marshall, E. L.; Gibson, V. C.; White, A. J. P.; Williams, D. J. Remarkable Stereocontrol in the Polymerization of Racemic Lactide Using Aluminum Initiators Supported by Tetradentate Aminophenoxide Ligands. *J. Am. Chem. Soc.* **2004**, *126* (9), 2688–2689.

(53) Du, H.; Velders, A. H.; Dijkstra, P. J.; Sun, J.; Zhong, Z.; Chen, X.; Feijen, J. Chiral Salan Aluminium Ethyl Complexes and Their Application in Lactide Polymerization. *Chem. Eur. J.* **2009**, *15* (38), 9836–9845.

(54) Press, K.; Goldberg, I.; Kol, M. Mechanistic Insight into the Stereochemical Control of Lactide Polymerization by Salan–Aluminum Catalysts. *Angew. Chem. In. Ed.* **2015**, *54* (49), 14858–14861.

(55) Trofimenko, S. Boron-Pyrazole Chemistry. *J. Am. Chem. Soc.* **1966**, *88* (8), 1842–1844.

(56) Trofimenko, Swiatoslaw. Transition Metal Poly(1-Pyrazolyl)Borates Containing Other Ligands. *J. Am. Chem. Soc.* **1967**, *89* (15), 3904–3905.

(57) Trofimenko, Swiatoslaw. Coordination Chemistry of Pyrazole-Derived Ligands. *Chem. Rev.* **1972**, *72* (5), 497–509.

(58) Owen, G. R. Functional Group Migrations between Boron and Metal Centres within Transition Metal–Borane and –Boryl Complexes and Cleavage of H–H, E–H and E–E′ Bonds. *Chem. Commun.* **2016**, *52* (71), 10712–10726.

(59) Pettinari, C.; Pettinari, R.; Marchetti, F. Chapter Four - Golden Jubilee for Scorpionates: Recent Advances in Organometallic Chemistry and Their Role in Catalysis. In *Advances in Organometallic Chemistry*; Pérez, P. J., Ed.; Academic Press, 2016; Vol. 65, pp 175–260.

(60) Wang, Y.; Zhang, B.; Guo, S. Transition Metal Complexes Supported by N-Heterocyclic Carbene-Based Pincer Platforms: Synthesis, Reactivity and Applications. *Eur. J. Inorg. Chem.* **2021**, *2021* (3), 188–204.

(61) Taakili, R.; Canac, Y. NHC Core Pincer Ligands Exhibiting Two Anionic Coordinating Extremities. *Molecules* **2020**, *25* (9), 2231.

(62) Silva, F.; Fernandes, C.; Campello, M. P. C.; Paulo, A. Metal Complexes of Tridentate Tripod Ligands in Medical Imaging and Therapy. *Polyhedron* **2017**, *125*, 186–205.

(63) Martins, L. M. D. R. S. C-Scorpionate Complexes: Ever Young Catalytic Tools. *Coord. Chem. Rev.* **2019**, *396*, 89–102.

(64) Santini, C.; Marinelli, M.; Pellei, M. Boron-Centered Scorpionate-Type NHC-Based Ligands and Their Metal Complexes. *Eur. J. Inorg. Chem.* **2016**, *2016* (15–16), 2312–2331.

(65) Otero, A.; Fernández-Baeza, J.; Antiñolo, A.; Tejeda, J.; Lara-Sánchez, A. Heteroscorpionate Ligands Based on Bis(Pyrazol-1-Yl)Methane: Design and Coordination Chemistry. *Dalton Trans.* **2004**, *10*, 1499–1510.

(66) de la Cruz-Martínez, F.; Martínez, J.; Gaona, M. A.; Fernández-Baeza, J.; Sánchez-Barba, L. F.; Rodríguez, A. M.; Castro-Osma, J. A.; Otero, A.; Lara-Sánchez, A.

Bifunctional Aluminum Catalysts for the Chemical Fixation of Carbon Dioxide into Cyclic Carbonates. *ACS Sustainable Chem. Eng.* **2018**, *6* (4), 5322–5332.

(67) Garcés, A.; Sánchez-Barba, L. F.; Fernández-Baeza, J.; Otero, A.; Fernández, I.; Lara-Sánchez, A.; Rodríguez, A. M. Organo-Aluminum and Zinc Acetamidinates: Preparation, Coordination Ability, and Ring-Opening Polymerization Processes of Cyclic Esters. *Inorg. Chem.* **2018**, *57* (19), 12132–12142.

(68) Su, W.-J.; Liang, L.-C. Elusive Scorpionates: C3-Symmetric, Formally Dianionic, Facially Tridentate Ligands. *Inorg. Chem.* **2018**, *57* (2), 553–556.

(69) Martínez, J.; Castro-Osma, J. A.; Alonso-Moreno, C.; Rodríguez-Diéguez, A.; North, M.; Otero, A.; Lara-Sánchez, A. One-Component Aluminum(Heteroscorpionate) Catalysts for the Formation of Cyclic Carbonates from Epoxides and Carbon Dioxide. *ChemSusChem* **2017**, *10* (6), 1175–1185.

(70) Martínez, J.; Castro-Osma, J. A.; Earlam, A.; Alonso-Moreno, C.; Otero, A.; Lara-Sánchez, A.; North, M.; Rodríguez-Diéguez, A. Synthesis of Cyclic Carbonates Catalysed by Aluminium Heteroscorpionate Complexes. *Chem. Eur. J.* **2015**, *21* (27), 9850–9862.

(71) Chen, H.-Y.; Lee, Y.-H.; Chiang, M. Y.; Lu, W.-Y.; Tseng, H.-C.; Tsai, H.-Y.; Chen, Y.-H.; Lai, Y.-C.; Chen, H.-Y. Coordinating Effect in Ring-Opening Polymerization of ε-Caprolactone Using Aluminum Complexes Bearing Bisphenolate as Catalysts. *RSC Adv.* **2015**, *5* (100), 82018–82026.

(72) Castro-Osma, J. A.; Alonso-Moreno, C.; Márquez-Segovia, I.; Otero, A.; Lara-Sánchez, A.; Fernández-Baeza, J.; Rodríguez, A. M.; Sánchez-Barba, L. F.; García-Martínez, J. C. Synthesis, Structural Characterization and Catalytic Evaluation of the Ring-Opening

Polymerization of Discrete Five-Coordinate Alkyl Aluminium Complexes. *Dalton Trans.* **2013**, *42* (25), 9325–9337.

(73) Otero, A.; Lara-Sánchez, A.; Fernández-Baeza, J.; Alonso-Moreno, C.; Castro-Osma, J. A.; Márquez-Segovia, I.; Sánchez-Barba, L. F.; Rodríguez, A. M.; Garcia-Martinez, J. C. Neutral and Cationic Aluminum Complexes Supported by Acetamidate and Thioacetamidate Heteroscorpionate Ligands as Initiators for Ring-Opening Polymerization of Cyclic Esters. *Organometallics* **2011**, *30* (6), 1507–1522.

(74) A. Castro-Osma, J.; Alonso-Moreno, C.; Lara-Sánchez, A.; Otero, A.; Fernández-Baeza, J.; F. Sánchez-Barba, L.; M. Rodríguez, A. Catalytic Behaviour in the Ring-Opening Polymerisation of Organoaluminiums Supported by Bulky Heteroscorpionate Ligands. *Dalton Trans.* **2015**, *44* (27), 12388–12400.

(75) Castro-Osma, J. A.; Alonso-Moreno, C.; García-Martinez, J. C.; Fernández-Baeza, J.; Sánchez-Barba, L. F.; Lara-Sánchez, A.; Otero, A. Ring-Opening (ROP) versus Ring-Expansion (REP) Polymerization of ε-Caprolactone To Give Linear or Cyclic Polycaprolactones. *Macromolecules* **2013**, *46* (16), 6388–6394.

(76) Gazizov, A. S.; Burilov, A. R.; Khakimov, M. S.; Kharitonova, N. I.; Pudovik, M. A.; Konovalov, A. I. Reaction of α-Aminoacetals with 2-Methylresorcinol. *Russ. J. Gen. Chem.* **2009**, *79* (9), 1929-1930.

(77) Aoyama, K. Latent Epoxy Curing Catalyst or Curing Agent. WO 2018181045, October 4, 2018.

(78) Yu, R.-C.; Hung, C.-H.; Huang, J.-H.; Lee, H.-Y.; Chen, J.-T. Four- and Five-Coordinate Aluminum Ketiminate Complexes: Synthesis, Characterization, and Ring-Opening Polymerization. *Inorg. Chem.* **2002**, *41* (24), 6450–6455.

(79) Silvestri, A.; Grisi, F.; Milione, S. Ring Opening Polymerization of Lactide Promoted by Alcoholyzed Heteroscorpionate Aluminum Complexes. *J. Polym. Sci. Part A: Polym. Chem.* **2010**, *48* (16), 3632–3639.

(80) Arbaoui, A.; Redshaw, C. Metal Catalysts for ε-Caprolactone Polymerisation. *Polym. Chem.* **2010**, *1* (6), 801–826.

(81) Huang, T.-W.; Su, R.-R.; Lin, Y.-C.; Lai, H.-Y.; Yang, C.-Y.; Senadi, G. C.; Lai, Y.-C.; Chiang, M. Y.; Chen, H.-Y. Improvement in Aluminum Complexes Bearing a Schiff Base in Ring-Opening Polymerization of ε-Caprolactone: The Synergy of the N,S-Schiff Base in a Five-Membered Ring Aluminum System. *Dalton Trans.* **2018**, *47* (43), 15565–15573.

(82) Lu, W.-Y.; Chang, Y.-C.; Lian, C.-J.; Wu, K.-H.; Chiang, M. Y.; Chen, H.-Y.; Lin, C.-C.; Ko, B.-T. Optimization of Six-Membered Ring Aluminum Complexes in ε-Caprolactone Polymerization. *Eur. Polym. J.* **2019**, *114*, 151–163.

Chapter 3 - Molybdenum and Tungsten Alkylidene Complexes

3.1 Olefin Metathesis

Olefin metathesis is a powerful reaction for the formation of new alkene bonds, as shown in Figure 3.1. This is achieved through the exchange of alkylidene fragments.[1,2] A transition metal complex is needed to act as a catalyst for this reaction. Specifically, a metal carbene complex is needed, denoted by [M] in Figure 3.1.

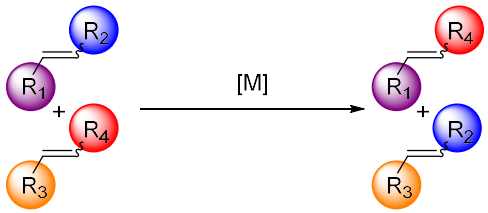

Figure 3.1: Olefin cross metathesis.

The generally accepted mechanism of olefin metathesis is shown in Figure 3.2.[3] The cycle starts with the metal carbene in *A*. An olefin with substituents R_3 and R_4 then binds to the metal carbene complex and a metallocyclobutane intermediate is formed in *C* with substituents R_1, R_3, and R_4 in the four-membered ring. This step will only happen if there is an open site *cis* to the carbene on the metal. This open *cis* site allows for the olefin to react with the nucleophiliccarbene to form the metallocyclobutane ring. In transition state *D*, the ring starts to cyclorevert. The original R_1 group on the carbene is starting to form an alkene bond to the carbon with the substituent group R_4. Once cycloreversion is complete, the new structure *E* contains a newly formed carbene complex containing the R_3 substituent group, while an olefin with substituents R_1 and R_4 is generated. Similar then to intermediate *C*, in intermediate *G*, another new olefin, this time with substituent groups R_1 and R_2 forms a metallocyclobutane intermediate. This structure then starts to cyclorevert through transition state *H*. The olefin with substituents R_2

and R_3 is then formed along with the original metal carbene with the substituent R_1 to complete the cycle.

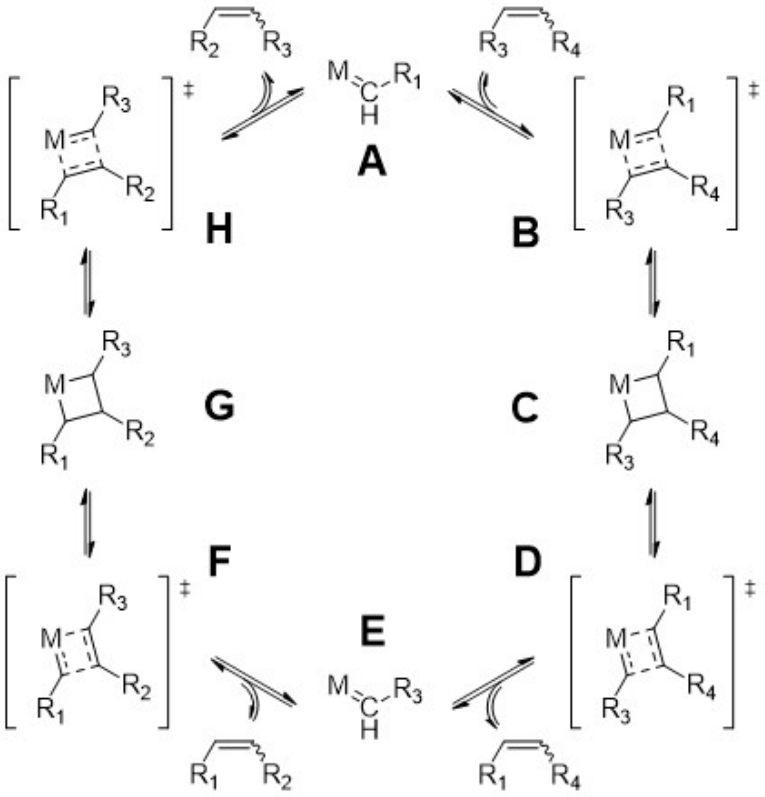

Figure 3.2: Mechanism of olefin metathesis.

3.2 The Fischer-Tropsch Process and Alkane Metathesis

The Fischer-Tropsch process is a method used by industry to produce linear alkanes from syngas, a mixture of hydrogen and carbon monoxide. This is a large-scale route for producing high grade diesel and other fuels for consumption.[4] Syngas can be derived from renewable biomass, which is a more sustainable approach to producing fuels. Syngas is converted into *n*-alkanes through a stepwise chain growth process involving a catalyst. The desired products from the Fischer-Tropsch process are the C9-C19 range of linear alkanes, but due to the stepwise chain growth mechanism, a highly disproportionate number of alkanes in the C4-C8 range are formed, Figure 3.3.

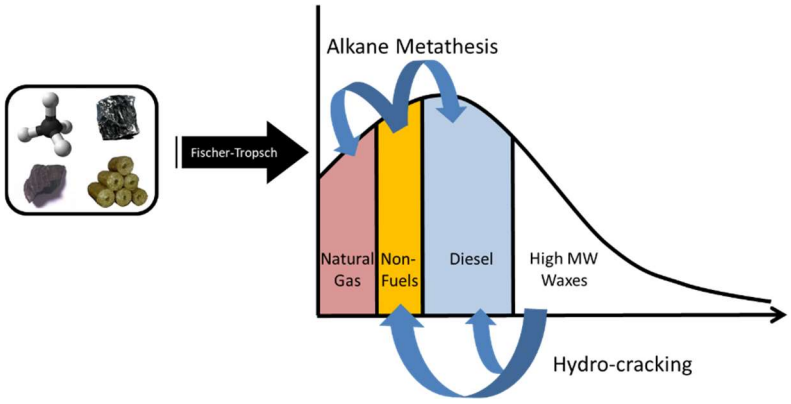

Figure 3.3: Alkane distribution from Fischer-Tropsch process.

Upgrading the alkanes in the C4-C8 range to diesel fuels would increase the efficiency of the Fischer-Tropsh process and make sustainable biofuels much more viable. One approach to transform shorter chain alkanes into longer chain alkanes is through a process called alkane metathesis. This method utilizes iridium pincer C-H activation catalysts in conjunction with olefin metathesis catalysts, Figure 3.4.[5,6] The iridium species activate the alkanes generating alkenes and iridium hydrides, while the olefin metathesis catalysts clip together the alkenes to form longer alkenes and ethylene gas. These are subsequently hydrogenated by the iridium hydrides, completing the catalytic cycle, Figure 3.4.

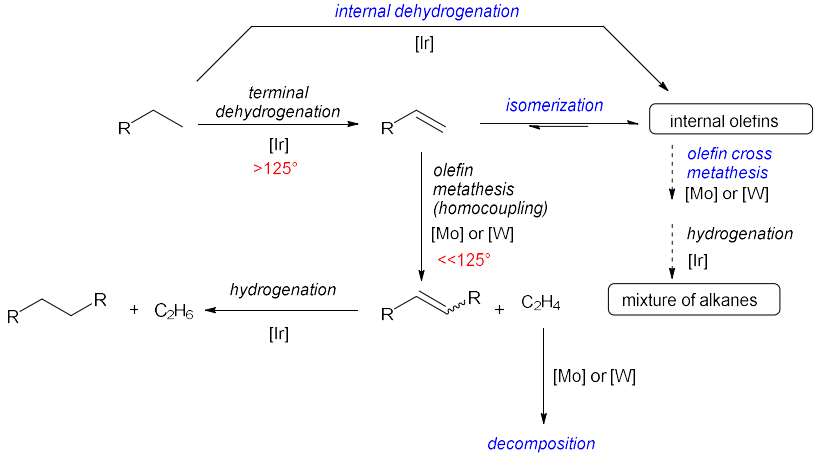

Figure 3.4: Alkane metathesis and potential side reactions.

3.3 Current Olefin Metathesis Catalysts

Currently two main types of olefin metathesis catalysts are used for olefin metathesis, Schrock-type and Grubbs-type catalysts, Figure 3.5. Schrock-type catalysts are based on the early transition metals molybdenum and tungsten with variable imido, alkoxide, and carbene ligands. These variable ligands allow Schrock-type catalysts to be highly selective and highly active. The drawback of Schrock-type catalysts is the use of early transition metals which makes the compounds highly air- and moisture- sensitive.[7,8] Grubbs-type catalysts use ruthenium, a late transition metal, and employ less variable ligands. The use of a late transition metal allows the catalysts to be more stable to air and water as well as more functional group tolerant, but the non-variable ligands make the catalysts less selective.[9,10]

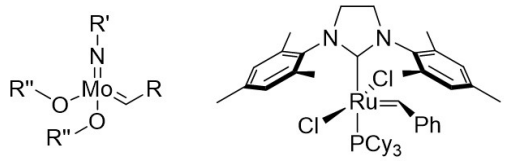

Figure 3.5: Examples of Schrock-type (left) and Grubbs-type (right) olefin metathesis catalysts.

One issue for alkane metathesis is that the activation of the alkanes by the iridium pincer complexes requires temperatures above 125°C. This poses a problem as current olefin metathesis catalysts readily decompose at these temperatures. Olefin metathesis catalysts also begin to decompose under ethylene gas, an intermediate of alkane metathesis.[11,12] This decomposition causes the formation of unwanted by-products as well as low turnover numbers.

The Schrock group has attempted to increase the stability of their catalysts in order to withstand the temperatures required for alkane metathesis. The method used was to utilize bidentate and tridentate ligands to stabilize the metal complexes at higher temperatures and to

reduce catalyst decomposition through biomolecular decomposition and hydride transfer mechanisms.

The first attempt utilized a dianionic biphenolate pincer ligand. As discussed in Chapter 1 of this thesis, pincer ligands are very stable and lead to thermally stable metal complexes due to their rigid structure.[13–15] Sues and coworkers used a $[ONO]^{2-}$ ligand, Figure 3.6, to form complexes with the structure $Mo(NC_6F_5)(CHCMe_2Ph)(ONO)$ and $W(O)(CHCMe_2Ph)(ONO)$.[16] When these complexes were reacted with ethylene, they produced six-coordinate metallocyclobutane species $Mo(NC_6F_5)(CH_2CH_2CH_2)(ONO)$ and $W(O)(CH_2CH_2CH_2)(ONO)$, which could be isolated. These octahedral geometries made it difficult for the metal complexes to undergo the cycloreversion step of olefin metathesis and it has been suggested that five-coordinate trigonal bipyramidal structures are needed for cycloreversion and olefin release.[12,17–19] Since the $[ONO]^{2-}$ ligand was rigid, the metallocyclobutane intermediates could not adopt a five-coordinate trigonal bipyramidal structure to allow for efficient catalysis.

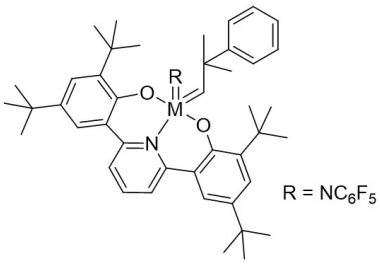

Figure 3.6: Molybdenum and tungsten based catalysts supported by a $[ONO]^{2-}$ ligand.

Next, Sues and coworkers moved on to a 2-pyridyl-substituted phenoxide ligands $[MesON]^-$ (2',4',5,6'-tetramethyl-3-(pyridine-2-yl)-[1,1'-biphenyl]-2-olate) and $[TripON]^-$ (2',3',6'-triisopropyl-5-methyl-3-(pyridin-2-yl)-[1,1'-biphenyl]-2-olate), Figure 3.7.[20] These ligands allowed the effects of sterically large bidentate ligands on 16-electron metal alkylidene complexes to be tested. The theory was that a bidentate ligand would allow for the necessary structural change into a trigonal bipyramidal metallocyclobutane intermediate, which is

necessary for cycloreversion in the olefin metathesis cycle. Although these complexes, Figure 3.7, were more active than the $[ONO]^{2-}$ ligand supported complexes, the activity was still low compared to other olefin metathesis catalysts. Additionally, when tested for alkane metathesis, there was no chain length selectivity, which is highly desirable for efficient alkane metathesis applications.

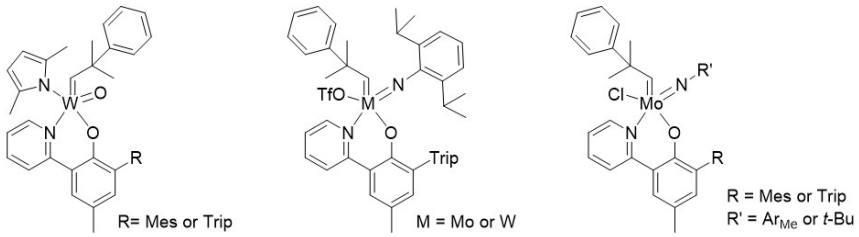

Figure 3.7: Molybdenum and tungsten based catalysts supported by $[MesON]^-$ and $[TripON]^-$ ligands.

3.4 Results and Discussion

The goal of this project was to stabilize a Schrock type catalyst with the scorpionate ligands discussed in Chapter 2 of this thesis. The synthetic route that was chosen utilized known starting material $Mo(NAr)(CHCMe_2Ph)(OTf)_2(DME)$ where Ar is 2,6-^{i}PrC_6H_2 and OTf is CF_3SO_3, Figure 3.8. This molybdenum complex was synthesized using known literature procedures.[21,22] From this starting material, it was hypothesized that a simple ligand exchange should be able to be carried out with a lithium or sodium salt of the ligand.[20] If successful, this synthetic route would provide a modular pathway for accessing the desired molybdenum product as well as a variety of analogues.

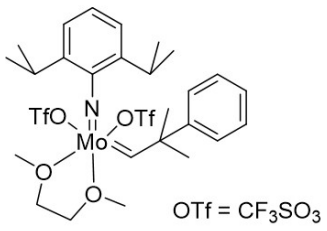

Figure 3.8: The $Mo(NAr)(CHCMe_2Ph)(OTf)_2(DME)$ starting material.

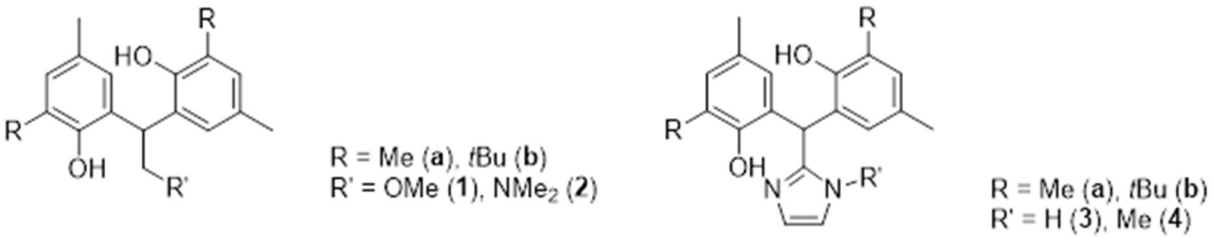

Figure 3.9: Ligands 1-4.

The same ligands discussed in Chapter 2, Figure 3.9, were utilized in the work with molybdenum using the synthetic route shown in Scheme 3.1. The first ligand used was a sodium salt of **2a**, **$Na_2$2a**. To synthesize this salt, **2a** was dissolved in ethanol and two equivalents of sodium hydroxide were added, Scheme 3.2.

Scheme 3.1: Initial proposed synthetic route to install scorpionate ligand.

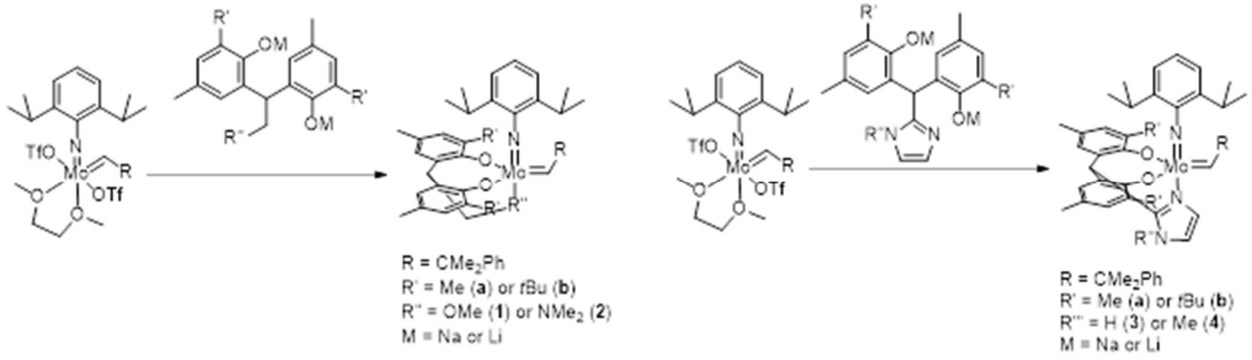

Scheme 3.2: Deprotonation of 1-4.

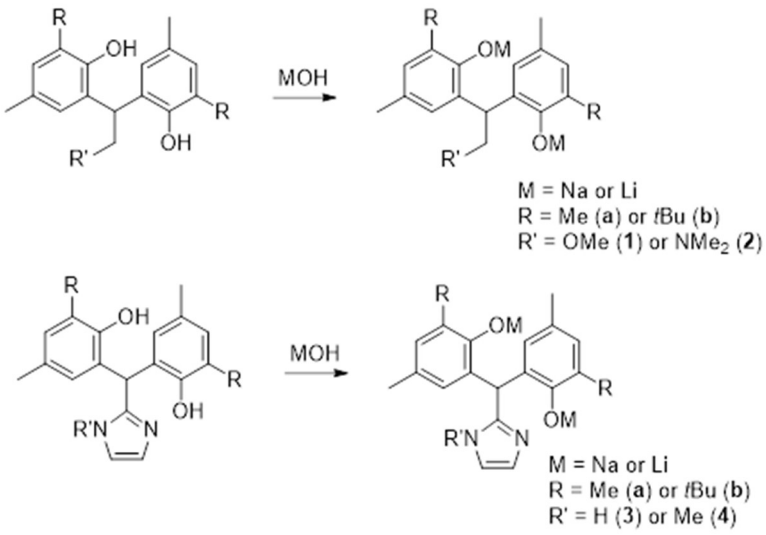

This reaction was allowed to stir overnight and then the solvent was evaporated. Through ^{1}H NMR spectroscopy, it was seen that ethanol remained coordinated to product **Na$_2$2a**, likely forming strong hydrogen bonds in the solid state. As molybdenum alkylidene structures are sensitive to alcohols and decompose in their presence, **Na$_2$2a** was recrystallized using dry DME in the glovebox to produce **Na$_2$2a** without any ethanol present in the product. Attempts to coordinate **Na$_2$2a** to Mo(NAr)(CHCMe$_2$Ph)(OTf)$_2$(DME) were unsuccessful after multiple attempts under various reaction conditions and in various solvents. The alkylidene proton was used as a handle to monitor the reaction progress and product purity. The desired product was not able to be purified from the reaction mixture, even after multiple purification attempts including recrystallizations and filtrations. The next step taken was to look at the formation of this compound over a set amount of time and analyze it by ^{1}H NMR spectroscopy, specifically

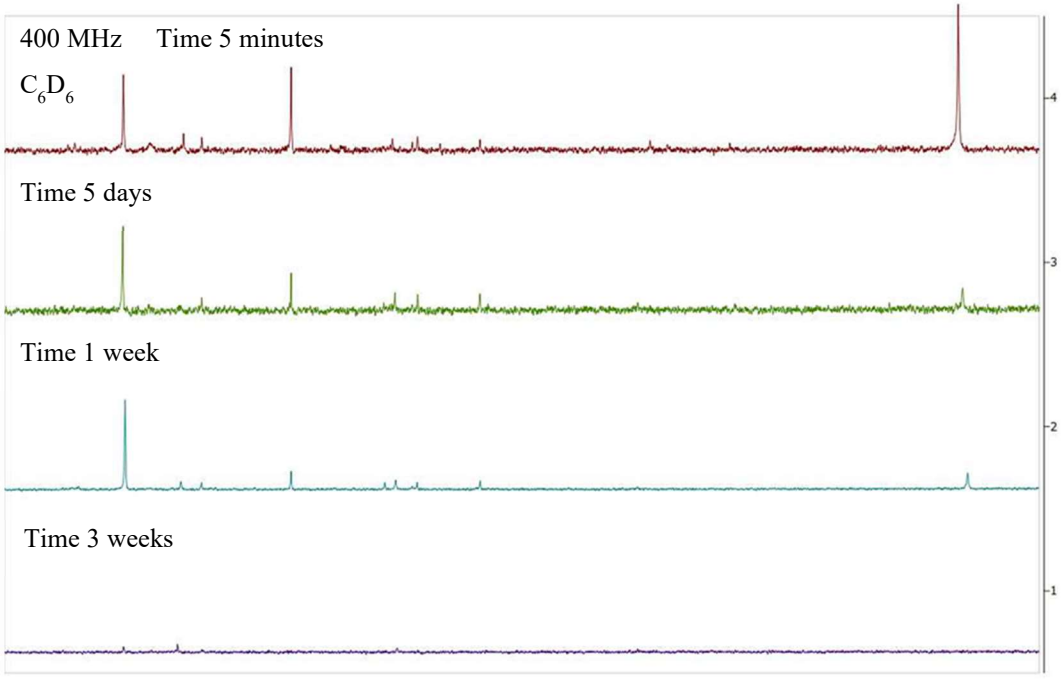

Figure 3.10: Following the reaction between Na$_2$2a and Mo(NAr)(CHCMe$_2$Ph)(OTf)$_2$(DME) by ^{1}H NMR spectroscopy in the alkylidene region.

between 10 and 20 ppm where the alkylidene peak is generally seen. What was seen in this region of the ^{1}H NMR spectrum were multiple alkylidene peaks when taking the ^{1}H NMR spectrum immediately after mixing the reactants. In Figure 3.10, it can be seen that the peaks at 15.3 ppm and 10.96 ppm were the most prominent alkylidene peaks present. The peak at 14.45 ppm, which is the alkylidene associated with the starting molybdenum complex, was set at an integration of 1 and the peak integrations at 10.96 and 15.3 ppm were monitored. The peak at 15.3 ppm increased from 1.02 at 5 minutes, to 13.6 at 5 days to 2.54 at 1 week. The peak at 10.96 ppm decreased from 2.33 to 1.33 to 1.37 over the same time periods. This initial high integration at 10.96 ppm and decrease indicated that it was most likely a kinetic product while the increase in the integration at 15.3 ppm indicated a thermodynamic product. After 3 weeks almost every alkylidene peak had disappeared, indicating complex decomposition.

From here, it was decided to look at the lithium salt of **2a** instead of the sodium salt. The difference in size of the cation can change the reactivity.[16,23] It was thought that the sodium cation might be coordinating to the ligand while it was attached to the molybdenum complex as was seen by Sues and co-workers in their work with ONO ligands.[16] The same general procedure for **Na$_2$2a** was used for the synthesis of **Li$_2$2a**, Scheme 3.2. With the switch from sodium to lithium salts, full conversion into the desired molybdenum complex was also difficult. Three major peaks in the alkylidene region appeared at 15.01 ppm, 14.45 ppm, and 12.64 ppm, Figure 3.11. The peak at 14.45 ppm was the alkylidene proton of the starting material, Mo(NAr)(CHCMe$_2$Ph)(OTf)$_2$(DME). Attempts to isolate a single alkylidene complex through various purification methods were ultimately unsuccessful.

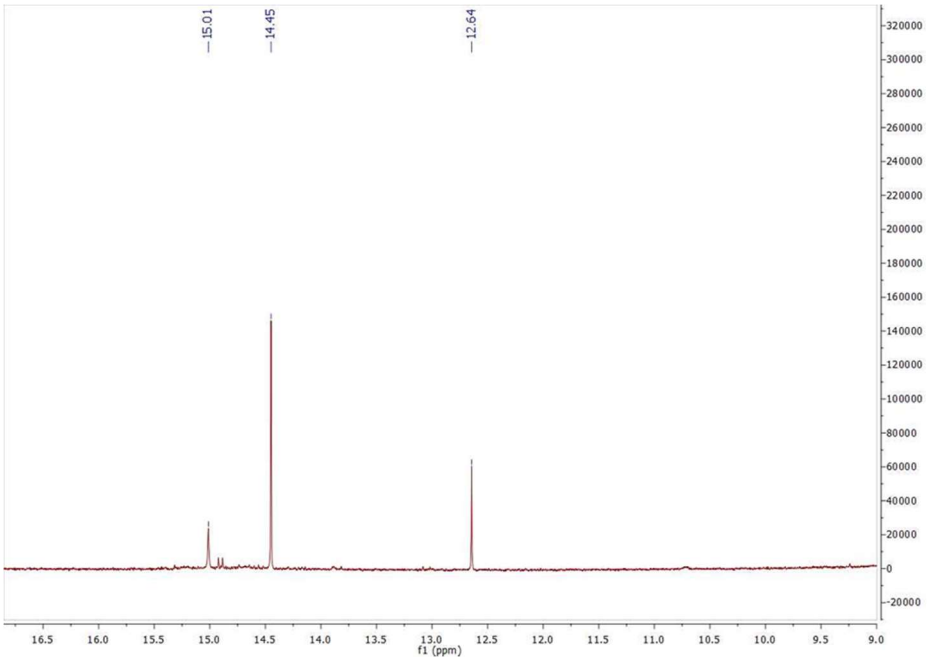

Figure 3.12: ^{1}H NMR spectrum of alkylidene region of initial reaction between $Li_2$2b and Mo(NAr)(CHCMe$_2$Ph)(OTf)$_2$(DME) in C_6D_6.

Using the same synthetic approach (Scheme 3.1) the generation of Mo(NAr)(CHCMe$_2$Ph)(**3b**) was attempted. It was found though that addition of **$Li_2$3b** caused rapid decomposition of the metal alkylidene moiety over the course of less than one day in

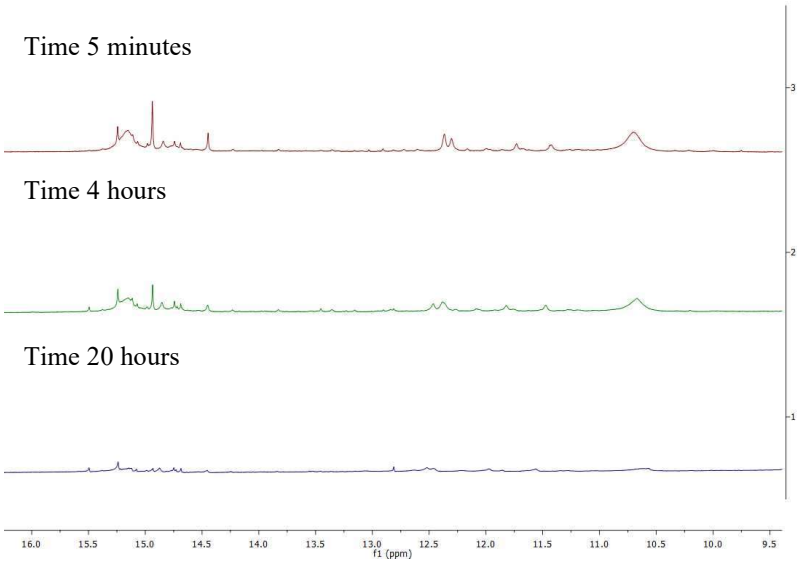

Figure 3.11: ^{1}H NMR spectrum of alkylidene region of initial reaction between $Li_2$3b and Mo(NAr)(CHCMe$_2$Ph)(OTf)$_2$(DME) in C_6D_6.

solution as tracked by ^{1}H NMR spectroscopy with the reaction in a J-Young NMR tube, Figure 3.12. The imidazole N-*H* was presumed to be too acidic and thus protonated the alkylidene carbon causing complex decomposition. Therefore, no more studies were performed using the imidazolyl scorpionate ligands.

Attempts to form the complex Mo(NAr)(CHCMe$_2$Ph)(**4b**) from **Li$_2$4b** and Mo(NAr)(CHCMe$_2$Ph)(OTf)$_2$(DME), Scheme 3.1, were also carried out. This, like the corresponding **2a** complexes also proved difficult to achieve. Typically, three major peaks would appear in the alkylidene region at 14.53 ppm, 14.16 ppm, and 13.55 ppm, Figure 3.13. The peak at 10.11 ppm seen in Figure 3.13 corresponded with the phenol -OH of **4b**, indicating that the lithium salt was being protonated. This likely contributed to decomposition of the desired complex and difficulties associated with isolating a pure product.

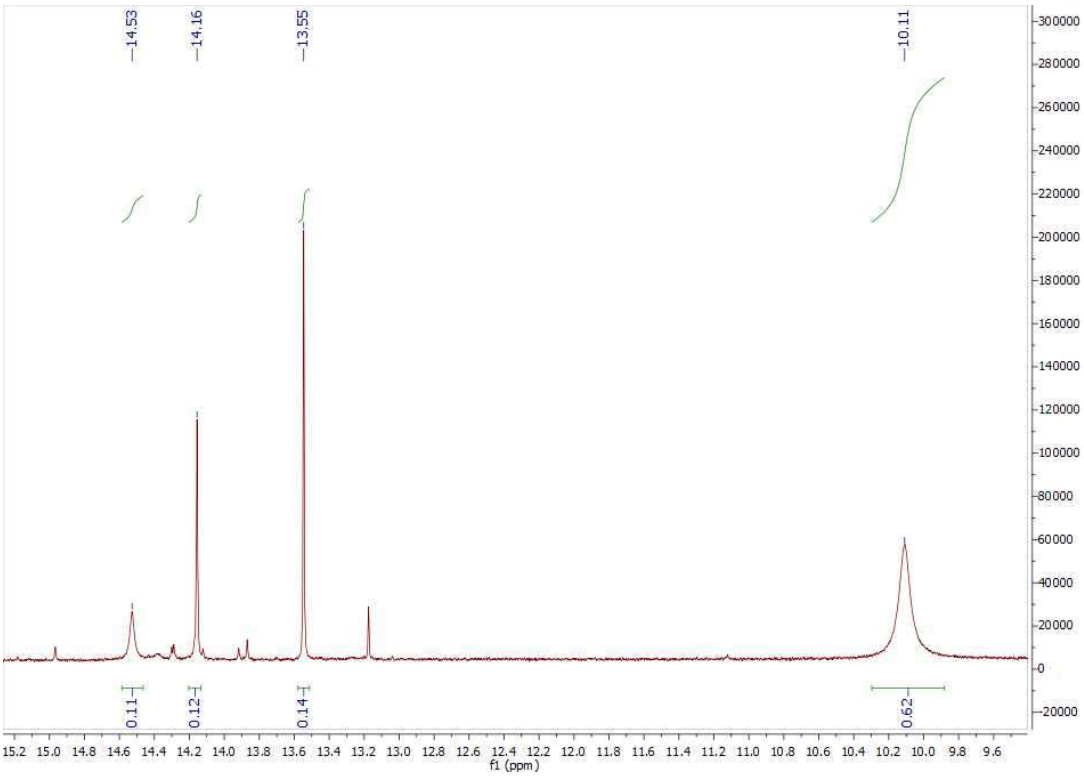

Figure 3.13: ^{1}H NMR spectrum of alkylidene region of initial reaction between Li$_2$4b and Mo(NAr)(CHCMe$_2$Ph)(OTf)$_2$(DME) in C$_6$D$_6$.

Crystals of Mo(NAr)(CHCMe$_2$Ph)(**4b**) were obtained and the crystal structure helped to explain some of the difficulties encountered in the synthesis and purification of this complex. The crystal structure seen in Figure 3.14 clearly shows that one triflate anion is still bound to the molybdenum center. Therefore, the two triflate anions were not being fully substituted by the incoming scorpionate ligand. This caused issues with purification as multiple species could be in solution. One avenue to avoid the incomplete substitution of the triflate anions by the incoming scoprionate ligand would be to utilize a molybdenum starting material that does not contain triflate. Additionally, the non-ligated phenoxide donor has become protonated, likely through deprotonation of an alkylidene carbon on another metal center. The X-ray structure shows that the metal center adopts a distorted square pyramidal structure. The complex crystalizes as the *syn* isomer with Mo(1))-C(40)-C(41) bond angle of 145.4(1)°. The imido ligand is found *trans* to the phenoxide donor with a N(1)- Mo(1)-O(4) angle of 158.6(4)°, while the triflate donor is found *trans* to the imidazole donor with a O(1)- Mo(1)-N(2) angle of 161.7(8)°.

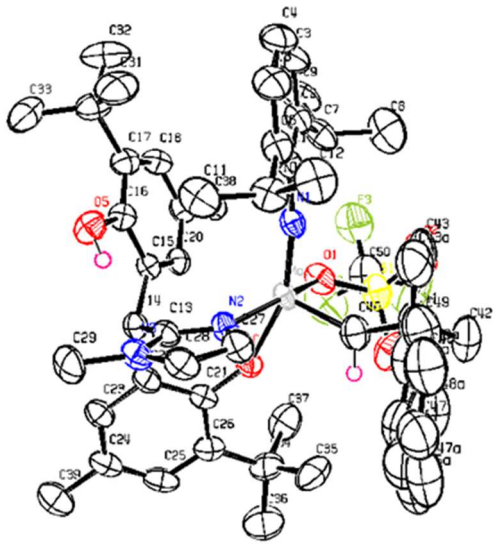

Figure 3.14: ORTEP3 representation (thermal ellipsoids at 50% probability) and atom numbering for Mo(NAr)(CHCMe$_2$Ph)(4b)(OTf) excluding most hydrogens for clarity.

Table 3.1: Selected bond distances (Å) and angles (deg) for Mo(NAr)(CHCMe$_2$Ph)(4b)(OTf).

Mo(NAr)(CHCMe$_2$Ph)(4b)(OTf)	
Bond Lengths (Å)	
Mo(1)-N(1)	1.76(8)
Mo(1)-N(2)	2.16(9)
Mo(1)-O(1)	2.16(8)
Mo(1)-O(4)	2.01(5)
Mo(1)-C(40)	1.90(1)
Bond Angles (deg)	
N(1)-Mo(1)-N(2)	95.0(3)
N(1)- Mo(1)-O(1)	96.6(4)
N(1)- Mo(1)-O(4)	158.6(4)
O(1)- Mo(1)-N(2)	161.7(8)
O(1)- Mo(1)-O(4)	83.1(4)
O(4)- Mo(1)-N(2)	80.9(1)
Mo(1)-C(40)-C(41)	145.4(1)

Table 3.2: Selected crystal data, data collection, and refinement parameters.

	Mo(NAr)(CHCMe$_2$Ph)(4b)(OTf)
empirical formula	$C_{50}H_{64}F_3O_5S$
FW	1044.22
lattice type	monoclinic

space group	$P12_1/n1$
T, K	199.9
a, Å	14.4832(5)
b, Å	25.1880(7)
c, Å	14.8606(5)
α, deg	90
β, deg	94.481(2)
γ, deg	90
V, Å^3	5404.6(3)
Z	4
ρ_{calc}/Mg m^{-3}	1.283
μ(Cu/Mo, Kα) mm^{-1}	2.820 (Cu)
F(000)	2040
cryst size, mm^3	0.14 x 0.02 x 0.015
range θ collected, deg	3.461 to 70.363
reflns collected/unique	40564/7325
abs cor	Semi-empirical from equivalents
Max and min transmn coeff.	0.7533 and 0.4922
goodness of fit	1.006
R_1(I>2σ(I))[a]	0.0643
wR_2 (all data)[a]	0.1813
peak and hole, e Å^{-3}	1.118 and -0.824

[a] Definition of R indices: $R_1 = \Sigma(F_O - F_C)/\Sigma(F_O)$; $wR_2 = [\Sigma[w(F_O^2 - F_C^2)^2]/[\ \Sigma[w(F_O^2)^2]]]^{1/2}$

The first synthetic route avoiding $Mo(NAr)(CHCMe_2Ph)(OTf)_2(DME)$ as the starting material is shown in Scheme 3.3. This route utilized the $Mo(NAr)_2(CH_2CHMe_2Ph)_2$ precursor which was initially used to generate $Mo(NAr)(CHCMe_2Ph)(OTf)_2(DME)$.[21,22] In the literature synthesis triflic acid is used to protonate one NAr group in order to generate an ammonium salt and as the triflate anions bind the molybdenum center, the increased steric bulk forces one CH_2CHMe_2Ph group to abstract a proton from the other CH_2CHMe_2Ph to form an alkylidene. Using $Mo(NAr)_2(CH_2CHMe_2Ph)_2$, **2a-HCl**, **2b-HCl**, or **3b** were added at -30°C and allowed to mix and warm to room temperature. There was no reaction seen for any of the ligands. The next step was to add small portions of triflic acid to see if this would help facilitate the *alpha*-abstraction to form the alkylidene. Unfortunately, this did not yield the desired results. Lastly, the reaction was heated at 50°C, but. these conditions also resulted in no reaction.

Scheme 3.3: First proposed synthetic route avoiding triflate anions.

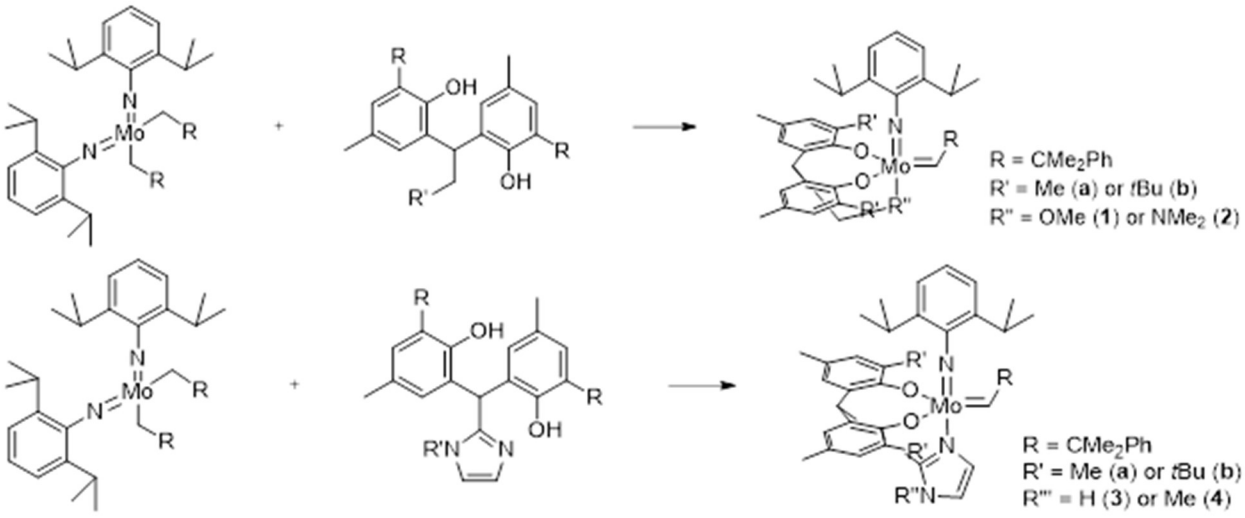

The next synthetic route tested made use of a known molybdenum alkylidene complex with no triflate anion. The molybdenum complex selected was $Mo(NAr)(CHCMe_2Ph)(NC_4H_4)_2$. The lithium pyrrolide[24] as well as the complex[25] was synthesized according to literature procedures. The neutral scorpionate ligands **2** and **4** were then added to the metal complex in

THF, Scheme 3.4. Other solvents like DME were utilized at first, but then put aside as the reactions in THF were much cleaner according to ^{1}H NMR spectroscopy for the reaction using **4b**, Figure 3.15 and Figure 3.16. As seen in the integrations in Figure 3.16, the complex is unsymmetrical. The complex was likely unsymmetrical due to the ligand binding unsymmetrically, Figure 3.17. Although these results were the most promising, a complex that was pure by ^{1}H NMR

Scheme 3.4: Second synthetic approach not involving triflate anions.

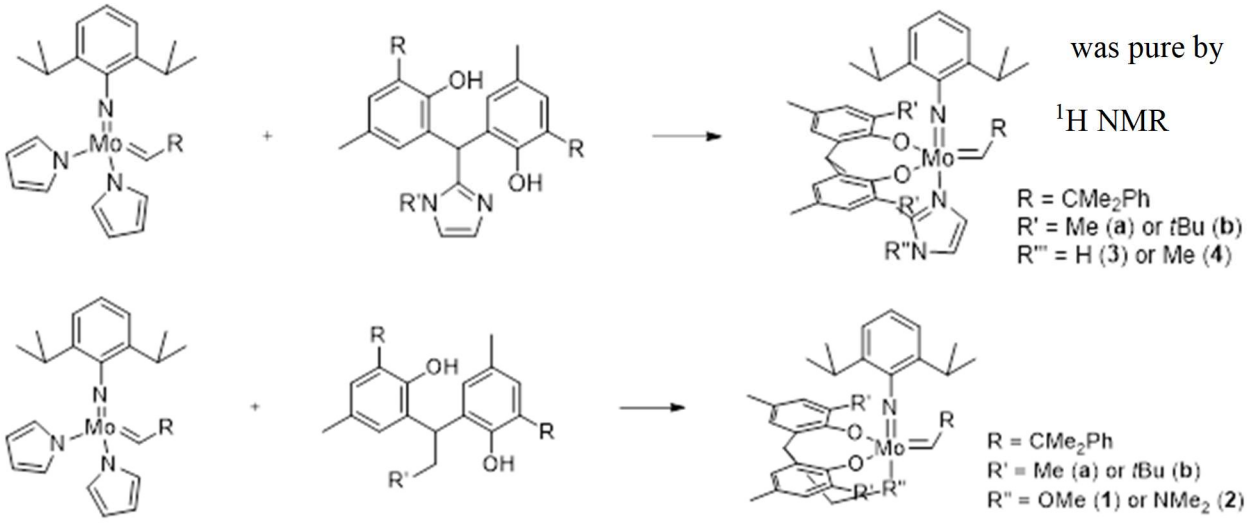

spectroscopy was not isolated.

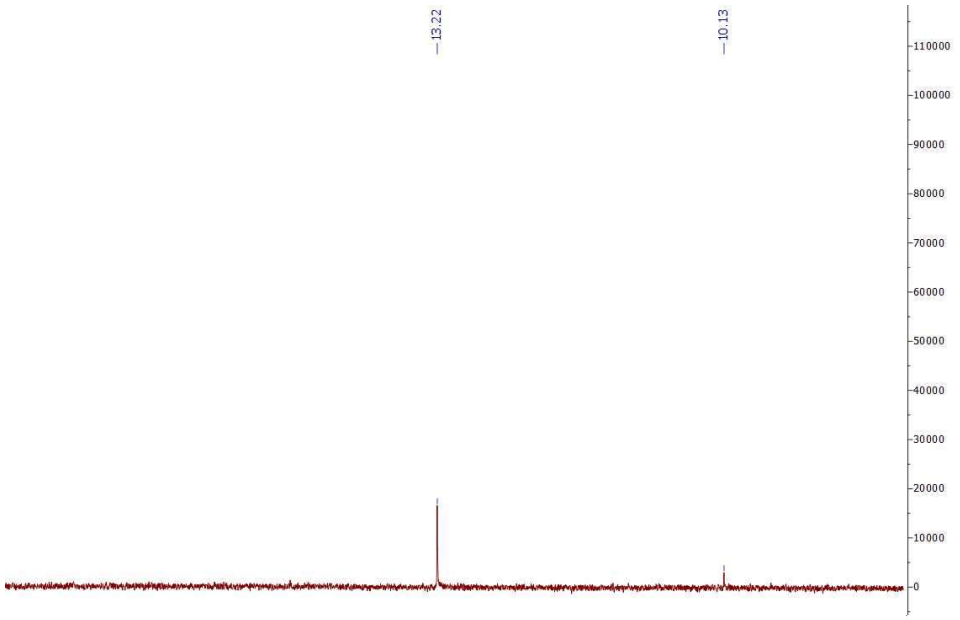

Figure 3.15: ^{1}H NMR spectrum of the alkylidene region of Mo(NAr)(CHCMe$_2$Ph)(4b) taken in C$_6$D$_6$.

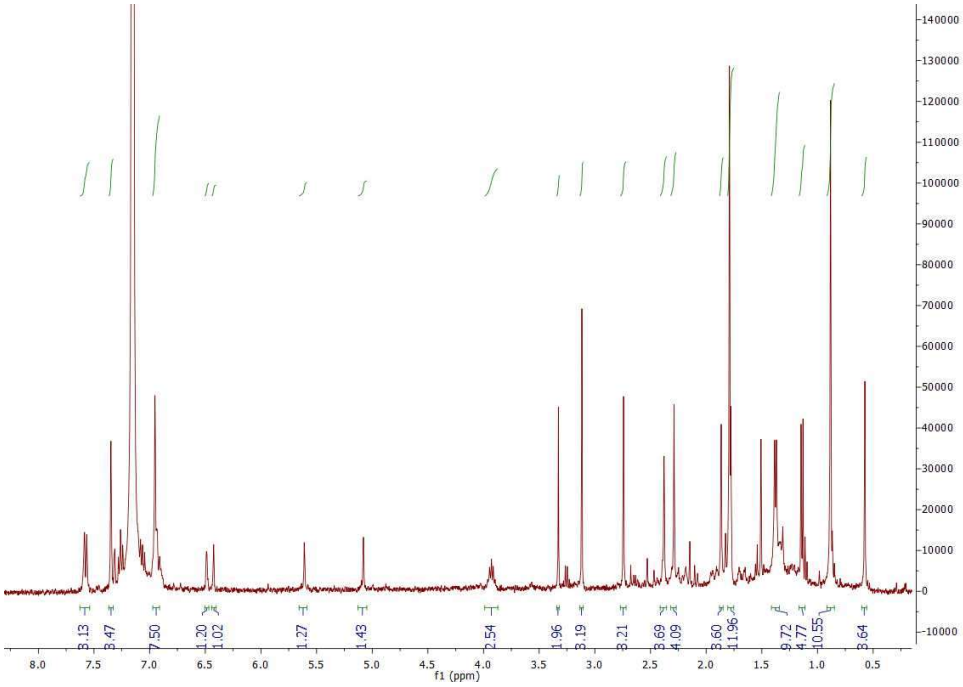

Figure 3.16: ^{1}H NMR spectrum of Mo(NAr)(CHCMe$_2$Ph)(4b) excluding the alkylidene region taken on 400 mHz in C$_6$D$_6$.

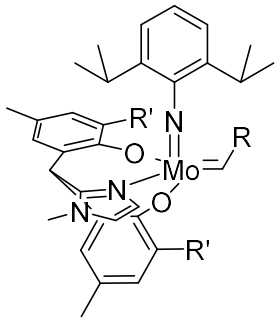

Figure 3.17: Unsymmetric binding of 4b to molybdenum.

3.5 Conclusions

This project was not completed as attempts to synthesize a molybdenum complex stabilized by the dianionic scoprionate ligands were not successful. However, the structure obtained by single crystal X-ray diffraction did lend some insight as to the reasons for the failed reactions. Future attempts should utilize molybdenum starting materials that do not have triflate anions. Or, at the minimum, ^{19}F NMR should be utilized to ensure that complete installation of the scorpionate ligand and dissociation of both triflate anions has occurred. More experiments utilizing the molybdenum bispyrrolide species as a starting material are needed. This synthetic route allowed for the reaction to be free of triflate, which was seen to be an issue with ligand substitution.

3.6 Experimental

General Considerations. All procedures and manipulations were performed under an argon or nitrogen atmosphere using standard Schlenk-line and glove box techniques unless stated otherwise. Solvents were dried and deoxygenated under argon using a LC Technology Solutions Inc. SP-1 stand-alone solvent purification system. All alcohols were dried and distilled over activated magnesium (magnesium turnings and a crystal of iodine) under a nitrogen atmosphere. Deuterated solvents were purchased from Cambridge Isotope Laboratories, Sigma Aldrich,

Acros Organics, or Alfa Aesar degassed, and dried over activated molecular sieves prior to use. All other reagents were purchased from commercial sources and utilized without further purification unless stated otherwise. NMR spectra were recorded at ambient temperature and pressure using a Bruker 400 MHz spectrometer (400 MHz for ^{1}H, and 100 MHz for ^{13}C). The ^{1}H and ^{13}C NMR spectra were measured relative to partially deuterated solvent peaks but are reported relative to tetramethylsilane (TMS). Single crystal X-ray data were collected using a Brunker Proteum diffractometer equipped with dual CCD detectors (Apex II and Platinum 135) and a shared Brunker MicroStar microfocus rotating anode generator running at 45 mA and 60 kV (Cu Kα λ = 1.54178 Å). The data collection strategy was calculated using the Bruker APEX2 software package to ensure desired data redundancy and percent completeness. Unit cell determination, initial indexing, data collection, frame integration, Lorentz-polarization corrections and final cell parameter calculations were carried out using the Bruker APEX2 software package. An absorption correction was performed using the SADABS. The structure was solved using the ShelXT structure solution program using Intrinsic Phasing and refined by Least Squares using the ShelXL program. All non-hydrogen atoms were refined anisotropically. Hydrogen atom positions were calculated geometrically and refined using the riding model. Olex2 was used for the preparation of the publication materials.

Synthesis of $Na_2$2a. To a solution of 1.913 g (1 equiv., 6.10 mmol) **2a** in 10 mL ethanol, 0.510 g (2 equiv., 12.7 mmol) NaOH in 25 mL ethanol was added and stirred overnight. The solvent was then removed in vacuo and the resulting residue was recrystallized in DME and isolated as a white solid containing 4 equivalents of DME. Yield: 2.8941 g. (66%) **^{1}H NMR** (400 MHz, CD_3CN) δ: 6.70 (s, 2H), 6.63 (s, 2H), 4.72 (t, 1H), 2.96 (d, 2H), 2.27 (s, 6H), 2.14 (s, 6H), and 2.13 (s, 6H) ppm.

Synthesis of $Li_2$2a. To a solution of 0.222 g (1 equiv., 0.71 mmol) **2a** in 5 mL THF at -30°C, 0.88 mL 1.6 M (2 equiv., 1.4 mmol) *n*-butyllithium was added and stirred for 1 hour and evaporated. The solution was stirred in toluene overnight and evaporated to isolate the product as a white solid. Yield: 0.228 g, (50%). **^{1}H NMR** (400 MHz, CD_3CN) δ: 6.58 (s, 2H), 6.37 (s, 2H), 3.35 (br. s, 1H), 2.56 (br. s, 2H), 2.09 (s, 6H), 2.04 (s, 6H), and 1.97 (s, 6H) ppm.

Synthesis of $Li_2$3b. To a solution of 0.102 g (1 equiv., 0.25 mmol) **3b** in 1 mL ethanol, 0.0143 g (2 equiv., 0.59 mmol) anhydrous LiOH in 4 mL ethanol was added and stirred for an hour. The solvent was then removed in vacuo. The product was recrystallized using THF layered with pentane at -30°C. The product was isolated as a white solid with 3 equivalents of THF. Yield: 0.0622 g. (39%) **^{1}H NMR** (400 MHz, C_6D_6) δ: 8.29 (s, 1H), 7.40 (s, 1H), 7.37 (s, 2H), 6.29 (s, 1H), 5.54 (s, 1H), 2.29 (br. s, 6H), and 1.65 (s, 18H) ppm.

Synthesis of $Li_2$4a. To a solution of 0.3263 g (1 equiv., 0.78 mmol) **4a** in 5 mL ethanol, 0.0483 g (2 equiv., 2.0 mmol) anhydrous LiOH in 15 mL ethanol was added and stirred for an hour. The solvent was then removed in vacuo and 10 mL THF was added and filtered. The filtrate was evaporated to yield the product as a white solid which contained 1 equivalent of THF. Yield: 0.2497 g. (61%) **^{1}H NMR** (400 MHz, DMSO) δ: 6.83 (s, 2H), 6.67 (s, 1H), 6.61 (s, 1H), 6.38 (s, 2H), 1.99 (s, 6H), and 1.97 (s, 6H) ppm.

Synthesis of $Li_2$4b. To a solution of 0.3025 g (1 equiv., 0.72 mmol) **4b** in 3 mL ethanol, 0.0372 g (2 equiv., 1.5 mmol) anhydrous LiOH in 12 mL ethanol was added and stirred for an hour. The solvent was then removed in vacuo. The residue was dissolved in THF and pentane was added to precipitate out the product. The solution was filtered yield the product as a white solid which contained 3 equivalents of THF. Yield: 0.2497 g. (54%) **^{1}H NMR** (400 MHz,

DMSO) δ: 7.28 (s, 2H), 6.96 (s, 1H), 6.83 (s, 1H), 6.50 (s, 2H), 6.31 (s, 1H), 2.03 (s, 6H), and 1.31 (s, 18H) ppm.

3.7 References

(1) Grubbs, R. H. Olefin-Metathesis Catalysts for the Preparation of Molecules and Materials (Nobel Lecture). *Angewandte Chemie International Edition* **2006**, *45* (23), 3760–3765.

(2) Schrock, R. R. Multiple Metal–Carbon Bonds for Catalytic Metathesis Reactions (Nobel Lecture). *Angewandte Chemie International Edition* **2006**, *45* (23), 3748–3759.

(3) Chauvin Yves. Olefin Metathesis: The Early Days (Nobel Lecture). *Angewandte Chemie International Edition* **2006**, *45* (23), 3740–3747.

(4) Goldman, A. S. Catalytic Alkane Metathesis by Tandem Alkane Dehydrogenation-Olefin Metathesis. *Science* **2006**, *312* (5771), 257–261.

(5) Dobereiner, G. E.; Yuan, J.; Schrock, R. R.; Goldman, A. S.; Hackenberg, J. D. Catalytic Synthesis of N-Alkyl Arenes through Alkyl Group Cross-Metathesis. *J. Am. Chem. Soc.* **2013**, *135* (34), 12572–12575.

(6) Bailey, B. C.; Schrock, R. R.; Kundu, S.; Goldman, A. S.; Huang, Z.; Brookhart, M. Evaluation of Molybdenum and Tungsten Metathesis Catalysts for Homogeneous Tandem Alkane Metathesis. *Organometallics* **2009**, *28* (1), 355–360.

(7) Schrock, R. R. Recent Advances in High Oxidation State Mo and W Imido Alkylidene Chemistry. *Chem. Rev.* **2009**, *109* (8), 3211–3226.

(8) Schrock, R. R. Synthesis of Stereoregular Polymers through Ring-Opening Metathesis Polymerization. *Acc. Chem. Res.* **2014**, *47* (8), 2457–2466.

(9) Vougioukalakis, G. C.; Grubbs, R. H. Ruthenium-Based Heterocyclic Carbene-Coordinated Olefin Metathesis Catalysts. *Chem. Rev.* **2010**, *110* (3), 1746–1787.

(10) Samojłowicz, C.; Bieniek, M.; Grela, K. Ruthenium-Based Olefin Metathesis Catalysts Bearing N-Heterocyclic Carbene Ligands. *Chem. Rev.* **2009**, *109* (8), 3708–3742.

(11) Marinescu, S. C.; King, A. J.; Schrock, R. R.; Singh, R.; Müller, P.; Takase, M. K. Simple Molybdenum(IV) Olefin Complexes of the Type Mo(NR)(X)(Y)(Olefin). *Organometallics* **2010**, *29* (24), 6816–6828.

(12) Schrock, R. R.; Jiang, A. J.; Marinescu, S. C.; Simpson, J. H.; Müller, P. Fundamental Studies of Molybdenum and Tungsten Methylidene and Metallacyclobutane Complexes. *Organometallics* **2010**, *29* (21), 5241–5251.

(13) Xu, W.; Rosini, G. P.; Krogh-Jespersen, K.; Goldman, A. S.; Gupta, M.; Jensen, C. M.; Kaska, W. C. Thermochemical Alkane Dehydrogenation Catalyzed in Solution without the Use of a Hydrogen Acceptor. *Chem. Commun.* **1997**, No. 23, 2273–2274.

(14) Haenel, M. W.; Oevers, S.; Angermund, K.; Kaska, W. C.; Fan, H.-J.; Hall, M. B. Thermally Stable Homogeneous Catalysts for Alkane Dehydrogenation. *Angewandte Chemie International Edition* **2001**, *40* (19), 3596–3600.

(15) Punji, B.; Emge, T. J.; Goldman, A. S. A Highly Stable Adamantyl-Substituted Pincer-Ligated Iridium Catalyst for Alkane Dehydrogenation. *Organometallics* **2010**, *29* (12), 2702–2709.

(16) Sues, P. E.; John, J. M.; Schrock, R. R.; Müller, P. Molybdenum and Tungsten Alkylidene and Metallacyclobutane Complexes That Contain a Dianionic Biphenolate Pincer Ligand. *Organometallics* **2016**, *35* (5), 758–761.

(17) Solans-Monfort, X.; Copéret, C.; Eisenstein, O. Metallacyclobutanes from Schrock-Type D0 Metal Alkylidene Catalysts: Structural Preferences and Consequences in Alkene Metathesis. *Organometallics* **2015**, *34* (9), 1668–1680.

(18) Jiang, A. J.; Simpson, J. H.; Müller, P.; Schrock, R. R. Fundamental Studies of Tungsten Alkylidene Imido Monoalkoxidepyrrolide Complexes. *J. Am. Chem. Soc.* **2009**, *131* (22), 7770–7780.

(19) Kress, J.; Osborn, J. A. Nachweis Der Carben-Olefin-Intermediate in Metathese-Katalysatoren Mit Wolfram in Hoher Oxidationsstufe. *Angewandte Chemie* **1992**, *104* (12), 1660–1662.

(20) Sues, P. E.; John, J. M.; Bukhryakov, K. V.; Schrock, R. R.; Müller, P. Molybdenum and Tungsten Alkylidene Complexes That Contain a 2-Pyridyl-Substituted Phenoxide Ligand. *Organometallics* **2016**, *35* (20), 3587–3593.

(21) Fox, H. H.; Yap, K. B.; Robbins, J.; Cai, S.; Schrock, R. R. Simple, High Yield Syntheses of Molybdenum(VI) Bis(Imido) Complexes of the Type Mo(NR)2Cl2(1,2-Dimethoxyethane). *Inorg. Chem.* **1992**, *31* (11), 2287–2289.

(22) Schrock, R. R.; Murdzek, J. S.; Bazan, G. C.; Robbins, J.; DiMare, M.; O'Regan, M. Synthesis of Molybdenum Imido Alkylidene Complexes and Some Reactions Involving Acyclic Olefins. *J. Am. Chem. Soc.* **1990**, *112* (10), 3875–3886.

(23) Schrock, R. R.; DePue, R. T.; Feldman, J.; Yap, K. B.; Yang, D. C.; Davis, W. M.; Park, L.; DiMare, M.; Schofield, M. Further Studies of Imido Alkylidene Complexes of Tungsten, Well-Characterized Olefin Metathesis Catalysts with Controllable Activity. *Organometallics* **1990**, *9* (8), 2262–2275.

(24) Deiter, T. Pyrrolylchromverbindungen. *Z. Anorg. Allg. Chem* **1971**, *384*, 136–146.

(25) Hock, A. S.; Schrock, R. R.; Hoveyda, A. H. Dipyrrolyl Precursors to Bisalkoxide Molybdenum Olefin Metathesis Catalysts. *J. Am. Chem. Soc.* **2006**, *128* (50), 16373–16375.

Chapter 4 - Conclusions and Future Work

4.1 Summary

In summary, the work discussed in this thesis covers the synthesis of eight novel ligands and eight aluminum complexes, as well as attempts to generate molybdenum complexes bearing the scorpionate ligands. The ligands contained anionic oxygen donors that acted as the "claws" of the scorpionate ligand and a nitrogen or oxygen "tail". The dianionic scorpionate ligands were synthesized using commercially available reagents and a modular Friedel-Crafts alkylation reaction which allowed the steric and electronic properties of the ligands **1-4** to be easily varied, Scheme 4.1.[1,2] The steric bulk was changed from a methyl group to a *tert*-butyl group *ortho* to the phenolate donor. The electronic behavior was varied through the scorpionate "tail" by changing from ethereal to amino, to imidazolyl moieties.

Scheme 4.1: Scorpionate ligand synthesis using a Friedel-Crafts alkylation.

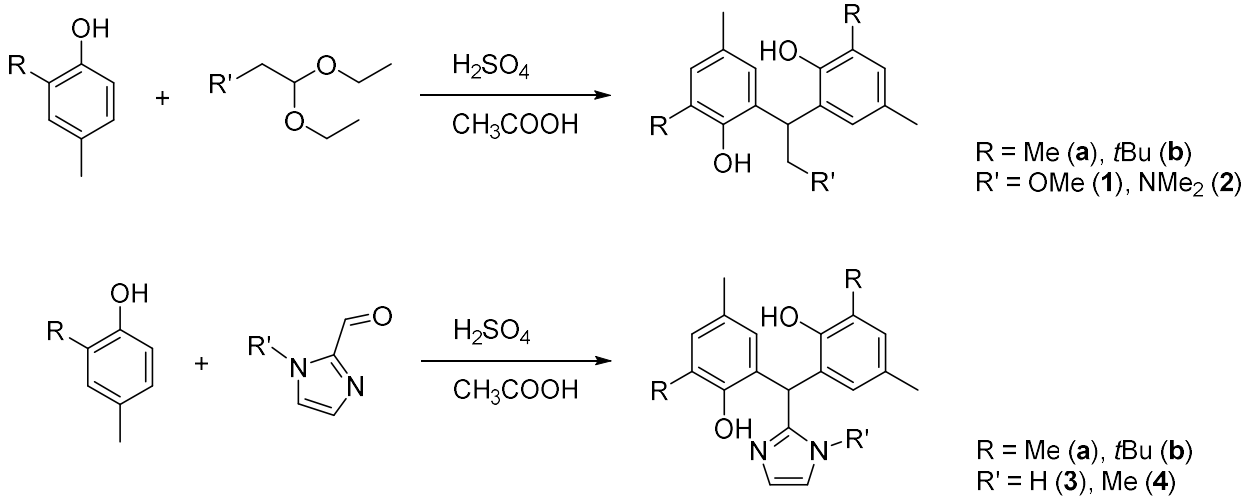

The aluminum complexes **5-8,** Scheme 4.2, were synthesized by adding ligands **1-4** to triethylaluminum to form tetrahedral complexes.[3–5] While the crystal structure indicated that **5a** formed dimers in the solid state, **5b**, **6a**, **6b**, **7a**, **7b** and **8a** formed monomeric species in the solid state. The combination of the weak donating ability of the ethereal tail and the small steric

size of the methyl substituent *ortho* to the phenolate donors caused **5a** to form bridging dimers. When in solution, however, the ^{1}H NMR spectrum suggested that a monomeric species formed and was the main species in solution. For **5b**, **6a**, **6b**, **7a**, **7b**, and **8a**, on the other hand, the crystal structures were able to confirm the donating ability of the "tail" of the scorpionate ligand through metal-ligand the bond distances. The trend followed our initial hypothesis, with the ethereal "tail" forming the weakest interaction, followed by the dimethylamino group, and the imidazolyl functionalities with the strongest interactions.

Scheme 4.2: Synthesis of aluminum scorpionate complexes.

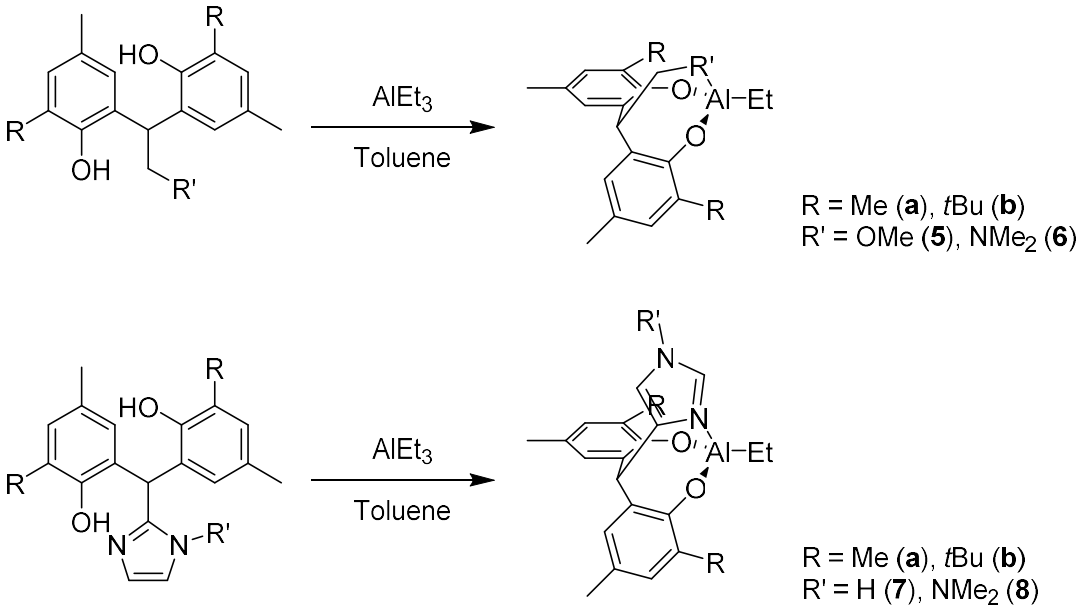

Predictably, the steric size as well as the electronic donating ability of each of the ligands influenced the activity of complexes **5-8** for ε-caprolactone polymerization. The less sterically crowded **a** series showed higher activities than the **b** series, except in the case of **5a**, where the dimers, trimers, and other clusters that formed in solution likely impeded polymerization activity. The donating strength of the "tail" also affected polymerization activity as it is hypothesized that the "tail" must de-coordinate during the catalytic cycle. As seen in the polymerization data, the polymerization activity correlated with the donating ability of the "tail".

Several synthetic strategies were employed in an attempt to access a molybdenum alkylidene complexes bearing ligands **1-4**, but no complexes were successfully synthesized and fully isolated. The ligand substitution with $Mo(NAr)(CHCMe_2Ph)(OTf)_2(DME)$[6,7] where Ar is 2,6-$^{i}PrC_6H_2$ and OTf is CF_3SO_3, was not successful. While one triflate was substituted, one triflate remained bound to the molybdenum center, as seen in the crystal structure in Figure 4.1.

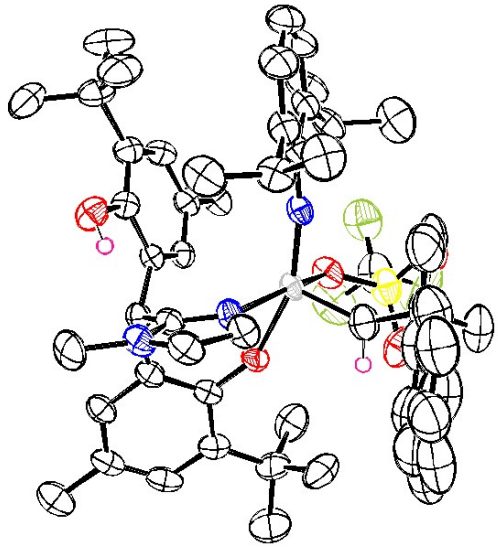

Figure 4.1: ORTEP3 representation (thermal ellipsoids at 50% probability) and atom numbering for Mo(NAr)(CHCMe$_2$Ph)(4b)(OTf) excluding most hydrogens for clarity.

4.2 Future Work

The scoripionate ligands **1-4** can potentially be utilized and studied in many systems. Continuing from the work discussed in Chapter 3 of this thesis, molybdenum and tungsten alkylidene species should be synthetically accessible. Now that it is known that the triflate anions were not being fully substituted, alternative synthetic pathways can be targeted. A synthetic strategy that could be viable, Scheme 4.3,[8,9] utilizes a known molybdenum starting material that does not contain triflate anions, although other alternative starting materials that do not contain triflate could be explored.[8–13] A few attempts utilizing this synthetic strategy were unsuccessful for the isolation of a spectroscopically pure complex. Further attempts using larger scale reactions to allow for easier purification and crystallization could prove successful.

Scheme 4.3: Proposed synthetic route to access molybdenum alkylidenes supported with scoprionate ligands.

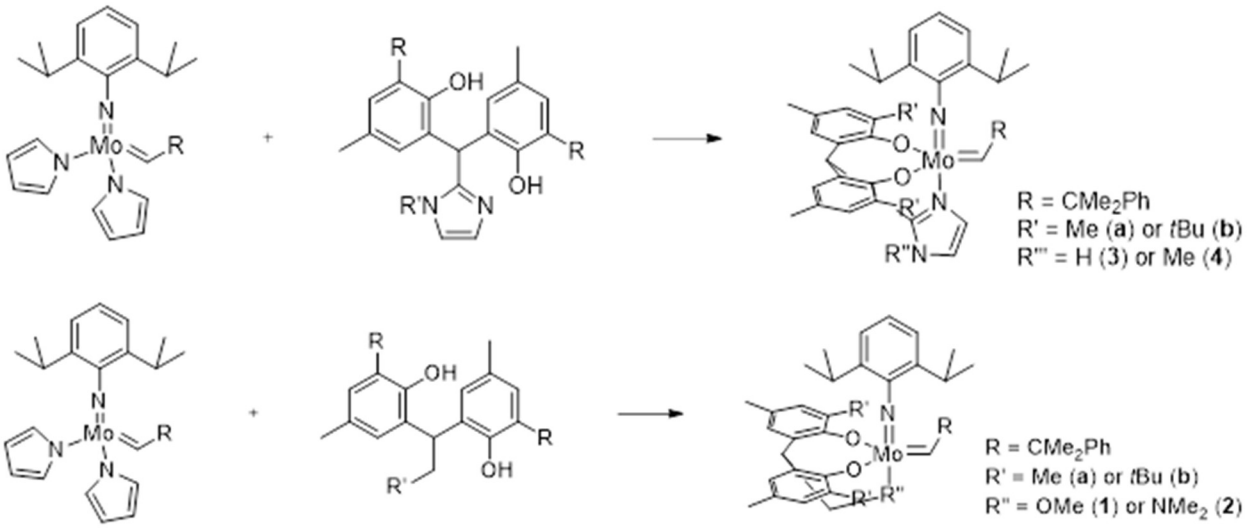

Once spectroscopically pure complexes have been synthesized utilizing ligands **1-4**, they should be characterized using NMR techniques including ^{1}H, ^{13}C, COSY, and HSQC experiments. Additionally, all complexes should be characterized by elemental analysis and single crystal X-ray crystallography. Next, the activity of the complexes for olefin metathesis

should be analyzed. First, the olefin metathesis activity at room temperature using 1-hexene and 1-octene should be investigated, Figure 4.2. It would not be surprising if olefin metathesis did not proceed at room temperature, however, similar to the results seen by Sues and co-workers with five coordinate molybdenum alkylidene complexes.[14,15] Increased temperatures should promote olefin metathesis activity, though, by labilizing the scorpionate ligand "tail". The complexes should also be tested at high temperatures over 125°C. Activity without decomposition at temperatures above 125°C would indicate that the catalysts would be compatible with iridium pincer complexes for alkane metathesis applications.[16] If the complexes are active and do not decompose at temperatures above 125°C, then alkane metathesis with iridium pincer complexes should be explored.[16]

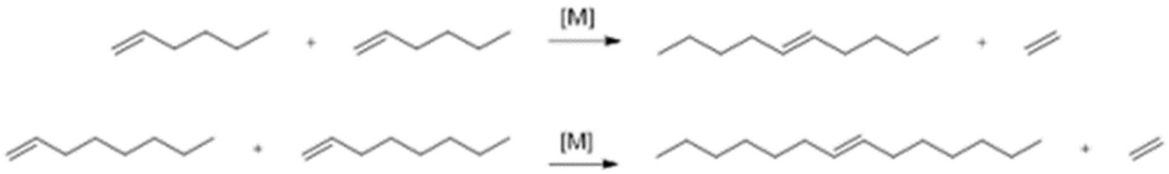

Figure 4.2: Cross metathesis with 1-hexene (top) and 1-octene (bottom).

These complexes could also be tested for ring opening metathesis polymerization using bicyclic monomers, Figure 4.3.[15,17–19] This would show if there is any preference to form *cis* or *trans* polymers as well as *syndiotactic*, *isotactic*, or *atactic* polymers.[20] The "tail" of the ligands could interact with the molybdenum or tungsten species during polymerization to give unique selectivity properties. Investigations into the mechanism by looking at the kinetics as well as

trapping intermediates could give insight into the coordination properties of the various "tails" in the scorpionate ligands.

In addition to synthesizing molybdenum and tungsten complexes, further variations of the ligand could be explored. A benzimidazole version of the ligand, **9**, Figure 4.4a, was synthesized using the same synthetic route as was used to produce ligands **1-4**. The synthesis of the

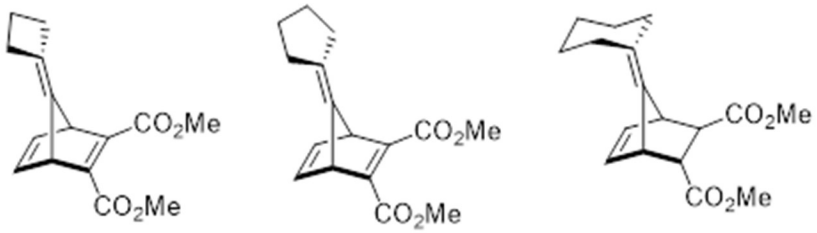

Figure 4.3: Bicyclic monomers for polymerization.

benzimidazole ligand, however, took a week stirring at room temperature and also required column chromatography for purification. This time prohibitive synthesis could be re-evaluated using elevated temperatures to increase reaction rates. Another ligand to potentially explore is the **4b**-half ligand, Figure 4.4b. During the synthesis of **4b**, small amounts of the monosubstituted ligand was isolated. Decreasing the ratio of 2-*tert*-butyl-4-methyl phenol to 1-methyl-2-imidazolecarboxaldehyde as well as decreasing the amount of sulfuric acid used to catalyze the reaction could lead to an increased yield of the half-substituted ligand.

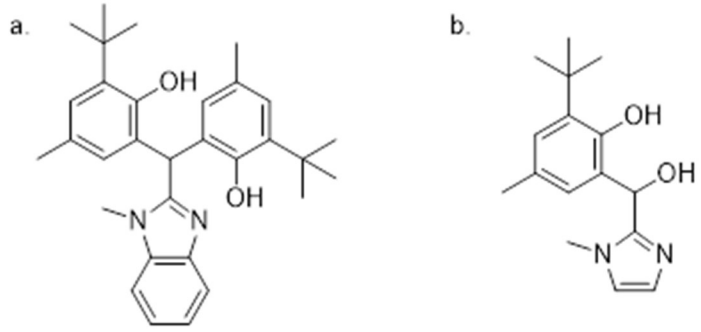

Figure 4.4: a. Benzimidazole ligand (9) and b. the half-4b ligand.

The **4b-**half ligand could then be utilized to generate aluminum, molybdenum, and tungsten complexes, potentially introducing chirality if an enantiopure ligand is used. Further, it is hypothesized that a secondary reaction, Scheme 4.4, could introduce a second "claw" to the

scorpionate ligand that has a different substituent *ortho* to the phenol. This proposed ligand would also introduce chirality to complexes, but with increased steric hinderance as compared to the **4b**-half ligand. These ligands and any subsequent metal complexes synthesized with them would need to be characterized using NMR techniques including ^{1}H, ^{13}C, COSY, and HSQC experiments as well as analyzed by elemental analysis and single crystal X-ray crystallography.

Scheme 4.4: Proposed mixed ligand synthesis.

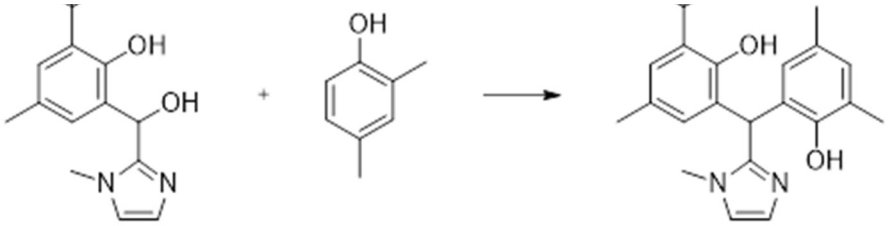

4.3 Experimental

General Considerations. All procedures and manipulations were performed under an argon or nitrogen atmosphere using standard Schlenk-line and glove box techniques unless stated otherwise. Solvents were dried and deoxygenated under argon using a LC Technology Solutions Inc. SP-1 stand-alone solvent purification system. All alcohols were dried and distilled over activated magnesium (magnesium turnings and a crystal of iodine) under a nitrogen atmosphere. Deuterated solvents were purchased from Cambridge Isotope Laboratories, Sigma Aldrich, Acros Organics, or Alfa Aesar degassed, and dried over activated molecular sieves prior to use. All other reagents were purchased from commercial sources and utilized without further purification unless stated otherwise. NMR spectra were recorded at ambient temperature and pressure using a Bruker 400 MHz spectrometer (400 MHz for ^{1}H, and 100 MHz for ^{13}C). The ^{1}H and ^{13}C NMR spectra were measured relative to partially deuterated solvent peaks but are reported relative to tetramethylsilane (TMS).

Synthesis of 9. A mixture of 0.519 g (1 equiv., 3.2 mmol) 1-methylbenzimidazole-2-carboxaldehyde and 1.425 g (2.5 equiv., 8.7 mmol) 2-*tert*-butyl-4-methylphenol in 6.2 ml acetic acid was stirred for 15 minutes. The solution was then cooled to 0°C and 8.2 ml of 1:3 sulfuric acid:acetic acid was added. The solution was allowed to stir for one week at room temperature. The solution was then cooled to 0°C. The reaction was diluted with 50 ml H_2O. The solution was neutralized using 10 M NaOH and then extracted using three times using 50 mL ethyl acetate. The combined organic layers were then washed with saturated $NaHCO_3$, then washed with brine, dried with MgSO4, filtered and concentrated in vacuo. The solid was then purified using a column with 50% ethyl acetate in hexanes. The first fraction was then further recrystallized using ethanol to yield the product as a white solid. Yield 0.4057 (26.5%) ^{1}H NMR (400MHz, DMSO) δ: 9.24 (s, 2H, -O*H*), 7.56 (t, 2H, Aromatic-C*H*), 7.25 (t, 1H, Aromatic-C*H*), 7.19 (t, 1H, Aromatic-C*H*), 6.93 (s, 2H, Aromatic-C*H*), 6.89 (s, 2H, Aromatic-C*H*), 6.02 (s, 2H, C*H*), 3.86 (s, 3H, N-CH_3), 2.14 (s, 6H, Aromatic-CH_3), 1.32 (s, 18H, C(CH_3)$_3$) ppm. ^{13}C NMR (100 MHz, DMSO) δ: 156.99 (Aromatic-*C*), 151.34 (Aromatic-*C*), 140.32 (Aromatic-*C*), 138.51 (Aromatic-*C*), 135.20 (Aromatic-*C*), 128.50 (Aromatic-*C*H), 127.91 (Aromatic-*C*), 126.33 (Aromatic-*C*H), 122.21 (Aromatic-*C*H), 121.94 (Aromatic-*C*H), 118.07 (Aromatic-*C*), 110.45 (Aromatic-*C*H), 41.57 (*C*H), 34.47 (*C*(CH$_3$)$_3$), 29.94 (N-*C*H$_3$), 29.86 (C(*C*H$_3$)$_3$), 20.80 (Aromatic-*C*H$_3$) ppm.

Synthesis of 4b-half ligand. A mixture of 0.368 g (1 equiv., 3.3 mmol) 1-methyl-2-imidazolecarboxaldehyde and 1.138 g (2 equiv., 6.9 mmol) of 2-*tert*-butyl-4-methylphenol in 5 mL acetic acid was stirred for 15 minutes. The solution was then cooled to 0°C and 3.3 mL of 1:3 sulfuric acid:acetic acid was added. The reaction was allowed to stir for two days at room temperature. The reaction was then cooled to 0°C and diluted with 5 mL H_2O. The reaction was neutralized with 10 M NaOH, allowed to warm to room temperature, and then extracted three

times using 25 mL ethyl acetate. The organic layers were combined, then washed twice with 25 mL water, dried with Mg_2SO_4, filtered, and concentrated in vacuo. The resulting residue was washed through a silica gel plug using 5% ethyl acetate in hexanes. The silica gel plug was then washed with ethyl acetate to elute the product and **4b** as a mixture. The **4b-**half ligand was isolated by adding hexanes to the ethyl acetate and filtering. **^{1}H NMR** (400 MHz, DMSO) δ: 12.36 (s, 1H) 7.32 (s, 1H), 7.16 (s, 1H), 7.01 (s, 1H), 5.99 (s, 1H), 5.90 (s, 1H), 3.18 (s, 3H), 2.07 (s, 3H), 1.43 (s, 9H) ppm.

4.4 References

(1) Gazizov, A. S.; Burilov, A. R.; Khakimov, M. S.; Kharitonova, N. I.; Pudovik, M. A.; Konovalov, A. I. Reaction of α-Aminoacetals with 2-Methylresorcinol. *Russ J Gen Chem* **2009**, *79* (9), 1929.

(2) Aoyama, K. Latent Epoxy Curing Catalyst or Curing Agent. Wo/2018/181045, April 10, 2018.

(3) Otero, A.; Lara-Sánchez, A.; Fernández-Baeza, J.; Alonso-Moreno, C.; Castro-Osma, J. A.; Márquez-Segovia, I.; Sánchez-Barba, L. F.; Rodríguez, A. M.; Garcia-Martinez, J. C. Neutral and Cationic Aluminum Complexes Supported by Acetamidate and Thioacetamidate Heteroscorpionate Ligands as Initiators for Ring-Opening Polymerization of Cyclic Esters. *Organometallics* **2011**, *30* (6), 1507–1522.

(4) A. Castro-Osma, J.; Alonso-Moreno, C.; Lara-Sánchez, A.; Otero, A.; Fernández-Baeza, J.; F. Sánchez-Barba, L.; M. Rodríguez, A. Catalytic Behaviour in the Ring-Opening Polymerisation of Organoaluminiums Supported by Bulky Heteroscorpionate Ligands. *Dalton Transactions* **2015**, *44* (27), 12388–12400.

(5) Castro-Osma, J. A.; Alonso-Moreno, C.; Márquez-Segovia, I.; Otero, A.; Lara-Sánchez, A.; Fernández-Baeza, J.; Rodríguez, A. M.; Sánchez-Barba, L. F.; García-Martínez, J. C. Synthesis, Structural Characterization and Catalytic Evaluation of the Ring-Opening Polymerization of Discrete Five-Coordinate Alkyl Aluminium Complexes. *Dalton Trans.* **2013**, *42* (25), 9325–9337.

(6) Fox, H. H.; Yap, K. B.; Robbins, J.; Cai, S.; Schrock, R. R. Simple, High Yield Syntheses of Molybdenum(VI) Bis(Imido) Complexes of the Type Mo(NR)2Cl2(1,2-Dimethoxyethane). *Inorg. Chem.* **1992**, *31* (11), 2287–2289.

(7) Schrock, R. R.; Murdzek, J. S.; Bazan, G. C.; Robbins, J.; DiMare, M.; O'Regan, M. Synthesis of Molybdenum Imido Alkylidene Complexes and Some Reactions Involving Acyclic Olefins. *J. Am. Chem. Soc.* **1990**, *112* (10), 3875–3886.

(8) Hock, A. S.; Schrock, R. R.; Hoveyda, A. H. Dipyrrolyl Precursors to Bisalkoxide Molybdenum Olefin Metathesis Catalysts. *J. Am. Chem. Soc.* **2006**, *128* (50), 16373–16375.

(9) Deiter, T. Pyrrolylchromverbindungen. *Z. Anorg. Allg. Chem* **1971**, *384*, 136–146.

(10) Kreickmann, T.; Arndt, S.; Schrock, R. R.; Müller, P. Imido Alkylidene Bispyrrolyl Complexes of Tungsten. *Organometallics* **2007**, *26* (23), 5702–5711.

(11) Arndt, S.; Schrock, R. R.; Müller, P. Synthesis and Reactions of Tungsten Alkylidene Complexes That Contain the 2,6-Dichlorophenylimido Ligand. *Organometallics* **2007**, *26* (5), 1279–1290.

(12) Jeong, H.; Kozera, D. J.; Schrock, R. R.; Smith, S. J.; Zhang, J.; Ren, N.; Hillmyer, M. A. *Z* -Selective Ring-Opening Metathesis Polymerization of 3-Substituted Cyclooctenes by

Monoaryloxide Pyrrolide Imido Alkylidene (MAP) Catalysts of Molybdenum and Tungsten. *Organometallics* **2013**, *32* (17), 4843–4850.

(13) Jeong, H.; Axtell, J. C.; Török, B.; Schrock, R. R.; Müller, P. Syntheses of Tungsten *Tert* -Butylimido and Adamantylimido Alkylidene Complexes Employing Pyridinium Chloride As the Acid. *Organometallics* **2012**, *31* (18), 6522–6525.

(14) Sues, P. E.; John, J. M.; Schrock, R. R.; Müller, P. Molybdenum and Tungsten Alkylidene and Metallacyclobutane Complexes That Contain a Dianionic Biphenolate Pincer Ligand. *Organometallics* **2016**, *35* (5), 758–761.

(15) Sues, P. E.; John, J. M.; Bukhryakov, K. V.; Schrock, R. R.; Müller, P. Molybdenum and Tungsten Alkylidene Complexes That Contain a 2-Pyridyl-Substituted Phenoxide Ligand. *Organometallics* **2016**, *35* (20), 3587–3593.

(16) Bailey, B. C.; Schrock, R. R.; Kundu, S.; Goldman, A. S.; Huang, Z.; Brookhart, M. Evaluation of Molybdenum and Tungsten Metathesis Catalysts for Homogeneous Tandem Alkane Metathesis. *Organometallics* **2009**, *28* (1), 355–360.

(17) Jeong, H.; John, J. M.; Schrock, R. R.; Hoveyda, A. H. Synthesis of Alternating Trans-AB Copolymers through Ring-Opening Metathesis Polymerization Initiated by Molybdenum Alkylidenes. *J. Am. Chem. Soc.* **2015**, *137* (6), 2239–2242.

(18) Jeong, H.; John, J. M.; Schrock, R. R. Formation of Alternating Trans-A-Alt-B Copolymers through Ring-Opening Metathesis Polymerization Initiated by Molybdenum Imido Alkylidene Complexes. *Organometallics* **2015**, *34* (20), 5136–5145.

(19) Bazan, G. C.; Khosravi, E.; Schrock, R. R.; Feast, W. J.; Gibson, V. C.; O'Regan, M. B.; Thomas, J. K.; Davis, W. M. Living Ring-Opening Metathesis Polymerization of 2,3-

Difunctionalized Norbornadienes by Mo(:CHBu-Tert)(:NC6H3Pr-Iso2-2,6)(OBu-Tert)2. *J. Am. Chem. Soc.* **1990**, *112* (23), 8378–8387.

(20) Schrock, R. R. Synthesis of Stereoregular Polymers through Ring-Opening Metathesis Polymerization. *Acc. Chem. Res.* **2014**, *47* (8), 2457–2466.